

# **INTRINSIC FUNCTIONAL BRAIN NETWORKS IN HEALTH AND DISEASE**

**PhD thesis  
at the Graduate School of Systemic Neurosciences  
Ludwig-Maximilians Universität  
by  
Dr.med. Valentin Riedl**

**March 2012  
Munich, Germany**

**Supervisor: Dr Afra Wohlschläger  
2<sup>nd</sup> expert appraiser: Prof Dr Anna Schubö  
Oral defense: 19.07.2012**

**Content**

<b>1 Abbreviations</b>	<b>3</b>
<b>2 List of publications</b>	<b>4</b>
<b>3 Declaration of contribution as co-author</b>	<b>4</b>
<b>4 Summary</b>	<b>5</b>
<b>5 Aims of the thesis</b>	<b>5</b>
<b>6 Introduction</b>	<b>6</b>
6.1 Imaging cognitive processes with functional magnetic resonance imaging	7
6.2 Imaging the brain's resting state	8
6.3 Intrinsic connectivity networks in the resting state	9
6.4 Investigating modulations and plasticity of intrinsic connectivity networks	12
<b>7 Paper 1: Towards discovery science of human brain function (PNAS 2010)</b>	<b>14</b>
<b>8 Paper 2: Repeated pain induces adaptations of intrinsic brain activity to reflect past and predict future pain (Neuroimage 2011)</b>	<b>30</b>
<b>9 Paper 3: Intrinsic network connectivity reflects consistency of synesthetic experiences (J Neurosci 2012)</b>	<b>40</b>
<b>10 Paper 4: Selective changes of resting-state networks in individuals at risk for Alzheimer's disease (PNAS 2007)</b>	<b>48</b>
<b>11 Paper 5: Increased intrinsic brain activity in the striatum reflects symptom dimensions in schizophrenia (Schizophr Bull 2012)</b>	<b>59</b>
<b>12 Discussion</b>	<b>73</b>
12.1 Organized intrinsic brain activity influences behavior in healthy subjects	73
12.2 Intrinsic connectivity networks and neuropsychiatric diseases	76
12.3 Overall conclusion on organized intrinsic brain activity	78
<b>13 References</b>	<b>80</b>
<b>14 Acknowledgments</b>	<b>85</b>
<b>15 Statutory declaration and statement</b>	<b>85</b>
<b>16 CV</b>	<b>86</b>

## 1 Abbreviations

AD	- Alzheimer's Disease
ADHD	- Attention Deficit Hyperactivity Disorder
BLP	- Band-Limited Power
BOLD	- Blood-Oxygen-Level-Dependent
DMN	- Default Mode Network (ICN)
EEG	- Electroencephalography
ECoG	- Electrocorticography
FC	- Functional Connectivity
fMRI	- Functional MRI
ICA	- Independent Component Analysis
ICN	- Intrinsic Connectivity Network
FC	- Intrinsic FC
LFF	- Low Frequency Fluctuations
MCI	- Mild Cognitive Impairment
MRI	- Magnetic Resonance Imaging
PET	- Positron-Emission-Tomography
ROI	- Region-of-interest
rs-fMRI	- resting state fMRI
SC	- Structural Connectivity
SMN	- Sensorimotor Network (ICN)
SN	- Salience Network (ICN)
vmPFC	- Ventromedial Prefrontal Cortex

## 2 List of publications

### Toward discovery science of human brain function.

Biswal BB, Mennes M, Zuo XN, Gohel S, Kelly C, Smith SM, Beckmann CF, Adelstein JS, Buckner RL, Colcombe S, Dogonowski AM, Ernst M, Fair D, Hampson M, Hoptman MJ, Hyde JS, Kiviniemi VJ, Kotter R, Li SJ, Lin CP, Lowe MJ, Mackay C, Madden DJ, Madsen KH, Margulies DS, Mayberg HS, McMahon K, Monk CS, Mostofsky SH, Nagel BJ, Pekar JJ, Peltier SJ, Petersen SE, **Riedl V**, Rombouts SA, Rypma B, Schlaggar BL, Schmidt S, Seidler RD, Siegle GJ, Sorg C, Teng GJ, Veijola J, Villringer A, Walter M, Wang L, Weng XC, Whitfield-Gabrieli S, Williamson P, Windischberger C, Zang YF, Zhang HY, Castellanos FX, Milham MP.

Proc Natl Acad Sci U S A. 2010 Mar 9;107(10):4734-9. **IF:9,8**

### Repeated pain induces adaptations of intrinsic brain activity to reflect past and predict future pain.

**Riedl V**, Valet M, Wöller A, Sorg C, Vogel D, Sprenger T, Boecker H, Wohlschläger AM, Tölle TR.

Neuroimage. 2011 Jul 1;57(1):206-13. **IF:6,0**

### Intrinsic network connectivity reflects consistency of synesthetic experiences.

Dovern A, Fink GR, Fromme CB, Wohlschlaeger AM, Weiss PH, **Riedl V**.

J Neurosci. 2012 May 30;32(22):7614-21. **IF:7,3**

### Selective changes of resting-state networks in individuals at risk for Alzheimer's disease.

Sorg C, **Riedl V**, Mühlau M, Calhoun VD, Eichele T, Läer L, Drzezga A, Förstl H, Kurz A, Zimmer C, Wohlschläger AM.

Proc Natl Acad Sci U S A. 2007 Nov 20;104(47):18760-5. **IF:9,6**

### Increased intrinsic brain activity in the striatum reflects symptom dimensions in schizophrenia.

Sorg C, Manoliu A, Neufang S, Myers N, Peters H, Schwerthoeffer D, Scherr M, Muehlau M, Zimmer C, Drzega A, Foerstl H, Baeumli J, Eichele T, Wohlschlaeger AM, **Riedl V**.

Schizophr Bull. 2012 Jan 12 [Epub ahead of print] **IF:8,3**

## 3 Declaration of contribution as co-author

Valentin Riedl (VR) designed the study, analyzed the data and co-wrote the paper **Sorg et al (2007)** resulting in a shared 1st authorship. VR analyzed the data and wrote the paper **Riedl et al (2011)**. VR supervised data analyses and co-wrote the papers **Dovern et al (2012)** and **Sorg et al (2012)** resulting in the senior position. VR performed research and contributed analytic tools to the paper **Biswal et al (2010)**.

## 4 Summary

The majority of energy consumed by the brain is dedicated to intrinsic neuronal signaling. Recently, methods emerged that allow the investigation of intrinsic brain activity in the resting brain with functional magnetic resonance imaging (fMRI). These functional connectivity (FC) methods detect large scale brain networks of coherent, ongoing signal fluctuations, called resting state or intrinsic connectivity networks (ICN). ICNs consistently occur in humans across the whole life span, during waking, sleep, and altered levels of consciousness. Furthermore ICNs have been detected in other species like rats and monkeys. Therefore, the intrinsic functional architecture of coherent brain activity is a fundamental organizational principle of the brain.

The papers of this thesis cover resting-state fMRI (rs-fMRI) studies with healthy subjects and patients with neuropsychiatric diseases. We report FC methods to analyze organized intrinsic brain activity as an emerging tool for discovery science of the brain. We then revealed plasticity in the intrinsic network connectivity of healthy subjects that repeatedly experienced pain. Furthermore, we showed that altered sensory experiences in healthy individuals with synesthesia correlate with altered connectivity between sensory ICNs in the resting state. We also investigated ICNs in patients with neuropsychiatric diseases. First, we showed selective changes in two cortical ICNs in patients with early Alzheimer's Disease. And second, we revealed altered intrinsic FC in a subcortical ICN that correlates with symptom dimensions in patients with schizophrenia. These data show that networks of ongoing brain activity form an intrinsic functional architecture in the human brain that is robustly detectable in rs-fMRI data. Moreover, dynamic changes occur in organized intrinsic brain activity in healthy and diseased brains and these changes are related to differences in sensory experiences or behavior.

## 5 Aims of the thesis

Analysis of resting state fMRI data with multivariate methods to characterize and detect

- ICNs as the organizational principle of intrinsic brain activity
- Plasticity of ICNs in healthy subjects after sensory experiences
- Alterations of ICNs in neuropsychiatric diseases

## 6 Introduction

In the last three decades, **neuroimaging** evolved as a new discipline to investigate the neurobiological correlates of human behavior. The two major techniques, positron-emission-tomography (PET) and functional magnetic resonance imaging (fMRI), allow the mapping of human brain function by revealing spatial patterns of brain regions that activate or deactivate in a variety of cognitive tasks, from simple sensory to complex cognitive processing like emotions and decision-making<sup>1,2</sup>. Still, the brain consumes most energy already in the **resting state** when a subject is not involved in performing any externally oriented task<sup>3</sup> (see Figure 1). So far, this **intrinsic brain activity** has not been the focus of interest in the analysis of neuroimaging data, but only served as a reference, or baseline in comparison to task conditions<sup>4</sup>. To fully understand the neurobiological correlate of human behavior it is crucial not only to investigate the causes of regional activations or deactivations but also to explore the organizational principle of the intrinsic brain state and how its activity influences immediate behavior. This thesis will approach these questions by investigating organized intrinsic brain activity with rs-fMRI and its modulation by sensory experiences and in neuropsychiatric diseases.

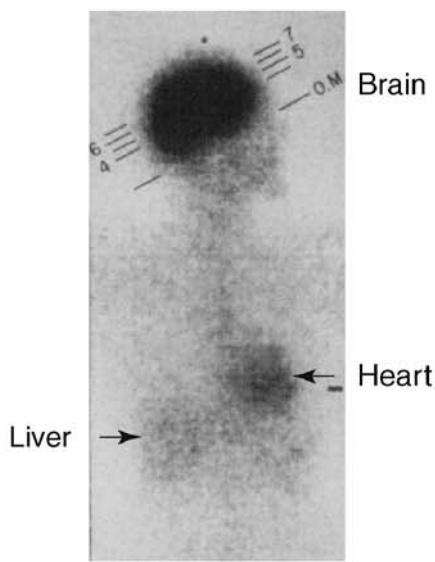
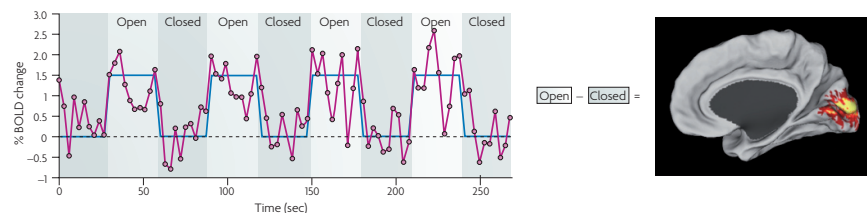


Figure 1: Whole body glucose consumption. In the resting state brain blood flow accounts for 11% of the cardiac output and brain metabolism accounts for 20% of the energy consumption of the body, overshadowing the metabolism of other organs such as the heart, liver and skeletal muscle as shown in this classic image of whole body glucose consumption. Taken from<sup>5</sup>.

### 6.1 Imaging cognitive processes with functional magnetic resonance imaging

Functional neuroimaging is a noninvasive method for mapping human brain function with PET and fMRI<sup>6</sup> (for review, see<sup>2,7,8</sup>). FMRI indirectly measures mass neuronal activity in circumscribed volumes, or voxels, of the brain<sup>9</sup>. The method relies on the fact that increased neuronal activity induces increased blood flow in the same voxel or brain region. As a consequence, the ratio of available oxygen bound to oxygenated hemoglobin, also increases. All these parameters, i.e. tissue perfusion, blood-volume changes, and changes in the concentration of oxygen can be used to indirectly infer changes in neuronal activity. However, the blood-oxygen-level-dependent (BOLD) signal is the parameter most often reported since its discovery in animal<sup>10</sup> and human brain imaging studies<sup>11-13</sup>.



**Figure 2: Traditional fMRI analysis and BOLD noise.** BOLD signal time course (magenta) from a region in the primary visual cortex during a simple task paradigm that requires subjects to open and close their eyes. The paradigm is shown in blue. Traditional fMRI analysis involves correlating BOLD data with a stimulation time-course across multiple blocks. In this case, subtraction of the eyes-closed condition from the eyes-open condition identifies a BOLD signal intensity difference in the primary visual cortex (shown on the right). Taken from<sup>14</sup>.

The traditional approach to investigate the involvement of a brain region in a cognitive task is the voxel-wise comparison of the BOLD signal during a condition of high task demand (e.g. viewing pictures of faces) with that during a lesser demanding baseline state (for review, see<sup>4,5</sup>). The following two experiments illustrate this BOLD-subtraction method to map human brain function. When a black and white checkerboard is visually presented to human subjects for several minutes, primary and secondary visual areas in the occipital cortex activate above baseline (when no visual stimulation is present) as shown in Figure 2. A more complex task of allocating attention to detect a certain target in a visual scene reveals a distributed attention related network of fronto-parietal cortices (see Figure 3). This means that certain brain regions increase their activity consistently above baseline when an experimentally controlled task is performed.

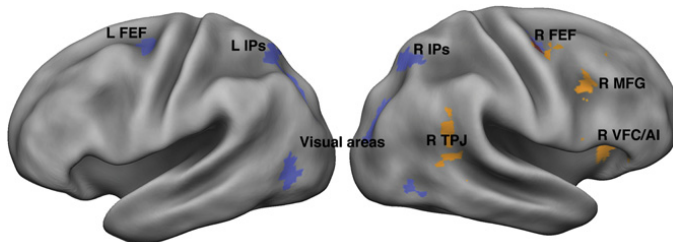


**Figure 3: Definition of dorsal and ventral networks from activation data and putative interactions. Results from a meta-analysis of activation data. Regions in blue are consistently activated by central cues, indicating where a peripheral object will subsequently appear or what is the feature of an upcoming object. Regions in orange are consistently activated when attention is reoriented to an unexpected but behaviorally relevant object. Taken from<sup>15</sup>.**

## 6.2 Imaging the brain's resting state

During the baseline condition, however, the resting brain is by no means in an idle state (for review, see<sup>3</sup>). PET, a method measuring the voxel-wise distribution of glucose consumption, revealed that the resting brain consumes ~20% of the body's energy (see Figure 1). The vast majority of this energy is provided by aerobic glycolysis, the metabolism of glucose to carbon dioxide and water. Up to 80% of the entire energy consumption at rest is devoted to glutamate cycling and, hence, neural signaling processes<sup>16</sup>. This means that the majority of energy consumed by the brain is dedicated to intrinsic, ongoing neuronal signaling while the processing of an external task as described above (Figure 2) increases local energy consumption only in the range of additional 3-5%<sup>17</sup> (see Figure 4).

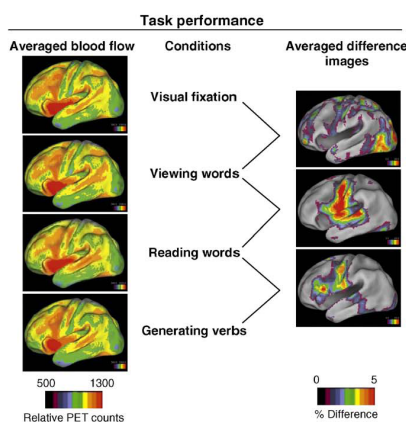


**Figure 4: The changes in regional blood flow associated with task performance are often no more than 5% of the resting blood flow of the brain from which they were derived (center) and, hence, only discernible in difference images averaged across subjects as shown above on the left. These modest modulations in ongoing circulatory and metabolic activity rarely affect the overall rate of brain blood flow and metabolism during even the most arousing perceptual and vigorous motor activity. Taken from<sup>5</sup>**

During a resting state scan, subjects lie in the scanner without performing an experimentally controlled cognitive task. Therefore, the classical procedure of analyzing fMRI data by subtracting the voxel-wise BOLD signal of two cognitive conditions from each other is not applicable to resting state data. Instead, **functional connectivity (FC)** methods have been developed to detect correlations in the rs-fMRI BOLD-signal between voxels<sup>18-20</sup>: (i) Seed-based correlational analyses detect the FC of a region-of-interest (ROI) to any other ROI or ultimately to any other voxel in the brain. This results in a whole brain connectivity map indicating voxels with significant FC to the seed region. (ii) Data-driven methods, such as independent component analysis (ICA) are approaches where no a priori hypothesis about a seed region is needed. The ICA-algorithm simultaneously detects independent spatial maps of coherent, ongoing brain activity in the rs-fMRI data set. (iii) Finally, frequency-domain analyses target differences in the amplitude of certain frequency components in the BOLD signal<sup>21</sup>. After transforming the time series into the frequency domain, the power spectrum of low-frequency (<0.1 Hz) fluctuations (LFF) is calculated for each voxel and compared across conditions or groups. While this last approach tests for correlations in amplitudes across voxels it differs from the other two measures that test for coherence between voxel time-series. A single rs-fMRI scan (as brief as 5 min) can thus be used to interrogate a multitude of functional circuits simultaneously, without the requirement of selecting a priori hypotheses<sup>22</sup>. Building on the term “connectome,” initially applied to the comprehensive map of structural connections in the human brain<sup>23</sup>, the term “functional connectome” describes the collective set of functional connections in the human brain<sup>24</sup>.

### 6.3 Intrinsic connectivity networks in the resting state

Analyzing **intrinsic FC** of rs-fMRI data reveals spontaneous fluctuations in the low frequency band of the BOLD signal that are temporally correlated across functionally related areas<sup>14,25</sup> (see Figure 5). These spatial patterns of coherent intrinsic brain activity have been termed resting state or **intrinsic connectivity networks (ICN)**. In 1995, Bharat Biswal and colleagues described the first ICN in the motor system<sup>25</sup>. They found that ongoing BOLD signal fluctuations in the right primary motor cortex are highly correlated with the resting state BOLD signal in contralateral primary motor cortex, premotor cortices and regions in the cerebellum. Thus, they detected a whole network

of distributed brain regions characterized by coherent ongoing neuronal activity in the resting state that is usually activated together during motor tasks.

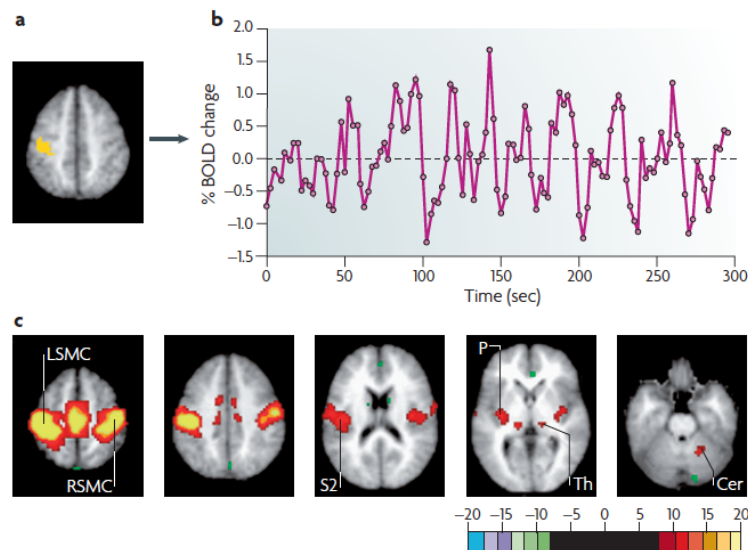


**Figure 5: Generation of resting-state correlation maps.** a) Seed region in the left somatomotor cortex (LSMC) is shown in yellow. b) Time course of spontaneous BOLD activity recorded during resting fixation and extracted from the seed region. c) Statistical z-score map showing voxels that are significantly correlated with the extracted time course. In addition to correlations with the right somatomotor cortex (RSMC) and medial motor areas, correlations are observed with the secondary somatosensory association cortex (S2), the posterior nuclei of the thalamus (Th), putamen (P) and cerebellum (Cer).

Taken from<sup>14</sup>.

After the initial description of this motor network in rs-fMRI data, further ICNs have been repeatedly reported<sup>26-34</sup>. These ICNs cover occipital, temporal and fronto-parietal cortices that show strong correspondence to spatial patterns known from task-fMRI studies mapping visual, sound or attention processing. One can distinguish primary ICNs covering sensori-motor cortices and spatially distributed ICNs similar to networks related to higher cognitive functions like attention, emotion and cognitive control processing (see Figure 6). The primary ICNs cover primary and secondary visual cortices, primary auditory cortices, somatosensory and motor/premotor cortices. ICNs similar to higher cognitive functions are fronto-parietal networks mimicking dorsal (spatial) and ventral attention networks, insular networks related to emotion and cognitive/executive control and a self related default mode network.

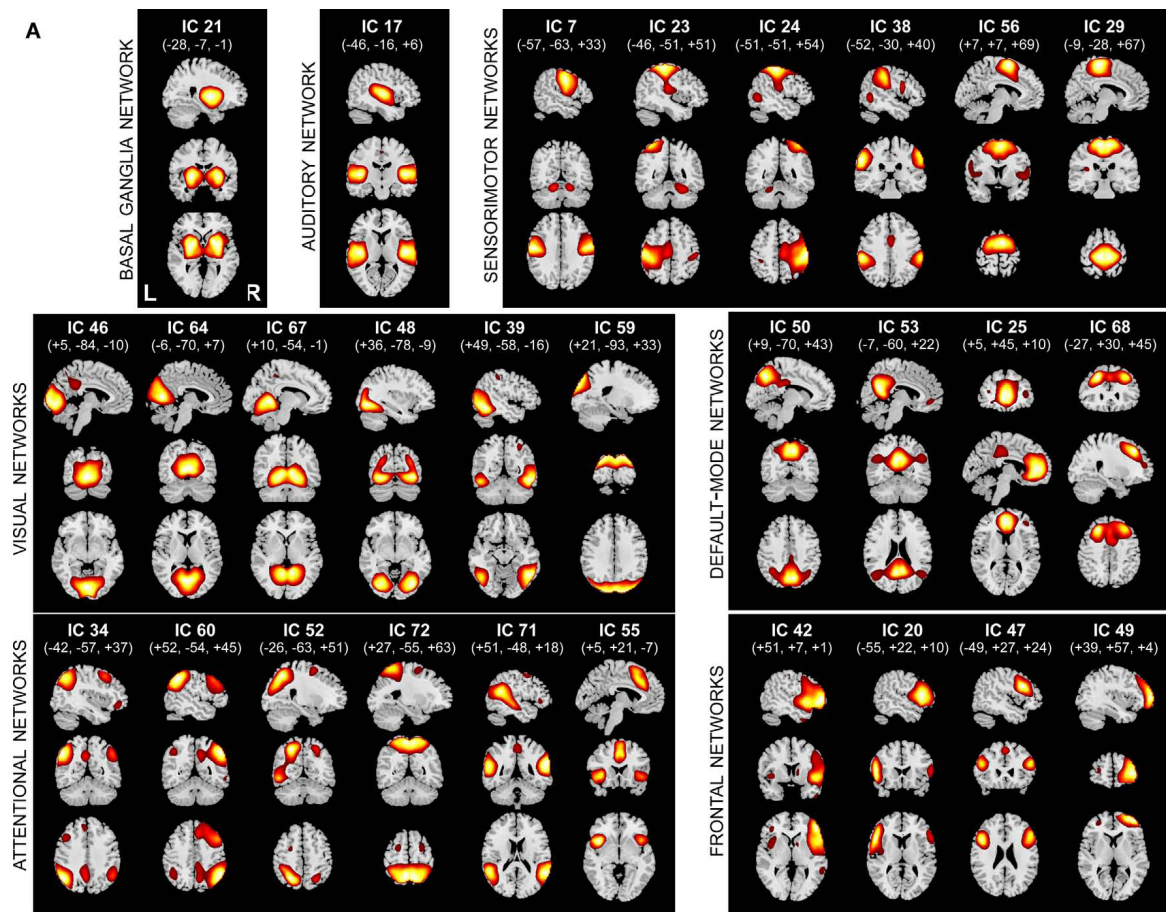


**Figure 6: FC within and between ICNs. (A)** In this publication by Allen et al, 28 components of an ICA were identified as ICNs. ICNs are divided into groups based on their anatomical and functional properties and include basal ganglia, auditory, sensorimotor, visual, default-mode, attentional, and frontal networks. Taken from<sup>32</sup>.

This intrinsic network architecture of ongoing brain activity has now emerged as a common organizational principle in humans, monkeys, and rats<sup>30,35-37</sup>. Studies have provided insight into the development of ICNs in the maturing and aging brain<sup>38-41</sup>, and delineated the effects of sleep<sup>42,43</sup>, anesthesia<sup>44,45</sup>, and pharmacologic agents on rs-fMRI measures<sup>46,47</sup>. Others have investigated the anatomical properties of intrinsically coupled brain regions. In the beginning, it was suggested that patterns of FC rather reflect underlying anatomical connections, or structural connectivity (SC)<sup>36,48</sup>. While connections between certain core regions indeed show this similarity, the majority of functionally coupled regions (like homotopic functional regions) are not directly anatomically connected<sup>49</sup>. This suggests a layer of functional processing in the intrinsic functional architecture that reaches beyond mimicking anatomical connections.

Finally, a large body of literature analyzed the neurophysiological underpinnings of ongoing, coherent BOLD signal fluctuations (for review, see<sup>50</sup>). Typically, coherence of rs-fMRI signal fluctuations between cortical and subcortical brain regions occurs in distinct bins of the low frequency domain (<0.1Hz)<sup>51</sup>. However, the BOLD-signal is heavily blurred and temporally sampled only every 2-3s. Therefore, these MRI parameters might be responsible for the strong representation of LFF. Combined fMRI-electrophysiological recordings found evidence for additional representations of higher frequencies in the electrical signal. In primates, neural spiking activity and the band-limited power (BLP) of high-frequency gamma oscillations correlated best with ongoing BOLD-signal fluctuations<sup>52</sup>. In humans, electrocorticography (ECoG) found correlated spontaneous neuronal activity between both hemispheres of the sensorimotor ICN in slow frequencies as well as in the gamma-range BLP<sup>53,54</sup>. Furthermore, studies have investigated the spatial similarity of electrophysiological and BOLD FC patterns and found strong overlap for ECoG recordings<sup>53,55</sup> and electroencephalography (EEG) recordings<sup>56</sup>. Together, these data suggest that the networks of ongoing BOLD signal fluctuations reflect an intrinsic functional architecture of neuronal activity in the resting state that is more than a mere copy of anatomical connections. This assumption is supported by the studies presented in this thesis as well as by an increasing amount of work by others that show modulations of coherent, intrinsic brain activity by cognitive<sup>57-60</sup> or emotional<sup>61,62</sup> states.

#### 6.4 Investigating modulations and plasticity of intrinsic connectivity networks

The studies presented in this thesis investigate organized intrinsic brain activity with rs-fMRI and its modulation by sensory experiences and in neuropsychiatric diseases. We studied ICNs in healthy subjects and patients with neuropsychiatric diseases. We participated in a multicenter study of 35 research sites to describe a comprehensive and ubiquitous set of ICNs in the resting state forming the human **functional connectome**<sup>37</sup>. Although stable across individuals, we revealed **modulations** of intrinsic network connectivity in healthy subjects that repeatedly experienced pain<sup>59</sup> (*1<sup>st</sup> author*). Furthermore, we showed that altered sensory experiences in healthy individuals, here **synesthesia**, correlate with altered connectivity between sensory ICNs in the resting state (Dovern 2011, J Neurosci, under revision) (*senior author*). We also investigated ICNs in patients with neuropsychiatric diseases. First, we showed selective changes in

two cortical ICNs in patients with early **Alzheimer's Disease** (AD) that precede structural changes in the same brain regions<sup>63</sup> (*shared 1<sup>st</sup> author*). And second, we revealed altered FC in a subcortical ICN that correlates with symptom dimensions in patients with **schizophrenia**<sup>64</sup> (*senior author*). Together, these data show that dynamic changes occur in the intrinsic architecture of ongoing brain activity in healthy and diseased brains and these changes are related to differences in sensory experiences or behavior.

## 7 Paper 1: Towards discovery science of human brain function (PNAS 2010)

# Toward discovery science of human brain function

Bharat B. Biswal<sup>a</sup>, Maarten Mennes<sup>b</sup>, Xi-Nian Zuo<sup>b</sup>, Suril Goel<sup>a</sup>, Clare Kelly<sup>b</sup>, Steve M. Smith<sup>c</sup>, Christian F. Beckmann<sup>c</sup>, Jonathan S. Adelstein<sup>b</sup>, Randy L. Buckner<sup>d</sup>, Stan Colcombe<sup>e</sup>, Anne-Marie Dogonowski<sup>f</sup>, Monique Ernst<sup>g</sup>, Damien Fair<sup>h</sup>, Michelle Hampson<sup>i</sup>, Matthew J. Hoptman<sup>j</sup>, James S. Hyde<sup>k</sup>, Vesa J. Kiviniemi<sup>l</sup>, Rolf Kötter<sup>m</sup>, Shi-Jiang Li<sup>n</sup>, Ching-Po Lin<sup>o</sup>, Mark J. Lowe<sup>p</sup>, Clare Mackay<sup>c</sup>, David J. Madden<sup>q</sup>, Kristoffer H. Madsen<sup>f</sup>, Daniel S. Margulies<sup>r</sup>, Helen S. Mayberg<sup>s</sup>, Katie McMahon<sup>t</sup>, Christopher S. Monk<sup>u</sup>, Stewart H. Mostofsky<sup>v</sup>, Bonnie J. Nagel<sup>w</sup>, James J. Pekar<sup>x</sup>, Scott J. Peltier<sup>y</sup>, Steven E. Petersen<sup>z</sup>, Valentin Riedl<sup>aa</sup>, Serge A. R. B. Rombouts<sup>bb</sup>, Bart Rypma<sup>cc</sup>, Bradley L. Schlaggar<sup>dd</sup>, Sein Schmidt<sup>ee</sup>, Rachael D. Seidler<sup>ff,u</sup>, Greg J. Siegle<sup>gg</sup>, Christian Sorg<sup>hh</sup>, Gao-Jun Teng<sup>ii</sup>, Juha Veijola<sup>jj</sup>, Arno Villringer<sup>ee,kk</sup>, Martin Walter<sup>ll</sup>, Lihong Wang<sup>q</sup>, Xu-Chu Weng<sup>mm</sup>, Susan Whitfield-Gabrieli<sup>nn</sup>, Peter Williamson<sup>oo</sup>, Christian Windischberger<sup>pp</sup>, Yu-Feng Zang<sup>qq</sup>, Hong-Ying Zhang<sup>ii</sup>, F. Xavier Castellanos<sup>bj</sup>, and Michael P. Milham<sup>b,1</sup>

<sup>a</sup>Department of Radiology, New Jersey Medical School, Newark, NJ 07103; <sup>b</sup>Phyllis Green and Randolph Cowen Institute for Pediatric Neuroscience, New York University Child Study Center, NYU Langone Medical Center, New York, NY 10016; <sup>c</sup>FMRIB Centre, Oxford University, Oxford OX3 9DU, UK; <sup>d</sup>Howard Hughes Medical Institute, Harvard University, Cambridge, MA 02138; <sup>e</sup>School of Psychology, University of Wales, Bangor, UK; <sup>f</sup>Danish Research Centre for Magnetic Resonance, Copenhagen University Hospital Hvidovre, Hvidovre, Denmark; <sup>g</sup>Mood and Anxiety Disorders Program, National Institute of Mental Health/National Institutes of Health, Department of Health and Human Services, Bethesda, MD 20892; <sup>h</sup>Behavioral Neuroscience Department, Oregon Health & Science University, Portland, OR 97239; <sup>i</sup>Department of Diagnostic Radiology, Yale University School of Medicine, New Haven, CT 06511; <sup>j</sup>Division of Clinical Research, Nathan S. Kline Institute for Psychiatric Research, Orangeburg, NY 10962; <sup>k</sup>Biophysics Research Institute, Medical College of Wisconsin, Milwaukee, WI 53226; <sup>l</sup>Department of Diagnostic Radiology, Oulu University Hospital, Oulu, Finland; <sup>m</sup>Donders Institute for Brain, Cognition, and Behavior, Center for Neuroscience, Radboud University Nijmegen Medical Center, 6500 HB Nijmegen, The Netherlands; <sup>n</sup>Biophysics Research Institute, Medical College of Wisconsin, Milwaukee, WI 53226; <sup>o</sup>Institute of Neuroscience, National Yang-Ming University, Taiwan; <sup>p</sup>Imaging Institute, The Cleveland Clinic, Cleveland, OH 44195; <sup>q</sup>Brain Imaging and Analysis Center, Duke University Medical Center, Durham, NC, 27710; <sup>r</sup>Department of Cognitive Neurology, Max Planck Institute for Human Cognitive and Brain Sciences, 04103 Leipzig, Germany; <sup>s</sup>Department of Psychiatry and Department of Neurology, Emory University School of Medicine, Atlanta, GA 30322; <sup>t</sup>Centre for Advanced Imaging, University of Queensland, Brisbane, Australia; <sup>u</sup>Department of Psychology, University of Michigan, Ann Arbor, MI 48109; <sup>v</sup>Laboratory for Neurocognitive and Imaging Research, Kennedy Krieger Institute, Baltimore, MD, 21205; <sup>w</sup>Department of Psychiatry, Oregon Health & Science University, Portland, OR 97239; <sup>x</sup>F.M. Kirby Research Center for Functional Brain Imaging, Kennedy Krieger Institute, Baltimore, MD 21205; <sup>y</sup>Functional MRI Laboratory, University of Michigan, Ann Arbor, MI 48109; <sup>z</sup>McDonnell Center for Higher Brain Functions, Washington University School of Medicine, St. Louis, MO 63110; <sup>aa</sup>Departments of Neurology and Neuroradiology, Klinikum Rechts der Isar, Technische Universität München, 81675 Munich, Germany; <sup>bb</sup>Institute of Psychology and Department of Radiology, Leiden University Medical Center, Leiden University, Leiden, The Netherlands; <sup>cc</sup>Center for Brain Health and School of Behavioral and Brain Sciences, University of Texas at Dallas, Richardson, TX 75080; <sup>dd</sup>Department of Neurology, Washington University School of Medicine, St. Louis, MO 63110; <sup>ee</sup>Department of Neurology, Charité Universitätsmedizin-Berlin, 10117 Berlin, Germany; <sup>ff</sup>School of Kinesiology, University of Michigan, Ann Arbor, MI 48109; <sup>gg</sup>Department of Psychiatry, University of Pittsburgh, Pittsburgh, PA 15213; <sup>hh</sup>Department of Psychiatry, Klinikum Rechts der Isar, Technische Universität München, D-81675 Munich, Germany; <sup>ii</sup>Jiangsu Key Laboratory of Molecular and Functional Imaging, Department of Radiology, Zhong-Da Hospital, Southeast University, Nanjing 210009, China; <sup>jj</sup>Department of Psychiatry, Institute of Clinical Medicine and Department of Public Health Science, Institute of Health Science, University of Oulu, Oulu 90014, Finland; <sup>kk</sup>Berlin Neuroimaging Center, 10099 Berlin, Germany; <sup>ll</sup>Department of Psychiatry, Otto-von-Guericke University of Magdeburg, Magdeburg 39106, Germany; <sup>mm</sup>Laboratory for Higher Brain Function, Institute of Psychology, Chinese Academy of Sciences, Beijing 100864, China; <sup>nn</sup>Department of Brain and Cognitive Sciences, Harvard-MIT Division of Health Sciences and Technology, Massachusetts Institute of Technology, Boston, MA 02139; <sup>oo</sup>Department of Psychiatry, University of Western Ontario, London, ON N6A3H8, Canada; <sup>pp</sup>Center for Medical Physics and Biomedical Engineering, Medical University of Vienna, Vienna, Austria; and <sup>qq</sup>State Key Laboratory of Cognitive Neuroscience and Learning, Beijing Normal University, Beijing 100875, China

Edited\* by Marcus E. Raichle, Washington University, St. Louis, MO, and approved January 20, 2010 (received for review October 14, 2009)

Although it is being successfully implemented for exploration of the genome, discovery science has eluded the functional neuro-imaging community. The core challenge remains the development of common paradigms for interrogating the myriad functional systems in the brain without the constraints of *a priori* hypotheses. Resting-state functional MRI (R-fMRI) constitutes a candidate approach capable of addressing this challenge. Imaging the brain during rest reveals large-amplitude spontaneous low-frequency (<0.1 Hz) fluctuations in the fMRI signal that are temporally correlated across functionally related areas. Referred to as functional connectivity, these correlations yield detailed maps of complex neural systems, collectively constituting an individual's "functional connectome." Reproducibility across datasets and individuals suggests the functional connectome has a common architecture, yet each individual's functional connectome exhibits unique features, with stable, meaningful interindividual differences in connectivity patterns and strengths. Comprehensive mapping of the functional connectome, and its subsequent exploitation to discern genetic influences and brain-behavior relationships, will require multicenter collaborative datasets. Here we initiate this endeavor by gathering R-fMRI data from 1,414 volunteers collected independently at 35 international centers. We demonstrate a universal architecture of positive and negative functional connections, as well as consistent loci of inter-individual variability. Age and sex emerged as significant determinants. These results demonstrate that independent R-fMRI datasets can be aggregated and shared. High-throughput R-fMRI can provide quantitative phenotypes for molecular genetic studies and biomarkers of developmental and

pathological processes in the brain. To initiate discovery science of brain function, the 1000 Functional Connectomes Project dataset is freely accessible at [www.nitrc.org/projects/fcon\\_1000/](http://www.nitrc.org/projects/fcon_1000/).

database | neuroimaging | open access | reproducibility | resting state

**M**uch like the challenge of decoding the human genome, the complexities of mapping human brain function pose a challenge to the functional neuroimaging community. As dem-

Author contributions: B.B.B., R.L.B., J.S.H., R.K., A.V., Y.Z., F.X.C., and M.P.M. designed research; B.B.B., M.M., X.N.Z., S.G., C.K., S.M.S., C.F.B., J.S.A., R.L.B., S.C., A.-M.D., M.E., D.F., M.H., M.J.H., J.S.H., V.J.K., R.K., S.J.L., C.P.L., M.J.L., C.E.M., D.M., K.H.M., D.S.M., H.S., M., K.M., C.S.M., S.M., B.J.N., J.J.P., S.J.P., S.E.P., V.R., S.A.R., B.R., B.L.S., S.S., R.D.S., G.S., C.S., G.J.T., J.M.V., A.V., M.W., L.W., X.C.W., S.W.-G., P.W., C.W., Y.Z., H.Y.Z., B.B.B., F.X.C., and M.P.M. performed research; S.M.S., C.F.B., R.L.B., S.C., A.-M.D., M.E., D.F., M.H., M.J.H., J.S.H., V.J.K., R.K., S.J.L., C.P.L., M.J.L., C.E.M., D.M., K.H.M., D.S.M., H.S.M., K.M., C.S.M., S.M., B.J.N., J.J.P., S.J.P., S.E.P., V.R., S.A.R., B.R., B.L.S., S.S., R.D.S., G.S., C.S., G.J.T., J.M.V., A.V., M.W., L.W., X.C.W., S.W.-G., P.W., C.W., Y.Z., H.Y.Z., B.B.B., F.X.C., and M.P.M. contributed new reagents/analytic tools; B.B.B., M.M., X.N.Z., S.G., C.K., F.X.C., and M.P.M. analyzed data; and B.B.B., M.M., X.N.Z., C.K., J.S.A., F.X.C., and M.P.M. wrote the paper.

The authors declare no conflict of interest.

\*This Direct Submission article had a prearranged editor.

Freely available online through the PNAS open access option.

Data deposition: All data used in this work were released on December 11, 2009 via [www.nitrc.org/projects/fcon\\_1000/](http://www.nitrc.org/projects/fcon_1000/).

To whom correspondence should be addressed. E-mail: michael.milham@nyumc.org.

This article contains supporting information online at [www.pnas.org/cgi/content/full/0911855107/DCSupplemental](http://www.pnas.org/cgi/content/full/0911855107/DCSupplemental).

onstrated by the 1000 Genomes Project (1), the accumulation and sharing of large-scale datasets for data mining is necessary for the first phase of discovery science.

Although the neuroimaging community has traditionally focused on hypothesis-driven task-based approaches, resting-state functional MRI (R-fMRI) has recently emerged as a powerful tool for discovery science. Imaging the brain during rest reveals large-amplitude spontaneous low-frequency ( $<0.1$  Hz) fluctuations in the fMRI signal that are temporally correlated across functionally related areas (2–5). A single R-fMRI scan (as brief as 5 min) can be used to interrogate a multitude of functional circuits simultaneously, without the requirement of selecting a priori hypotheses (6). Building on the term “connectome,” coined to describe the comprehensive map of structural connections in the human brain (7), we use “functional connectome” to describe the collective set of functional connections in the human brain.

Buttressed by moderate to high test-retest reliability (8–10) and replicability (11, 12), as well as widespread access, R-fMRI has overcome initial skepticism (13) regarding the validity of examining such an apparently unconstrained state (5, 8, 14). Recent R-fMRI studies have identified putative biomarkers of neuropsychiatric illness (12, 15–18), provided insight into the development of functional networks in the maturing and aging brain (19–22), demonstrated a shared intrinsic functional architecture (23) between

humans and nonhuman primates (24, 25), and delineated the effects of sleep (26), anesthesia (27), and pharmacologic agents on R-fMRI measures (28, 29). Given the many sources of variability inherent in fMRI, the remaining challenge is to demonstrate the feasibility and utility of adopting a high-throughput model for R-fMRI, commensurate with the scale used by human genetics studies to have the power to detect both single gene and combinatorial genetic and environmental effects on complex phenotypes.

Accordingly, the 1000 Functional Connectomes Project was formed to aggregate existing R-fMRI data from collaborating centers throughout the world and to provide an initial demonstration of the ability to pool functional data across centers. As of December 11, 2009, the repository includes data from 1,414 healthy adult participants contributed by 35 laboratories (Table S1). The intent is to expand this open resource as additional data are made available.

Here we provide an initial demonstration of the feasibility of pooling R-fMRI datasets across centers. Specifically, we (i) establish the presence of a universal functional architecture in the brain, consistently detectable across centers; (ii) investigate the influence of center on R-fMRI measures; (iii) explore the potential impact of demographic variables (e.g., age, sex) on R-fMRI measures; and (iv) demonstrate the use of an intersubject variance-based method for identifying putative boundaries between functional networks.

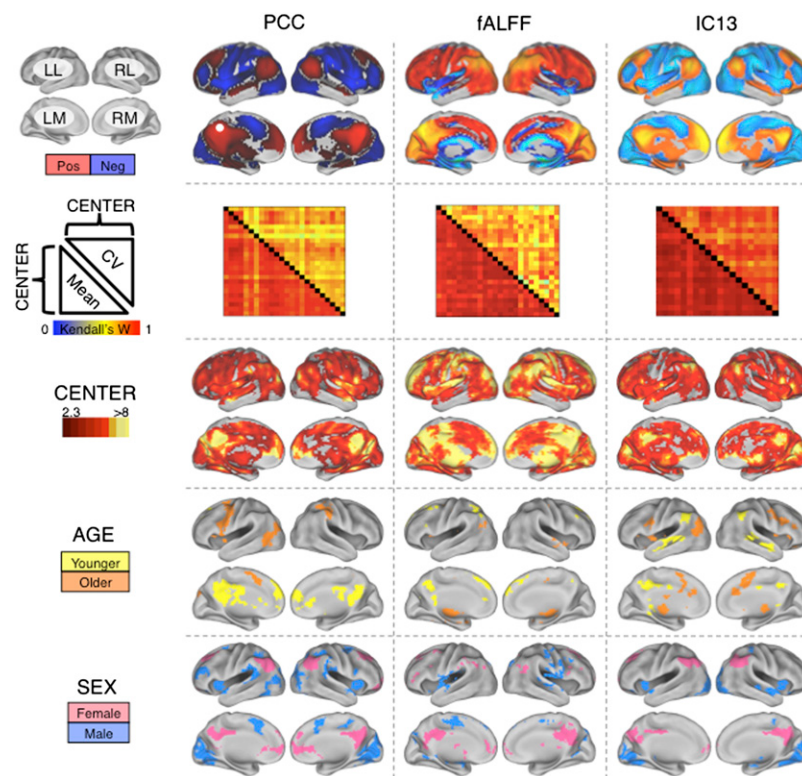


**Fig. 1.** Independent center-, age-, and sex-related variations detected in R-fMRI measures of functional connectivity and amplitude fluctuation. The first row depicts group-level maps for representative seed-based (column 1) and ICA-based (column 3) functional connectivity analyses (SI Results), as well as fALFF (column 2). Group-level maps were derived from one-way ANOVA across 1,093 participants from 24 centers (factor: center; covariates: age and sex). All group-level maps depicted were corrected for multiple comparisons at the cluster level using Gaussian random-field theory ( $Z > 2.3$ ;  $P < 0.05$ , corrected). For each measure, the second row shows robust between-center concordances (Kendall's  $W$ ), with the voxelwise coefficients of variation above the diagonal and the voxelwise means below the diagonal. Kendall's  $W$  concordance between any two centers was calculated across all voxels in the brain mask for the mean (or coefficient of variation) connectivity map across all participants included in each center. Rows 3, 4, and 5 depict voxels exhibiting significant effects of center, age, and sex, respectively, as detected by one-way ANOVA. “Male” refers to significantly greater connectivity (or amplitude, i.e., fALFF) in males; similarly, “female” refers to significantly greater connectivity (or amplitude) in females. “Older” refers to significantly increasing connectivity (or amplitude) with increasing age, whereas “younger” refers to significantly increasing connectivity (or amplitude) with decreasing age. “Pos” refers to positive functional connectivity, and “neg” refers to negative functional connectivity. The PCC seed region is indicated by a white dot. (Top Left) Surface map legend: LL, left lateral; RL, right lateral; LM, left medial; RM, right medial. All surface maps are rendered on the PALS-B12 atlas in CARET (<http://brainvis.wustl.edu>).

## Results

We applied three distinct analytic methods commonly used in the R-fMRI literature: seed-based functional connectivity, independent component analysis (ICA), and frequency-domain analyses. Across the three approaches, we found evidence of (i) a universal intrinsic functional architecture in the human brain, (ii) center-related variation in R-fMRI measures, and (iii) consistent effects of age and sex on R-fMRI measures, detectable across centers despite the presence of center-related variability (Fig. 1). Specifically, seed-based correlational analyses revealed highly consistent patterns of functional connectivity across centers for both the “default mode” (30) and “task-positive” networks (31), supporting a universal functional architecture (Fig. S1). Similarly, a data-driven, temporal concatenation ICA approach, combined with dual regression (32–34), revealed consistent patterns of functional connectivity across centers for 20 spatially independent functional networks (Fig. 1 and Figs. S2 and S3). In addition, for each of the functional connectivity measures, within-center coefficient of variation maps showed a high degree of concordance across centers (Fig. S4). This suggests that common loci of variation exist: centers demonstrated a high degree of agreement on which connections are characterized by relative variance or invariance. Despite the high degree of concordance between centers, there were appreciable center-related variations in the strength of functional connectivity throughout the brain (8). The effect of center was especially prominent in regions exhibiting greater interregional connection strength, because these have the least within-center variability (See SI Results and Fig. S5 for further discussion of center-related variability.) However, even when taking this center-related variability into account, robustly reliable effects of age and sex remained appreciable (Fig. 2 and Figs. S1 and S2). (See SI Results and Fig. S6 for an examination of the impact of sample size on effects of age and sex.)

The detection of sex differences was particularly noteworthy, because these differences are rarely appreciated in the R-fMRI

literature (35). Sexual dimorphism in human genomic expression (36) is known to affect numerous physiological variables that can influence the fMRI signal (37, 38). For example, males and females differ in terms of hemoglobin concentrations and hematocrit (39). However, global variables such as these do not explain the regionally specific sex-related phenomenon noted in the present work. Hormonal effects (e.g., estrogen), operating both during brain development (40) and acutely (41), are known to have regional specificity (42), making them potential contributors to the differences observed. Given the discovery nature of the present work and the lack of prior coordination among centers, the specific sex differences that we observed should be interpreted with caution until replicated in an independent sample.

Along with examining patterns of functional connectivity, we measured the amplitude of low-frequency fluctuations at each voxel using two common periodogram-based measures: amplitude of low frequency fluctuation (ALFF; total power <0.1 Hz) (2, 17, 43) and fractional ALFF (fALFF; total power <0.1 Hz/total power in the measured spectrum) (44). Concordant with previous work, the dominance of low-frequency fluctuations was consistently noted within gray matter regions, but not white matter (44). As with our analyses of functional connectivity, despite clear evidence of center-related effects, we were again able to demonstrate age- and sex-related differences in the magnitude of low-frequency fluctuations in various regions, particularly medial wall structures (Fig. 2 and Fig. S7).

Beyond data pooling for statistical analyses, we demonstrate the potential to use high-throughput datasets to develop normative maps of functional systems in the brain, which is a prerequisite for clinical applications. Specifically, we exploit a key property of functional connectivity maps, the presence of well-differentiated borders between functionally distinct regions (45). The voxelwise measures of coefficients of variation for each type of functional connectivity map delineate putative functional boundaries based on the presence of marked variability in func-

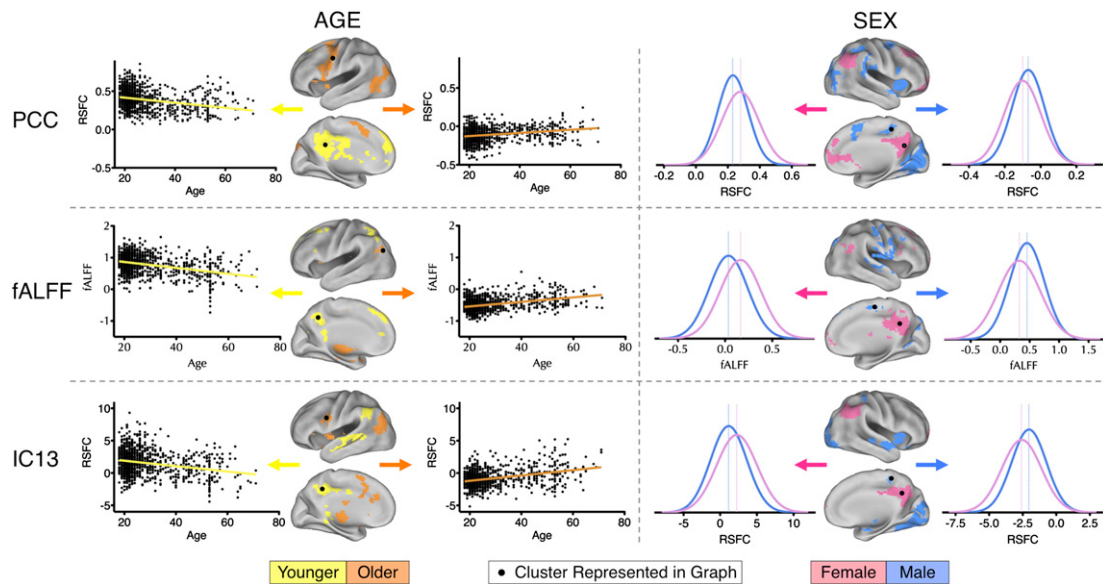


**Fig. 2.** Illustrative areas exhibiting age- and sex-related variation in R-fMRI properties. Significant group-level variance in functional connectivity maps was explained by age and sex (cluster-based Gaussian random-field corrected:  $Z > 2.3$ ;  $P < 0.05$ ). For each of three methods (seed-based, fALFF, and ICA), variance in connectivity strength explained by age (Left) and sex (Right) is illustrated both anatomically and graphically. Age-related differences are represented as scatterplots. Sex-related differences are represented as histograms depicting the distributions of resting-state functional connectivity (RSFC) values for males and females separately. Vertical lines indicate peak values. Corresponding topographical brain areas are indicated with dots. “Male” refers to significantly greater connectivity (or amplitude, i.e., fALFF) in males; similarly, “female” refers to significantly greater connectivity (or amplitude) in females. “Older” refers to significantly increasing connectivity (or amplitude) with increasing age, whereas “younger” refers to significantly increasing connectivity (or amplitude) with decreasing age.

tional connectivity across participants. The variation observed at these boundaries stands in contrast to the low degree of variability observed in regions exhibiting consistently positive or negative connectivity (Fig. 3). In addition, examination of the coefficients of variation for fALFF measures revealed sharp boundary zones between white matter and gray matter. It also identified areas of variability in the amplitude of spontaneous fluctuations that coincided with anatomic areas of notable sulcal variability (e.g., cingulate and frontal opercular regions).

## Discussion

The present work represents a watershed event in functional imaging: demonstration of the feasibility of sharing and pooling functional data across multiple centers, alongside the establishment of an open-access data repository. We have demonstrated (i) the presence of a universal functional architecture, with remarkable stability in the functional connectome and its loci of variation across participants and centers; (ii) evidence of systematic sex differences in R-fMRI measures, as well as age-related gradients even in middle adulthood; and (iii) a method for highlighting the complex array of putative functional boundaries between networks from which normative maps can be developed. Future work should focus on using the functional connectome to catalog phenotypic diversity in brain–behavior relationships.

Functional connectivity is both related to and distinct from anatomic connectivity. Specifically, a recent study reported that a structural core appears to play “a central role in integrating information across functionally segregated brain regions” (23). As such, our finding of a universal functional architecture was not unexpected. But structure and function are not completely coupled, as illustrated by the robust homotopic (i.e., contralateral) functional connectivity for such regions as the primary visual cortex or the amygdala, both of which lack direct callosal projections (24, 46). Such findings imply that functional connectivity is subserved by polysynaptic as well as monosynaptic anatomic circuits. In addition, functional connectivity exhibits dynamic properties that are absent

in structural connectivity. For instance, functional connectivity is modulated by cognitive (47) and emotional state (48), arousal, and sleep (26), whereas structural connectivity is grossly unaffected by such factors. In short, the presence of a demonstrable structural connection does not necessitate that of a functional connection, nor does the demonstration of a functional connection imply the presence of a direct structural connection.

Task-based fMRI and R-fMRI approaches have complementary roles in the study of human brain function. Task-based approaches require sufficient *a priori* knowledge to articulate specific hypotheses, and they are invaluable in refining such hypotheses. But when the knowledge base is insufficient, task-based approaches may be compared to candidate gene studies, which have had limited success when applied to complex genetic disorders. In contrast, genome-wide association studies are increasingly providing initial findings for complex traits (49) and diseases that are subsequently validated through replication, extension, and deep sequencing (50). Our demonstration that R-fMRI data can be aggregated and pooled, and that variability among individuals can be explained in terms of specific subject variables (e.g., sex, age), suggests that this approach can provide quantitative phenotypes to be integrated into molecular studies.

Our results must be considered in light of several limitations of the present study. First, we used a convenience sample comprising previously collected data from an array of centers, without prior coordination of acquisition parameters or scanning conditions. Although the robustness of our results attests to the consistency of intrinsic brain activity, it still represents a potential underestimate of the true across-center consistency. Our demographic data warrant caution, because centers were heterogeneous with respect to male:female ratio, mean age, and age range. Our findings should motivate more systematic exploration of these variables, because future high-throughput imaging studies will need to take such factors into account.

Despite the promise of R-fMRI, some theoretical and pragmatic issues need to be addressed. Examples include the determination of

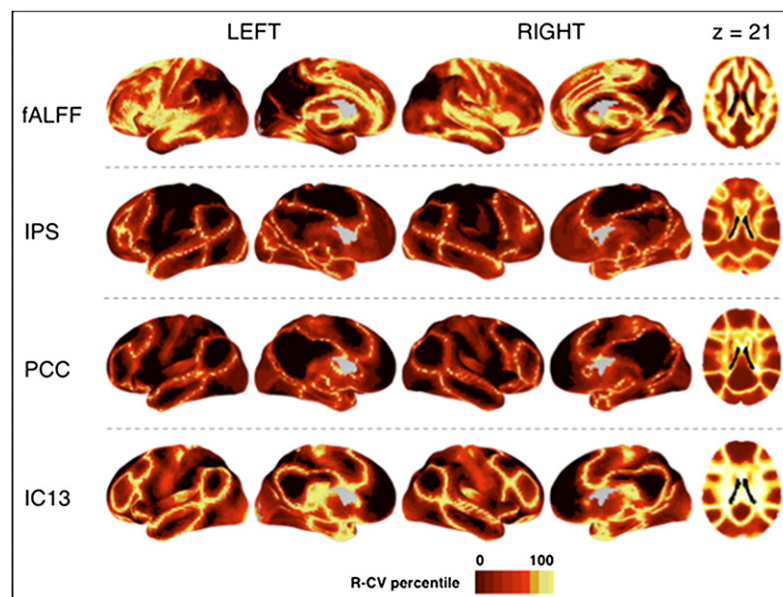


**Fig. 3.** Variation across individuals reveals functional boundaries. Previous work has noted that functionally segregated regions are frequently characterized by well-demarcated boundaries for an individual (45). As such, variability in boundary areas is detectable across participants. Here we detect functional boundaries via examination of voxelwise coefficients of variation (absolute value) for fALFF and selected seed-based [intraparietal sulcus (IPS), posterior cingulate/precuneus (PCC)] and ICA-based (IC13) functional connectivity maps. For the purpose of visualization, coefficients of variation were rank-ordered, whereby the relative degree of variation across participants at a given voxel, rather than the actual value, was plotted to better contrast brain regions. Ranking coefficients of variation efficiently identified regions of greatest interindividual variability, thus delineating putative functional boundaries.

the origins and biological significance of spontaneous low-frequency fluctuations of neuronal and hemodynamic activity, the impact of intrinsic activity on evoked responses (and vice versa), and the ideal means of acquiring, processing, and analyzing R-fMRI data. Nevertheless, the potential of discovery science is vast, from the development of objective measures of brain functional integrity to help guide clinical diagnoses and decision-making, to tracking treatment response and assessing the efficacy of treatment interventions. Finally, whereas the present work examines functional connectivity alone, future studies may combine R-fMRI with other modalities (e.g., EEG, magnetoencephalography, diffusion-tensor imaging, volumetrics) and genetics to achieve a more complete understanding of the human brain.

All data and analytic tools used in the present work will be made available at [www.nitrc.org/projects/fcon\\_1000/](http://www.nitrc.org/projects/fcon_1000/). We anticipate that the open availability of the 1000 Functional Connectomes dataset will recruit the broad participation and collaboration among the scientific community necessary for successful implementation of discovery-based science of human brain function. In addition, we hope that it will further advance the ethos of data sharing and collaboration initiated by such efforts as fMRIIDC ([www.fmridc.org](http://www.fmridc.org)), FBIRN ([www.birncommunity.org](http://www.birncommunity.org)), OASIS ([www.oasis-brains.org](http://www.oasis-brains.org)), BrainScape ([www.brainscape.org](http://www.brainscape.org)), and BrainMap ([www.brainmap.org](http://www.brainmap.org)).

## Methods

Resting-state fMRI scans were aggregated from 35 community-based datasets ( $n = 1,414$ ). The present analysis was restricted to 24 centers ( $n = 1,093$ ; 21 published, 3 unpublished; mean age <60 years; only participants over age 18; one scan per participant; duration: 2.2–20 min;  $n = 970$  at 3 T,  $n = 123$  at 1.5 T; voxel size, 1.5–5 mm within plane; slice thickness, 3–8 mm). Each contributor's respective ethics committee approved submission of deidentified data. The institutional review boards of NYU Langone Medical Center and New Jersey Medical School approved the receipt and dissemination of the data.

For functional connectivity, we used seed-based correlation analysis, based on six previously identified seed regions (31), and model-free ICA, using temporal

- Wise J (2008) Consortium hopes to sequence genome of 1000 volunteers. *BMJ* 336: 237.
- Biswal B, Yetkin FZ, Haughton VM, Hyde JS (1995) Functional connectivity in the motor cortex of resting human brain using echo-planar MRI. *Magn Reson Med* 34: 537–541.
- Fox MD, Raichle ME (2007) Spontaneous fluctuations in brain activity observed with functional magnetic resonance imaging. *Nat Rev Neurosci* 8:700–711.
- Margulies DS, et al. (2007) Mapping the functional connectivity of anterior cingulate cortex. *Neuroimage* 37:579–588.
- Smith SM, et al. (2009) Correspondence of the brain's functional architecture during activation and rest. *Proc Natl Acad Sci USA* 106:13040–13045.
- Van Dijk KR, et al. (2010) Intrinsic functional connectivity as a tool for human connectomics: Theory, properties, and optimization. *J Neurophysiol* 103:297–321.
- Sporns O, Tononi G, Kötter R (2005) The human connectome: A structural description of the human brain. *PLOS Comput Biol* 1:e42.
- Shehzad Z, et al. (2009) The resting brain: Unconstrained yet reliable. *Cereb Cortex* 19: 2209–2229.
- Zuo XN, et al. (2010) Reliable intrinsic connectivity networks: test-retest evaluation using ICA and dual regression approach. *Neuroimage* 49:2163–2177.
- Zuo XN, et al. (2010) The oscillating brain: Complex and reliable. *Neuroimage* 49: 1432–1445.
- He Y, et al. (2009) Uncovering intrinsic modular organization of spontaneous brain activity in humans. *PLOS One* 4:e5226.
- Buckner RL, et al. (2009) Cortical hubs revealed by intrinsic functional connectivity: Mapping, assessment of stability, and relation to Alzheimer's disease. *J Neurosci* 29: 1860–1873.
- Morcom AM, Fletcher PC (2007) Does the brain have a baseline? Why we should be resisting a rest. *Neuroimage* 37:1073–1082.
- Damoiseaux JS, et al. (2006) Consistent resting-state networks across healthy subjects. *Proc Natl Acad Sci USA* 103:13848–13853.
- Castellanos FX, et al. (2008) Cingulate precuneus interactions: A new locus of dysfunction in adult attention-deficit/hyperactivity disorder. *Biol Psychiatry* 63: 332–337.
- Church JA, et al. (2009) Control networks in paediatric Tourette syndrome show immature and anomalous patterns of functional connectivity. *Brain* 132:225–238.
- Zang YF, et al. (2007) Altered baseline brain activity in children with ADHD revealed by resting-state functional MRI. *Brain Dev* 29:83–91.
- Rombouts SA, et al. (2009) Model-free group analysis shows altered BOLD FMRI networks in dementia. *Hum Brain Mapp* 30:256–266.
- Kelly AMC, et al. (2009) Development of anterior cingulate functional connectivity from late childhood to early adulthood. *Cereb Cortex* 19:640–657.
- Supekar K, Musen M, Menon V (2009) Development of large-scale functional brain networks in children. *PLoS Biol* 7:e1000157.
- Fair DA, et al. (2009) Functional brain networks develop from a "local to distributed" organization. *PLoS Comput Biol* 5:e1000381.
- Andrews-Hanna JR, et al. (2007) Disruption of large-scale brain systems in advanced aging. *Neuron* 56:924–935.
- Hagmann P, et al. (2008) Mapping the structural core of human cerebral cortex. *PLoS Biol* 6:e159.
- Vincent JL, et al. (2007) Intrinsic functional architecture in the anaesthetized monkey brain. *Nature* 447:83–86.
- Margulies DS, et al. (2009) Precuneus shares intrinsic functional architecture in humans and monkeys. *Proc Natl Acad Sci USA* 106:20069–20074.
- Fukunaga M, et al. (2006) Large-amplitude, spatially correlated fluctuations in BOLD fMRI signals during extended rest and early sleep stages. *Magn Reson Imaging* 24: 979–992.
- Greicius MD, et al. (2008) Persistent default-mode network connectivity during light sedation. *Hum Brain Mapp* 29:839–847.
- Achard S, Bullmore E (2007) Efficiency and cost of economical brain functional networks. *PLoS Comput Biol* 3:e17.
- Kelly C, et al. (2009) L-dopa modulates functional connectivity in striatal cognitive and motor networks: A double-blind, placebo-controlled study. *J Neurosci* 29:7364–7378.
- Gusnard DA, Raichle ME, Raichle ME (2001) Searching for a baseline: Functional imaging and the resting human brain. *Nat Rev Neurosci* 2:685–694.
- Fox MD, et al. (2005) The human brain is intrinsically organized into dynamic, anticorrelated functional networks. *Proc Natl Acad Sci USA* 102:9673–9678.
- Beckmann CF, DeLuca M, Devlin JT, Smith SM (2005) Investigations into resting-state connectivity using independent component analysis. *Philos Trans R Soc Lond B Biol Sci* 360:1001–1013.
- Filippini N, et al. (2009) Distinct patterns of brain activity in young carriers of the APOE-epsilon4 allele. *Proc Natl Acad Sci USA* 106:7209–7214.
- Calhoun VD, Pekar JJ, Pearson GD (2004) Alcohol intoxication effects on simulated driving: Exploring alcohol-dose effects on brain activation using functional MRI. *Neuropsychopharmacology* 29:2097–3017.
- Liu H, Stufflebeam SM, Sepulcre J, Hedden T, Buckner RL (2009) Evidence from intrinsic activity that asymmetry of the human brain is controlled by multiple factors. *Proc Natl Acad Sci USA* 106:20499–20503.
- Ellegren H, Parsch J (2007) The evolution of sex-biased genes and sex-biased gene expression. *Nat Rev Genet* 8:689–698.

concatenation to generate group-level components and dual regression to generate individual participant maps. For amplitude measures at each voxel, we used the FFT-based ALFF (2, 17, 43) and its normalized variant, fALFF (44).

Standard image preprocessing was performed (i.e., motion correction, spatial filtering with FWHM = 6 mm, 12-dof affine transformation to MNI152 stereotactic space). For seed-based correlation approaches and dual regression following ICA analysis, nuisance signals (e.g., global signal, WM, CSF, motion parameters) were regressed out. Temporal filtering was tailored for each analytic approach (29, 31, 32, 44).

ICA components for dual regression analyses were determined by (i) low-dimensional (20 components) temporal concatenation ICA carried out 25 times (each with 18 participants randomly selected from each of 17 centers with minimum of 165 time points) and (ii) low-dimensional (20 components) meta-ICA, a second concatenation-based ICA using the component sets produced by the 25 runs (see *SI Results* for a description of an alternative method). For each participant, dual regression (32–34) was performed using the 20 components identified by the meta-ICA (Fig. S3), yielding a connectivity map for each component.

Aggregate statistical analyses of center, sex, and age effects were based on a generalized linear model implementation of one-way ANOVA (factor: center; covariates: age and sex). To identify functional boundaries, we calculated voxelwise coefficients of variation across all 1,093 participants, and ranked each voxel based on the absolute value of its coefficient of variation.

**ACKNOWLEDGMENTS.** We thank David Kennedy and [www.nitrc.org](http://www.nitrc.org) for supporting the 1000 Functional Connectomes Project data release, Avi Snyder for providing helpful insights and advice concerning project goals, and Cameron Craddock for helpful advice on this study. Financial support for the 1000 Functional Connectomes project was provided by grants from the National Institutes of Mental Health (R01MH083246 and R01MH081218 to F.X.C. and M.P.M.), National Institute on Drug Abuse (R03DA024775, to C.K.; R01DA016979, to F.X.C.), Autism Speaks, National Institute of Neurological Disorders and Stroke (R01NS049176, to B.B.), and the Howard Hughes Medical Institute (to J.S.A. and R.L.B.), as well as gifts to the NYU Child Study Center from the Stavros Niarchos Foundation, Leon Levy Foundation, Joseph P. Healy, Linda and Richard Schaps, and Jill and Bob Smith and an endowment provided by Phyllis Green and Randolph Cöwen. NITRC is funded by the National Institutes of Health's Blueprint for Neurosciences Research ([neuroscienceblueprint.nih.gov](http://neuroscienceblueprint.nih.gov)) (Contract N02-EB-6-4281, to TCG, Inc.).

1. Wise J (2008) Consortium hopes to sequence genome of 1000 volunteers. *BMJ* 336: 237.
2. Biswal B, Yetkin FZ, Haughton VM, Hyde JS (1995) Functional connectivity in the motor cortex of resting human brain using echo-planar MRI. *Magn Reson Med* 34: 537–541.
3. Fox MD, Raichle ME (2007) Spontaneous fluctuations in brain activity observed with functional magnetic resonance imaging. *Nat Rev Neurosci* 8:700–711.
4. Margulies DS, et al. (2007) Mapping the functional connectivity of anterior cingulate cortex. *Neuroimage* 37:579–588.
5. Smith SM, et al. (2009) Correspondence of the brain's functional architecture during activation and rest. *Proc Natl Acad Sci USA* 106:13040–13045.
6. Van Dijk KR, et al. (2010) Intrinsic functional connectivity as a tool for human connectomics: Theory, properties, and optimization. *J Neurophysiol* 103:297–321.
7. Sporns O, Tononi G, Kötter R (2005) The human connectome: A structural description of the human brain. *PLOS Comput Biol* 1:e42.
8. Shehzad Z, et al. (2009) The resting brain: Unconstrained yet reliable. *Cereb Cortex* 19: 2209–2229.
9. Zuo XN, et al. (2010) Reliable intrinsic connectivity networks: test-retest evaluation using ICA and dual regression approach. *Neuroimage* 49:2163–2177.
10. Zuo XN, et al. (2010) The oscillating brain: Complex and reliable. *Neuroimage* 49: 1432–1445.
11. He Y, et al. (2009) Uncovering intrinsic modular organization of spontaneous brain activity in humans. *PLOS One* 4:e5226.
12. Buckner RL, et al. (2009) Cortical hubs revealed by intrinsic functional connectivity: Mapping, assessment of stability, and relation to Alzheimer's disease. *J Neurosci* 29: 1860–1873.
13. Morcom AM, Fletcher PC (2007) Does the brain have a baseline? Why we should be resisting a rest. *Neuroimage* 37:1073–1082.
14. Damoiseaux JS, et al. (2006) Consistent resting-state networks across healthy subjects. *Proc Natl Acad Sci USA* 103:13848–13853.
15. Castellanos FX, et al. (2008) Cingulate precuneus interactions: A new locus of dysfunction in adult attention-deficit/hyperactivity disorder. *Biol Psychiatry* 63: 332–337.
16. Church JA, et al. (2009) Control networks in paediatric Tourette syndrome show immature and anomalous patterns of functional connectivity. *Brain* 132:225–238.
17. Zang YF, et al. (2007) Altered baseline brain activity in children with ADHD revealed by resting-state functional MRI. *Brain Dev* 29:83–91.
18. Rombouts SA, et al. (2009) Model-free group analysis shows altered BOLD FMRI networks in dementia. *Hum Brain Mapp* 30:256–266.
19. Kelly AMC, et al. (2009) Development of anterior cingulate functional connectivity from late childhood to early adulthood. *Cereb Cortex* 19:640–657.
20. Supekar K, Musen M, Menon V (2009) Development of large-scale functional brain networks in children. *PLoS Biol* 7:e1000157.
21. Fair DA, et al. (2009) Functional brain networks develop from a "local to distributed" organization. *PLoS Comput Biol* 5:e1000381.
22. Andrews-Hanna JR, et al. (2007) Disruption of large-scale brain systems in advanced aging. *Neuron* 56:924–935.
23. Hagmann P, et al. (2008) Mapping the structural core of human cerebral cortex. *PLoS Biol* 6:e159.
24. Vincent JL, et al. (2007) Intrinsic functional architecture in the anaesthetized monkey brain. *Nature* 447:83–86.
25. Margulies DS, et al. (2009) Precuneus shares intrinsic functional architecture in humans and monkeys. *Proc Natl Acad Sci USA* 106:20069–20074.
26. Fukunaga M, et al. (2006) Large-amplitude, spatially correlated fluctuations in BOLD fMRI signals during extended rest and early sleep stages. *Magn Reson Imaging* 24: 979–992.
27. Greicius MD, et al. (2008) Persistent default-mode network connectivity during light sedation. *Hum Brain Mapp* 29:839–847.
28. Achard S, Bullmore E (2007) Efficiency and cost of economical brain functional networks. *PLoS Comput Biol* 3:e17.
29. Kelly C, et al. (2009) L-dopa modulates functional connectivity in striatal cognitive and motor networks: A double-blind, placebo-controlled study. *J Neurosci* 29:7364–7378.
30. Gusnard DA, Raichle ME, Raichle ME (2001) Searching for a baseline: Functional imaging and the resting human brain. *Nat Rev Neurosci* 2:685–694.
31. Fox MD, et al. (2005) The human brain is intrinsically organized into dynamic, anticorrelated functional networks. *Proc Natl Acad Sci USA* 102:9673–9678.
32. Beckmann CF, DeLuca M, Devlin JT, Smith SM (2005) Investigations into resting-state connectivity using independent component analysis. *Philos Trans R Soc Lond B Biol Sci* 360:1001–1013.
33. Filippini N, et al. (2009) Distinct patterns of brain activity in young carriers of the APOE-epsilon4 allele. *Proc Natl Acad Sci USA* 106:7209–7214.
34. Calhoun VD, Pekar JJ, Pearson GD (2004) Alcohol intoxication effects on simulated driving: Exploring alcohol-dose effects on brain activation using functional MRI. *Neuropsychopharmacology* 29:2097–3017.
35. Liu H, Stufflebeam SM, Sepulcre J, Hedden T, Buckner RL (2009) Evidence from intrinsic activity that asymmetry of the human brain is controlled by multiple factors. *Proc Natl Acad Sci USA* 106:20499–20503.
36. Ellegren H, Parsch J (2007) The evolution of sex-biased genes and sex-biased gene expression. *Nat Rev Genet* 8:689–698.

37. Goldstein JM, et al. (2001) Normal sexual dimorphism of the adult human brain assessed by in vivo magnetic resonance imaging. *Cereb Cortex* 11:490–497.
38. Gur RC, et al. (1995) Sex differences in regional cerebral glucose metabolism during a resting state. *Science* 267:528–531.
39. Zeng SM, Yankowitz J, Widness JA, Strauss RG (2001) Etiology of differences in hematocrit between males and females: Sequence-based polymorphisms in erythropoietin and its receptor. *J Gend Specif Med* 4:35–40.
40. Lenroot RK, et al. (2007) Sexual dimorphism of brain developmental trajectories during childhood and adolescence. *Neuroimage* 36:1065–1073.
41. Protopopescu X, et al. (2008) Hippocampal structural changes across the menstrual cycle. *Hippocampus* 18:985–988.
42. McEwen BS (1999) Permanence of brain sex differences and structural plasticity of the adult brain. *Proc Natl Acad Sci USA* 96:7128–7130.
43. Cordes D, et al. (2001) Frequencies contributing to functional connectivity in the cerebral cortex in “resting-state” data. *AJNR Am J Neuroradiol* 22:1326–1333.
44. Zou QH, et al. (2008) An improved approach to detection of amplitude of low-frequency fluctuation (ALFF) for resting-state fMRI: Fractional ALFF. *J Neurosci Methods* 172:137–141.
45. Cohen AL, et al. (2008) Defining functional areas in individual human brains using resting-state functional connectivity MRI. *Neuroimage* 41:45–57.
46. Roy AK, et al. (2009) Functional connectivity of the human amygdala using resting-state fMRI. *Neuroimage* 45:614–626.
47. Albert NB, Robertson EM, Miall RC (2009) The resting human brain and motor learning. *Curr Biol* 19:1023–1027.
48. Harrison BJ, et al. (2008) Modulation of brain resting-state networks by sad mood induction. *PLoS ONE* 3:e1794.
49. Lettre G (2009) Genetic regulation of adult stature. *Curr Opin Pediatr* 21:515–522.
50. Manolio TA, et al. (2009) Finding the missing heritability of complex diseases. *Nature* 461:747–753.

# Supporting Information

Biswal et al. 10.1073/pnas.0911855107

## SI Methods

**Image Preprocessing. Overview.** All available resting-state scans were preprocessed using both AFNI (1) and FSL ([www.fmrib.ox.ac.uk](http://www.fmrib.ox.ac.uk)). Specific commands can be found in the preprocessing scripts that will be released at [www.nitrc.org/projects/fcon\\_1000/](http://www.nitrc.org/projects/fcon_1000/) on publication of this paper. After the first five time points of every scan were discarded, to remove possible T1 stabilization effects, the data were corrected for motion by aligning each volume to the mean image volume using Fourier interpolation in AFNI. Then the data were spatially smoothed using a 6-mm FWHM Gaussian kernel. Mean-based intensity normalization was done by scaling all volumes by the same factor (10,000).

**Seed-based correlation analyses.** The data were temporally filtered using both a high-pass (Gaussian-weighted least squares straight-line fitting, with  $\sigma = 100.0$  s) and low-pass (Gaussian low-pass temporal filtering, with a HWHM of 2.8 s) filter, followed by linear detrending to remove any residual drift.

**Independent component analysis. Temporal concatenation group analysis.** Consistent with common practice, temporal filtering for ICA analyses was limited to high-pass filtering (Gaussian-weighted least squares straight-line fitting, with  $\sigma = 100.0$  s).

**Dual regression.** This step used the same preprocessed data as used in the seed-based correlation analyses.

**ALFF/fALFF.** No temporal filtering was carried out, because the data were examined in the frequency domain within select bands (2, 3). Temporal despiking with a hyperbolic tangent squashing function was performed, however, to limit extreme values. Linear trends were then removed from the data.

**Registration and normalization.** After the skull was removed using AFNI, registration of each individual's high-resolution anatomic image to a common stereotactic space [the Montreal Neurological Institute's 152-brain template (MNI152); 3 mm isotropic voxel size] was done using a 12-degrees of freedom linear affine transformation (FLIRT) (4, 5). The resulting transformation was then applied to each individual's functional dataset. We did not further optimize the normalization with a nonlinear algorithm, because of concerns about image quality and limited coverage in some datasets.

**Functional Connectivity: Seed-Based Correlation Analysis. Nuisance signal regression.** Consistent with common practice in the fMRI literature, nuisance signals were removed from the data via multiple regression before functional connectivity analyses were performed. This step is designed to control for the effects of physiological processes, such as fluctuations related to motion and cardiac and respiratory cycles. Specifically, each individual's 4D time series data were regressed on nine predictors: white matter (WM), cerebrospinal fluid (CSF), the global signal, and six motion parameters. The global signal regressor was generated by averaging across the time series of all voxels in the brain. The WM and CSF covariates were generated by segmenting each individual's high-resolution structural image (using FAST in FSL). The resulting segmented WM and CSF images were thresholded to ensure 80% tissue type probability. These thresholded masks were then applied to each individual's time series, and a mean time series was calculated by averaging across time series of all voxels within each mask. The six motion parameters were calculated in the motion-correction step during preprocessing. Movement in each of the three cardinal directions (X, Y, and Z) and rotational movement around three axes (pitch, yaw, and roll) were included for each individual.

**Seed selection.** Six 7.5-mm-radius seed regions of interest (ROIs) (containing 33 voxels) centered on the coordinates previously used

by Fox et al. (6) were created to examine functional connectivity for each of six regions, three regions within the "task-positive" network and three within the "default mode" network. The ROIs within the task-positive network were located in the IPS (-25, -57, 46), the middle temporal region (MT+; -45, -69, -2), and the right frontal eye field (FEF) region of the precentral sulcus (25, -13, 50). The default mode network seed ROIs were located in the left lateral parietal cortex (LP; -45, -67, 36), medial prefrontal cortex (MPF; -1, 47, -4), and PCC (-5, -49, 40).

**Individual seed-based functional connectivity analysis.** First, each individual's residual 4D time series data were spatially normalized by applying the previously computed transformation to the MNI152 standard space. Then the time series for each seed was extracted from these data. Time series were averaged across all voxels in each seed's ROI. For each individual dataset, the correlation between the time series of the seed ROI and that of each voxel in the brain was determined. This analysis was implemented using 3dfim+ (AFNI) to produce individual-level correlation maps of all voxels that were positively or negatively correlated with the seed's time series. Finally, these individual-level correlation maps were converted to Z-value maps using Fisher's *r*-to-z transformation.

**Functional Connectivity: Independent Component Analysis. Overview.** Temporal-concatenation group ICA (TC-GICA) was used to generate group-level components for the dataset (7) using MELODIC (FSL). Given computational resource limitations (e.g., 32 GB of physical memory), as well as a number of centers with a small number of time points due to repetition times >2.0 s, each TC-GICA run was applied to a dataset consisting of 18 participants/center from the 17 centers that collected a minimum of 165 functional volumes per scan. This approach also ensured that a single center's data would not drive the ICA components detected. Consistent with recent work on low-dimensional ICA (8), the number of components was fixed at 20. Given the potential for such factors as initial random values and subject sampling to affect ICA results, 25 TC-GICA analyses were performed, each using a unique resampling from each of the 17 centers. A meta-ICA analysis was then carried out across the 25 runs to extract the 20 spatially independent components consistently identified across the 25 runs. An alternative hierarchical clustering approach based on ICASSO (9) is described below. The two approaches yielded similar results. Dual regression (10, 11) was then carried out using the 20 resulting components as templates, to produce individual participant maps for each of the 20 components.

**TC-GICA.** Specifically, TC-GICA comprised five fundamental steps:

1. Each individual's preprocessed data were first truncated to the same number of time points (i.e., 165 EPI volumes).
2. A bootstrapping dataset was generated by randomly choosing 18 individual datasets per center, resulting in 306 individual functional datasets.
3. All 306 individual functional datasets were spatially averaged in MNI152 standard space and then used to estimate the mean covariance matrix.
4. The number of components was set at 20, and all individual functional data were projected into a subspace spanned by the first 20 eigenvectors of the mean covariance matrix, resulting in reduced individual fMRI data (in a common subspace).

5. All 306 reduced individual datasets were temporally concatenated, reduced via principal component analysis to 20 dimensions, and fed into the probabilistic ICA algorithm with a random initial value (12).

This procedure produced 20 group-level components for each TC-GICA run. Finally, 500 ( $20 \times 25$ ) group-level components were generated from the 25 TC-GICA runs.

**Generation of component templates for dual regression (meta-ICA).** To provide more accurate and robust ICA component templates, we carried out another low-dimensional (20 components) TC-GICA. Here we concatenated the 500 components produced by the 25 TC-GICA runs as the input data of a single-session ICA in MELODIC. The resultant maps were used as final component templates for the dual regression procedure. Of note, this method was selected as the primary approach over the alternative approach described because it guarantees the spatial independence of the 20 components, whereas the alternative approach does not.

**Generation of component templates for dual regression model (alternative approach).** To emphasize the robustness of the findings of the meta-ICA, here we describe an alternative approach that yields nearly identical components to the meta-ICA. The findings of the two approaches differed notably for only one of the 20 components, for which the meta-ICA finding was more plausible. Given the high degree of similarity between the two methods, we present only the findings from the meta-ICA in the present work. In the alternative approach, we used the hierarchical clustering algorithm implemented in the ICASSO toolbox (9). ICASSO was designed for validating the robustness of ICA with respect to random initial values (of the ICA mixing matrix) and the ICA cost function optimization search strategy. However, due to limitations in computational resources (e.g., 32 GB of memory in the present work), TC-GICA cannot be carried out on the full datasets. Thus, we used the bootstrapping approach described above with 25 ICA analyses, in which initial values and the specific participants selected from each center varied from one ICA analysis to the next. Here the 500 group-level components (20 components per run  $\times$  25 runs) were sorted using hierarchical clustering. The number of clusters (20) was selected to match the number of components. The similarity between components was measured by the combination of both spatial  $R_s$  and temporal  $R_t$  correlations in Eq. (1) and the distance between components as defined in Eq. (2) (13):

$$S(i,j) = \lambda^* R_s(i,j) + (1 - \lambda)^* R_t(i,j) \quad (1)$$

$$D(i,j) = \sqrt{1 - S(i,j)}, \quad 1 \leq i, j \leq 500 \quad (2)$$

Considering the spatial ICA,  $\lambda = 0.8$  was chosen in our clustering procedure. Finally, the median value at each voxel for each of the 20 clusters was calculated to determine the final component templates for the dual regression procedure.

**Individual component reconstruction via the dual regression model.** To reconstruct component maps for each participant, the recently developed dual regression procedure (11, 14) was applied to each of the 1,093 individual participants' datasets. Specifically, in the present work, dual regression consisted of two linear regressions carried out independently for each of the 20 component maps identified in temporal concatenation ICA. For each component template, the first regression model used the template as a spatial predictor for the participant's 4D data, producing a set of individual regression weights in the time domain (i.e., a time series for each spatial map). Using this time series as a temporal predictor for the 4D BOLD data, the second regression equation estimated the individual regression weights in the spatial domain (i.e., the participant-level individual spatial map). Both regressions used the same data set used for the seed-based con-

nnectivity approaches, that is, each participant's 4D dataset after removal of the nine nuisance covariates. Component time series were demeaned in both regressions, but no variance normalization was used. The dual regression procedure was carried out for all 1,093 participants included across 24 centers, not just those used for the generation of ICA-based templates. For each component, these individual spatial maps were then used to evaluate group-level statistics.

**Amplitude of spontaneous low-frequency fluctuations.** To examine the potentially meaningful information contained within the ALFF, two fast-Fourier transformation (FFT)-based indices, ALFF and fALFF, were used to compute the amplitude of low-frequency fluctuations in the frequency domain (2, 3, 15). For each individual, ALFF and fALFF were computed to identify those voxels with significantly detectable low-frequency fluctuation amplitudes. Specifically, at each voxel, ALFF is calculated as the sum of amplitudes within a specific low frequency range (0.01–0.1 Hz). fALFF is the normalized ALFF, calculated by dividing the ALFF value by the total sum of amplitudes across the entire frequency range measured in a given time series. Voxelwise ALFF and fALFF maps were calculated for each participant in native space, and then transformed into the MNI152 standard brain space with 3-mm isotropic voxel size. Before statistical analyses, each individual ALFF or fALFF map was Z-transformed (i.e., by subtracting the mean voxelwise ALFF or fALFF obtained for the individual's entire brain, and then dividing by the corresponding SD) to improve its suitability for group-level parametric analyses. The individual Z-transformed ALFF or fALFF maps were used in subsequent group- and center-level analyses.

**Unified group-level statistical model.** For all three types of R-fMRI measures (seed-based correlations, ICA, and ALFF/fALFF), a unified general linear model frame was developed for center-level statistical analyses. The unified statistical model is a one-way ANOVA, treating centers as the between factor. F-contrasts were used to measure the effect of centers. Overall group mean contrasts across all centers were modeled as well. Specifically, a one-factor 24-level ANOVA (factor: center; 1,093 participants), with age and sex as covariates, was used to examine the effects of age, sex, and center on the three R-fMRI measures. Multiple comparisons were corrected at the cluster level using Gaussian random field theory (min  $Z > 2.3$ ; cluster significance:  $P < 0.05$ , corrected).

## SI Results

**Center-Related Variability.** The results presented in Fig. 1 show that the effects ascribable to center can be either interpreted as negligible, as indicated by the high between-center Kendall's  $W$  (row 2), or substantial, accounting for much of the variance (row 3). These opposite interpretations are not mutually exclusive. The high between-center Kendall's  $W$  indicates that the resting-state measures (i.e., functional connectivity, fluctuation amplitude) obtained from different centers have a high degree of similarity. Nevertheless, systematic differences exist between centers, and these are easily quantified by ANOVA. In Fig. S5 for each center, the mean functional connectivity across 40 peak voxels derived from the center effect map for the PCC seed is depicted. As the figure shows, there are between-center differences in the height of the functional connectivity values. Some centers have overall higher functional connectivity values than others; these differences in the height of functional connectivity values drive the significant between-center effects. The variability in functional connectivity values could be related to a number of factors (e.g., the specific scanner used, scanner sequence, sample characteristics, specific instructions to participants, degree of variability in participant wakefulness). Because there was no previous coordination among centers regarding scanning parameters, each of these parameters could contribute to across-center differences. Specific examination of these factors is beyond the scope of the present work, but we anticipate that it will be

the focus of future studies. Fortunately, as demonstrated by our analyses, these sources of variation did not preclude us from being able to effectively pool data and carry out discovery-based analyses.

**Effect of Sample Size on the Relationship Between RSFC and Age.** We investigated the effect of sample size on the strength of the correlation between RSFC and age in two regions identified by our group analyses. For this purpose, we randomly sampled participants from the entire study sample using subgroups of 10–1,090 individuals (of the total 1,093 participants), then calculated the correlation be-

tween age and connectivity strength for each subgroup. We repeated this procedure 10,000 times to optimize randomization. Finally, we calculated the mean correlation and SD across the 10,000 iterations. As shown in Fig. S6, the variability in the observed correlation naturally decreased as a function of sample size, with a tipping point observed when samples exceeded ~100–200 participants. This suggests that results obtained with sample sizes that have been presumed to be sufficient (e.g., 50 participants) are likely to lead to false-negative results for small effects.

1. Cox RW (1996) AFNI: Software for analysis and visualization of functional magnetic resonance neuroimages. *Comput Biomed Res* 29:162–173.
2. Zang YF, et al. (2007) Altered baseline brain activity in children with ADHD revealed by resting-state functional MRI. *Brain Dev* 29:83–91.
3. Zou QH, et al. (2008) An improved approach to detection of amplitude of low-frequency fluctuation (ALFF) for resting-state fMRI: Fractional ALFF. *J Neurosci Methods* 172:137–141.
4. Jenkinson M, Smith S (2001) A global optimisation method for robust affine registration of brain images. *Med Image Anal* 5:143–156.
5. Jenkinson M, Bannister P, Brady M, Smith S (2002) Improved optimization for the robust and accurate linear registration and motion correction of brain images. *Neuroimage* 17:825–841.
6. Fox MD, et al. (2005) The human brain is intrinsically organized into dynamic, anticorrelated functional networks. *Proc Natl Acad Sci USA* 102:9673–9678.
7. Beckmann CF, DeLuca M, Devlin JT, Smith SM (2005) Investigations into resting-state connectivity using independent component analysis. *Philos Trans R Soc Lond B Biol Sci* 360:1001–1013.
8. Smith SM, et al. (2009) Correspondence of the brain's functional architecture during activation and rest. *Proc Natl Acad Sci USA* 106:13040–13045.
9. Himberg J, Hyvärinen A, Esposito F (2004) Validating the independent components of neuroimaging time series via clustering and visualization. *Neuroimage* 22:1214–1222.
10. Filippini N, et al. (2009) Distinct patterns of brain activity in young carriers of the APOE-epsilon4 allele. *Proc Natl Acad Sci USA* 106:7209–7214.
11. Calhoun VD, Pekar JJ, Pearson GD (2004) Alcohol intoxication effects on simulated driving: Exploring alcohol-dose effects on brain activation using functional MRI. *Neuropsychopharmacology* 29:2097–3017.
12. Beckmann CF, Smith SM (2004) Probabilistic independent component analysis for functional magnetic resonance imaging. *IEEE Trans Med Imaging* 23:137–152.
13. Esposito F, et al. (2005) Independent component analysis of fMRI group studies by self-organizing clustering. *Neuroimage* 25:193–205.
14. Filippini N, et al. (2009) Regional atrophy of transcallosal prefrontal connections in cognitively normal APOE epsilon4 carriers. *J Magn Reson Imaging* 29:1021–1026.
15. Biswal B, Yetkin FZ, Haughton VM, Hyde JS (1995) Functional connectivity in the motor cortex of resting human brain using echo-planar MRI. *Magn Reson Med* 34:537–541.

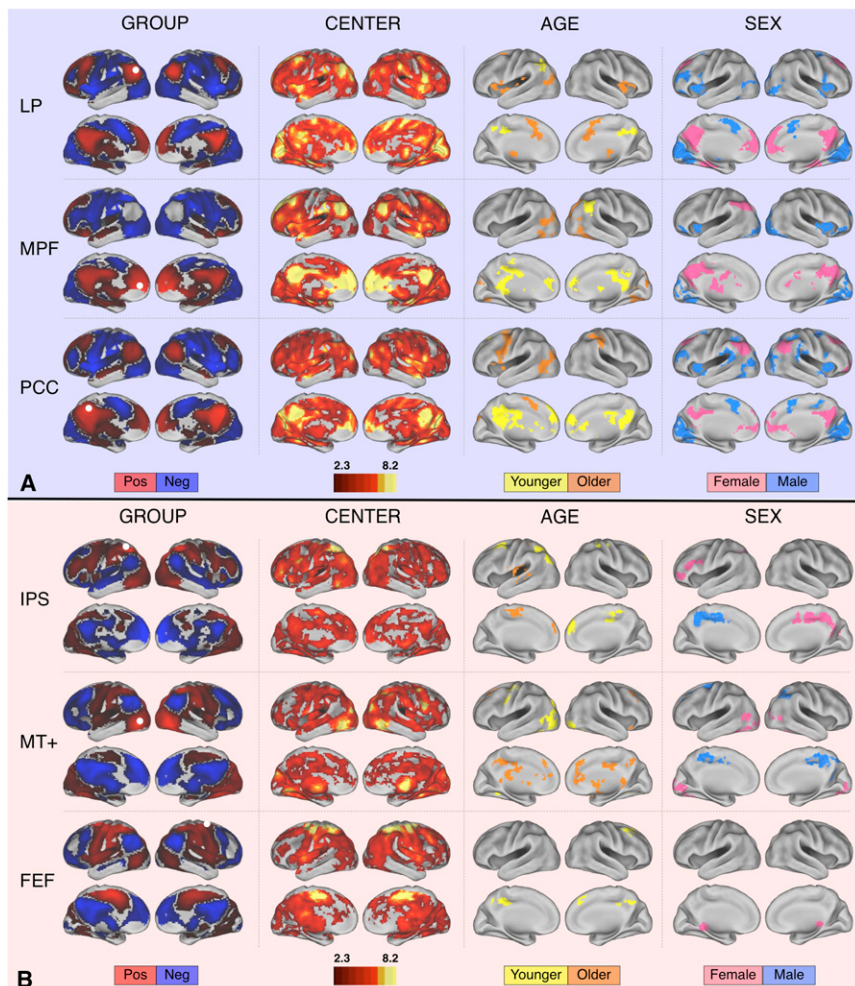


**Fig. S1.** Center-, age-, and sex-related variations detected in R-fMRI measures of functional connectivity using seed-based correlation analyses. The first column depicts group-level functional connectivity maps for three representative “default mode” seeds (*A*) and three “task-positive” network seeds (*B*). The seed ROIs are shown as white circles. The second column depicts voxels exhibiting significant effects of center, as detected by one-way ANOVA (across 24 centers, including 1,093 participants). Columns 3 and 4 depict voxels exhibiting age- and sex-related variations (modeled as covariates). Center, sex, and age findings were corrected for multiple comparisons ( $Z > 2.3$ ;  $P < 0.05$ , corrected). All supplementary cortical surface maps are arrayed as shown in Fig. 1, with lateral views in upper rows, medial views in lower rows, left hemisphere on the left, and right hemisphere on the right. “Male” refers to significantly greater connectivity in males; similarly, “female” refers to significantly greater connectivity in females. “Older” refers to significantly increasing connectivity with increasing age, whereas “younger” refers to significantly increasing connectivity with decreasing age. “Pos”, positive functional connectivity; “neg”, negative functional connectivity.

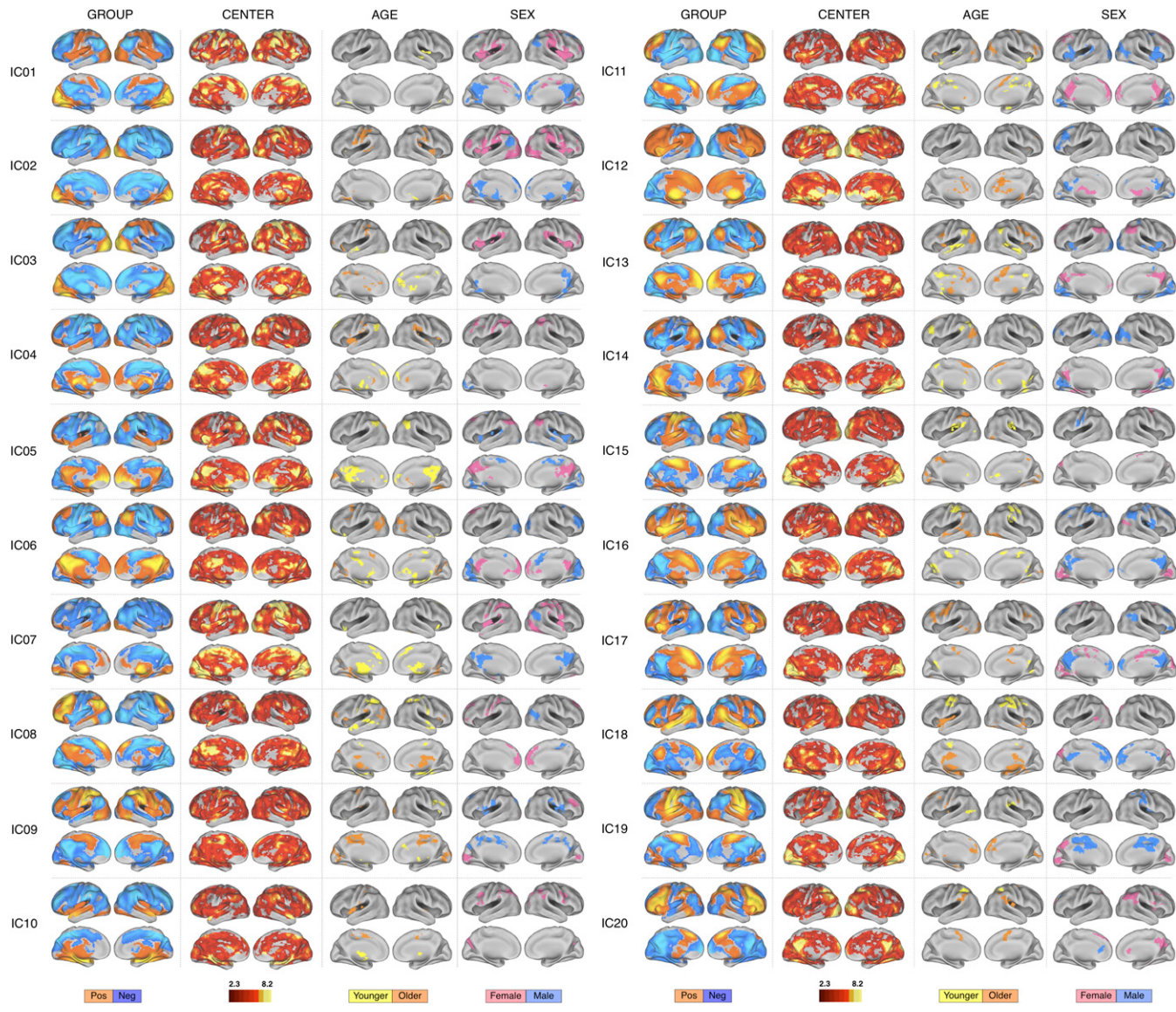


**Fig. S2.** Center-, age-, and sex-related differences detected in R-fMRI measures of functional connectivity combining independent component and dual regression analyses. The first column depicts group-level maps for 20 functional connectivity ICs. For each component, the second column depicts voxels exhibiting significant effects of center, as detected by one-way ANOVA (across 24 centers, including 1,093 participants). Columns 3 and 4 depict voxels exhibiting age- and sex-related variations. Center, age and sex findings were corrected for multiple comparisons ( $Z > 2.3$ ;  $P < 0.05$ , corrected). "Male" refers to significantly greater connectivity in males; similarly, "female" refers to significantly greater connectivity in females. "Older" refers to significantly increasing connectivity with increasing age, whereas "younger" refers to significantly increasing connectivity with decreasing age. "Pos," positive group effect; "neg," negative group effect.

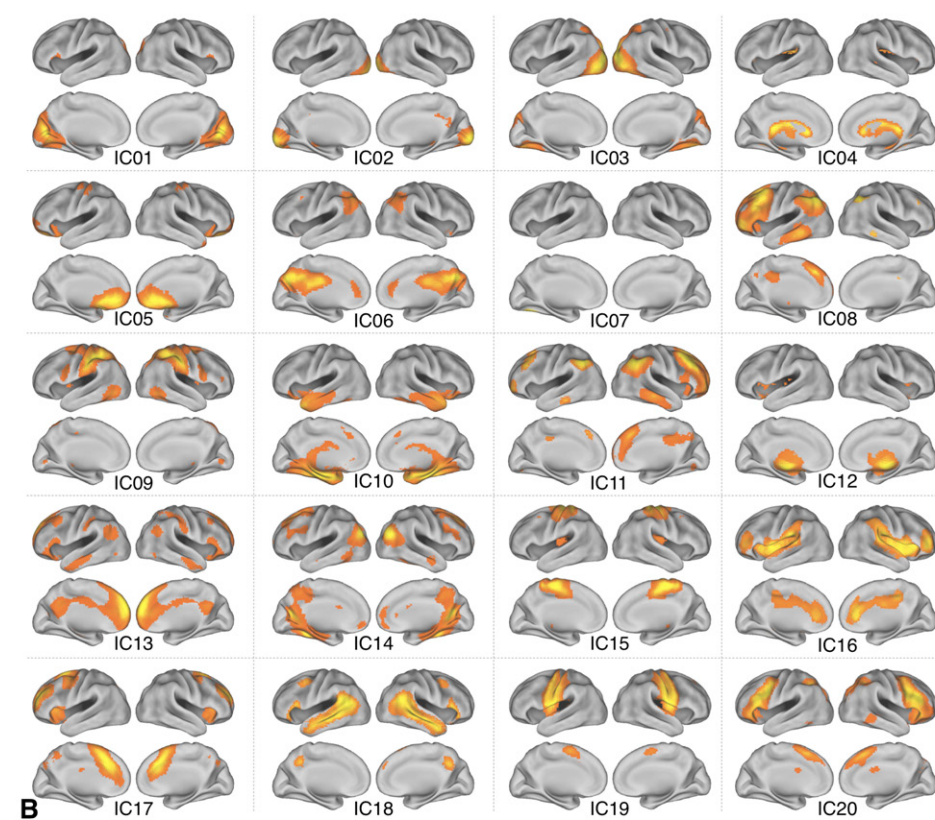
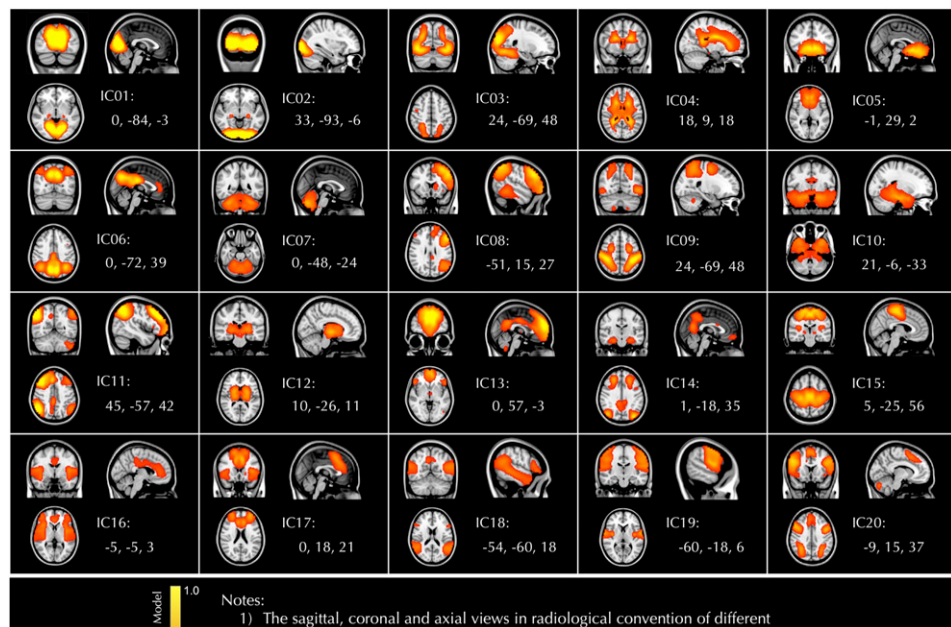


**Fig. S3.** IC templates used for dual regression analyses. Independent component maps resulting from the meta-ICA analysis shown on standard brain views (**A**) and surface maps (**B**). Component maps were thresholded at  $P > 0.05$  using spatial mixture modeling. Peak coordinates of each IC's activity are displayed in the lower right corner of each grid panel (MNI152 standard space).

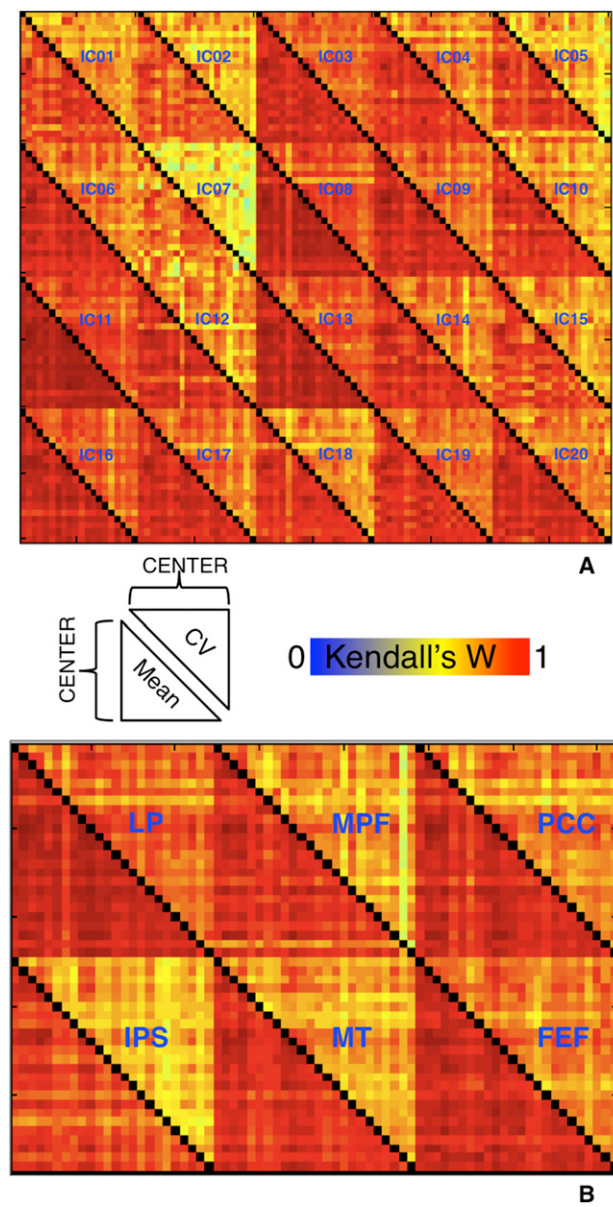


**Fig. S4.** Consistency of R-fMRI measures across centers: ICA combined with dual regression (*A*), and seed-based correlation (*B*). For each center, the voxelwise mean and coefficient of variation was calculated for each R-fMRI measure. The Kendall's *W* concordance of the mean or coefficient of variation maps between any two centers was calculated. The coefficient of variation is depicted above the diagonal, the mean below.

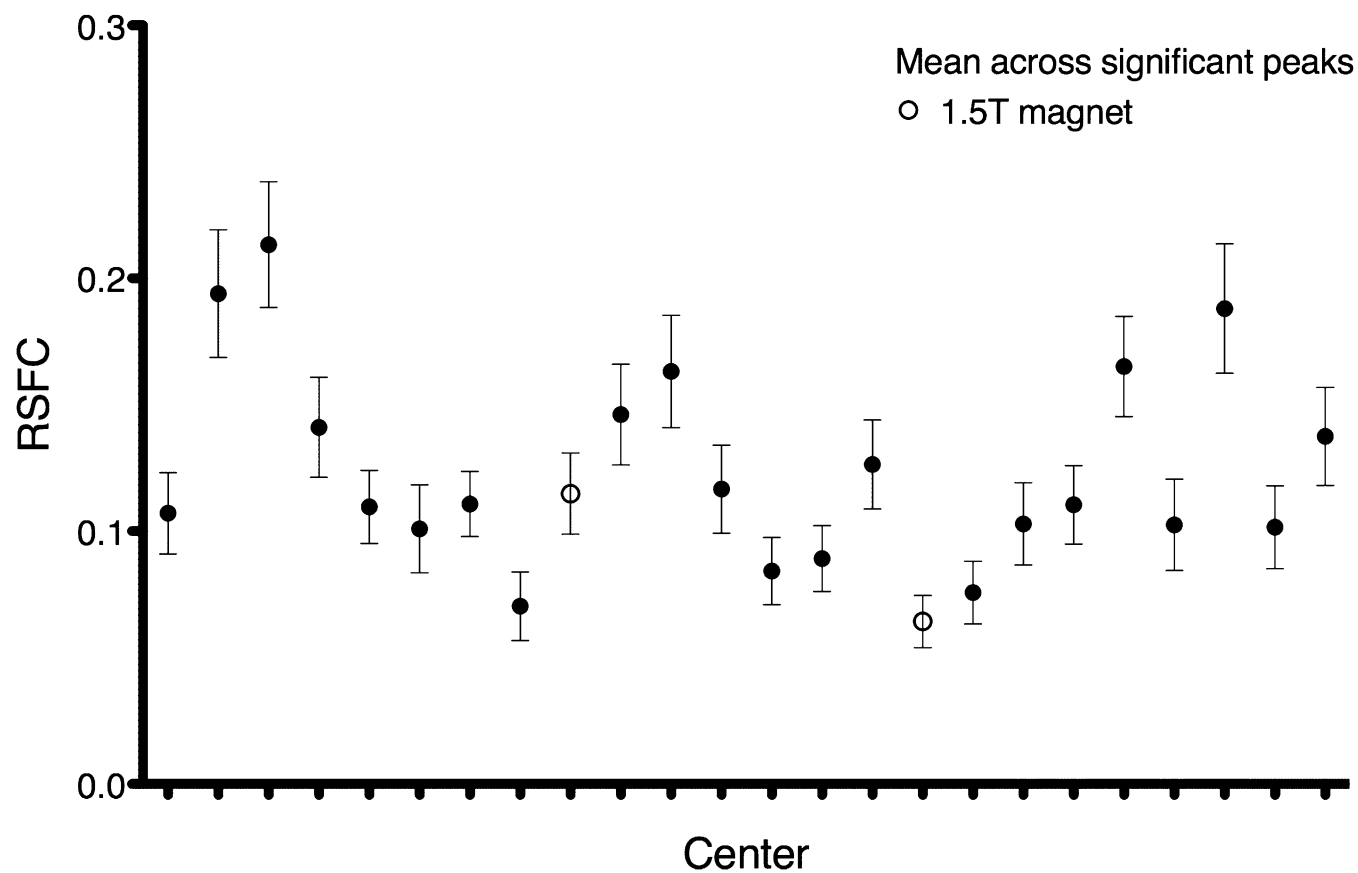


**Fig. S5.** Functional connectivity values observed at peak locations of between-center differences. For each center we calculated the mean across a 3 mm radius sphere centered at each of the 40 most significant voxels indexing the effect of center for the PCC seed ROI (Fig. 1, column 1, row 3). Connectivity values indexed the functional connectivity between the 3 mm radius sphere and the PCC seed ROI. All centers included in the analyses are shown ( $n = 24$ ). Although the strength of functional connectivity values observed across centers clearly varies, the within-center variability is relatively low. This indicates that the differences in functional connectivity strength among centers are relatively stable across the brain. A center that shows higher functional connectivity in one area of the brain compared with another center most likely also shows higher functional connectivity in other areas of the brain.

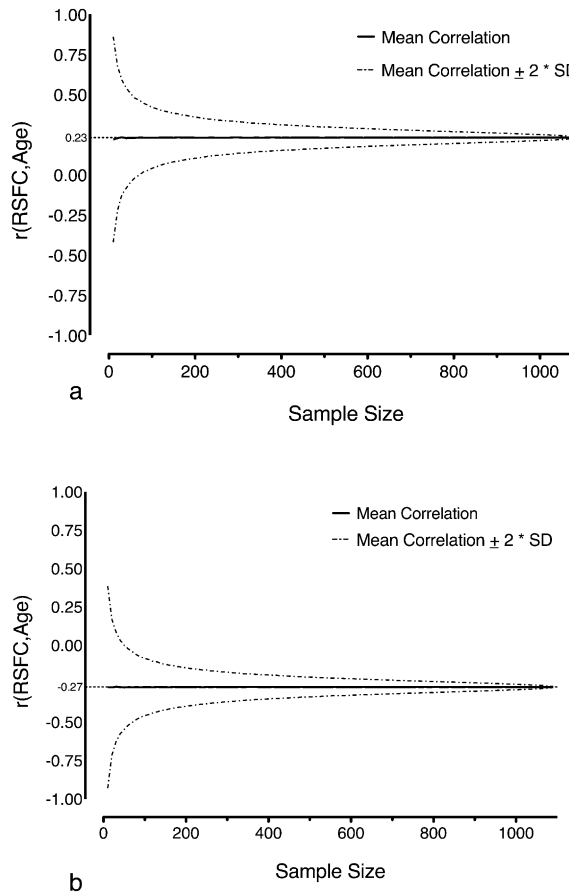


**Fig. S6.** Effect of sample size on the correlation between age and RSFC. Shown is the mean correlation  $\pm 2$  SD across 10,000 calculations of the correlation between age and functional connectivity strength as a function of sample size. For each of the two regions illustrating the effect of age for the PCC seed ROI in Fig. 2, we calculated the correlation between age and RSFC as a function of sample size. We randomly sampled subgroups, ranging in size from 10 to 1,090 participants, from the total of 1,093 participants. We then calculated the correlation between age and RSFC for each of the subgroups. This procedure was iterated 10,000 times to optimize randomization. (A) Mean correlation  $\pm 2$  times the SD across 10,000 iterations for the region illustrated in Fig. 2 that showed a positive correlation between age and RSFC with the PCC seed. (B) Mean correlation  $\pm 2$  times the SD across the 10,000 iterations for the region illustrated in Fig. 2 that showed a negative correlation between age and RSFC with the PCC seed. In each figure, the actually observed correlation is indicated on the y-axis in a smaller font.

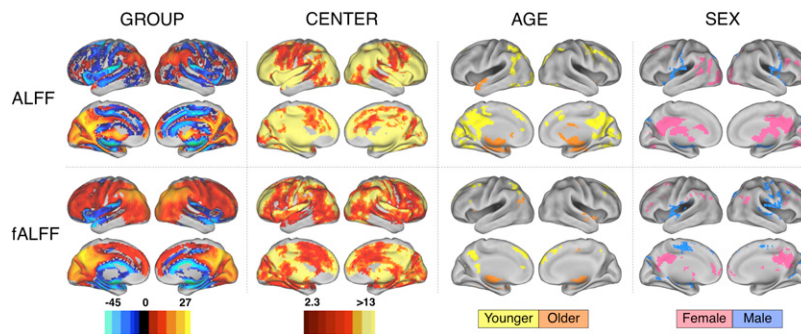


**Fig. S7.** Center-, age-, and sex-related variations in R-fMRI amplitude measures. The first column depicts group-level maps for voxelwise measures of ALFF (Upper) and fALFF (Lower). Before group-level analyses, each participant's ALFF/fALFF map is Z-transformed, such that positive voxels reflect greater low-frequency fluctuation amplitudes than baseline (whole brain mean) and negative voxels reflect low-frequency fluctuation amplitudes below baseline. The second column depicts voxels exhibiting significant effects of center, as detected by one-way ANOVA (across 24 centers, including 1,093 participants). Columns 3 and 4 depict voxels exhibiting age- and sex-related variations. Center, age, and sex findings were corrected for multiple comparisons ( $Z > 2.3$ ;  $P < 0.05$ , corrected). "Male" refers to significantly greater connectivity in males; similarly, "female" refers to significantly greater connectivity in females. "Older" refers to significantly increasing connectivity with increasing age, whereas "younger" refers to significantly increasing connectivity with decreasing age.

**Table S1.** Data currently included in the 1,000 Functional Connectomes Project

Center	PI	N	n*	Age	Age range	Male sex
				years, mean (SD)	years	%
1. Baltimore, MD	J. J. Pekar/S. H. Mostofsky	23		29.26 (5.46)	20–40	35%
2. Bangor, UK	S. Colcombe	20		23.4 (5.32)	19–38	100%
3. Beijing, China	YF. Zang	198	193	21.16 (1.83)	18–26	39%
4. Beijing, China	XC. Weng	28	27	20.41 (1.39)	18–24	27%
5. Berlin, Germany	D. Margulies	26		29.77 (5.21)	23–44	50%
6. Bethesda, MD	M. Ernst	18		33.00 (13.31)	18–53	22%
7. Cambridge, MA	R. L. Buckner	198		21.03 (2.31)	18–30	38%
8. Cambridge, MA	S. Whitfield-Gabrieli	39	35	25.09 (3.53)	20–32	49%
9. Cleveland, OH	M. J. Lowe	31		43.55 (11.14)	24–60	35%
10. Dallas, TX	B. Rypma	24		42.63 (20.07)	20–71	50%
11. Hvidovre, Denmark	A.-M. Dogonowski/K. Madsen	28		41.75 (10.7)	21–68	50%
12. Leiden, The Netherlands	S. A. R. B. Rombouts	31		22.19 (2.57)	18–28	74%
13. Leipzig, Germany	A. Villringer	37		26.22 (5)	20–42	43%
14. Magdeburg, Germany	M. Walter	29	28	30.43 (5.71)	22–43	93%
15. Milwaukee, WI	SJ. Li	64		53.59 (5.79)	44–65	64%
16. New Haven, CT	M. Hampson	19	18	31.61 (10.27)	18–48	56%
17. New York, NY <sup>†</sup>	M. Milham/F. X. Castellanos	59		32.78 (8.83)	20–49	68%
18. New York, NY <sup>†</sup>	M. Milham/F. X. Castellanos	20		29.75 (9.94)	18–46	40%
19. Newark, NJ	B. B. Biswal	19		24.11 (3.91)	21–39	47%
20. Orangeburg, NY <sup>‡</sup>	M. J. Hoptman	21	20	40.65 (11.03)	20–55	75%
21. Oulu, Finland <sup>‡</sup>	V. J. Kiviniemi/J. Veijola	103		21.52 (0.57)	20–23	36%
22. Oxford, UK	S. M. Smith/C. Mackay	22		29 (3.79)	20–35	55%
23. Queensland, Australia	K. McMahon	19	18	26.28 (3.71)	20–34	61%
24. St. Louis, MO	B. L. Schlaggar/S. E. Petersen	31		25.1 (2.31)	21–29	45%

Data from the following centers will be included in the 1000 Functional Connectomes data release but are not included in the current analyses: Ann Arbor, MI: C. S. Monk/R. D. Seidler/S. J. Peltier; Atlanta, GA: H. S. Mayberg; Berlin, Germany: S. Schmidt; Durham, NC: D. J. Madden; Durham, NC: L. Wang; London, Ontario, Canada: P. Williamson; Munich, Germany, C. Sorg/V. Riedl; Nanjing, China: G.J. Teng/H.Y. Zhang; Pittsburgh, PA: G.J. Siegle; Portland, OR: D. Fair/B. J. Nagel; Taipei, Taiwan: C.P. Lin; Vienna, Austria: C. Windischberger.

\*Actual number of participants included in the analysis, if different from N.

<sup>†</sup>Data from the same magnet, different sequence.

<sup>‡</sup>1.5-T magnet.

Funding sources for each contributor (numbered by site): 1: R01 MH085328, R01 MH078160, HD-24061 (Intellectual Disabilities Research Center), M01 RR00052 (Johns Hopkins General Clinical Research Center) and P41 RR15241 (National Center for Research Resources); 3: NSFC (No.30621130074); 4: Chinese Ministry of Science and Technology (No. 2007CB512300); 5: Berlin School of Mind and Brain (DFG); 7: Howard Hughes Medical Institute; 9: National Multiple Sclerosis Society; 13: Competence Net Stroke (BMBF) and Berlin School of Mind and Brain (DFG); 17-18: NIDA (R01DA016979), NIMH (R01MH083246), Stavros Niarchos Foundation; 19: NINDS (R01NS049176); 20: R01 MH064783, R21 MH084031, R01 MH0663674; 21: Academy of Finland (Grant codes 124257, 212181, 214273); 23: Australian Research Council (ARC) Discovery grant (DP0452264); 24: NIH NS053425; Atlanta, G.A.: H.S. Mayberg: URC Grant, Emory University; Durham, NC: D.J. Madden: NIH/NIA R01 AG011622; Durham, NC: L. Wang: Paul B. Beeson Career Developmental Awards (K23-AG028982); Portland, OR: D. Fair/B. Nagel: Oregon Clinical and Translational Research Institute, Medical Research Foundation, UNCF-Merck, Ford Foundation, Dana Foundation; Taipei, Taiwan: C-P. Lin: National Health Research Institute grant (NHRI-EX98-9813EC), Taiwan; Vienna, Austria: C. Windischberger: OeNB-P11468 and OeNB-P12982.

## 8 Paper 2: Repeated pain induces adaptations of intrinsic brain activity to reflect past and predict future pain (Neuroimage 2011)

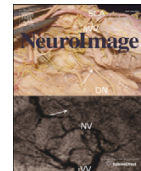
[NeuroImage 57 \(2011\) 206–213](#)



Contents lists available at [ScienceDirect](#)

**NeuroImage**

journal homepage: [www.elsevier.com/locate/ynimng](http://www.elsevier.com/locate/ynimng)



### Repeated pain induces adaptations of intrinsic brain activity to reflect past and predict future pain

Valentin Riedl <sup>a,c,\*</sup>, Michael Valet <sup>a</sup>, Andreas Wöller <sup>b</sup>, Christian Sorg <sup>b</sup>, Dominik Vogel <sup>a</sup>, Till Sprenger <sup>d</sup>, Henning Boecker <sup>e</sup>, Afra M. Wohlschläger <sup>c</sup>, Thomas R. Tölle <sup>a</sup>

<sup>a</sup> Department of Neurology, Klinikum rechts der Isar, Technische Universität München, Ismaningerstrasse 22, 81675 Munich, Germany

<sup>b</sup> Department of Psychiatry, Klinikum rechts der Isar, Technische Universität München, Ismaningerstrasse 22, 81675 Munich, Germany

<sup>c</sup> Department of Neuroradiology, Klinikum rechts der Isar, Technische Universität München, Ismaningerstrasse 22, 81675 Munich, Germany

<sup>d</sup> Department of Neurology and Division of Neuroradiology, University Hospital Basel, Petersgraben 4, 4031 Basel, Switzerland

<sup>e</sup> Functional Neuroimaging Group, Department of Radiology, Rheinische Friedrich-Wilhelms-Universität Bonn, Sigmund-Freud-Strasse 25, 53127 Bonn, Germany

#### ARTICLE INFO

##### Article history:

Received 15 November 2010

Revised 23 March 2011

Accepted 5 April 2011

Available online 13 April 2011

##### Keywords:

Intrinsic connectivity network  
Pain  
Resting state  
Plasticity  
Intrinsic brain activity  
Learning  
Prediction  
Memory

#### ABSTRACT

Recent neuroimaging studies have revealed a persistent architecture of intrinsic connectivity networks (ICNs) in the signal of functional magnetic resonance imaging (fMRI) of humans and other species. ICNs are characterized by coherent ongoing activity between distributed brain regions during rest, in the absence of externally oriented behavior. While these networks strongly reflect anatomical connections, the relevance of ICN activity for human behavior remains unclear. Here, we investigated whether intrinsic brain activity adapts to repeated pain and encodes an individual's experience. Healthy subjects received a short episode of heat pain on 11 consecutive days. Across this period, subjects either habituated or sensitized to the painful stimulation. This adaptation was reflected in plasticity of a sensorimotor ICN (SMN) comprising pain related brain regions: coherent intrinsic activity of the somatosensory cortex retrospectively mirrored pain perception; on day 11, intrinsic activity of the prefrontal cortex was additionally synchronized with the SMN and predicted whether an individual would experience more or less pain during upcoming stimulation. Other ICNs of the intrinsic architecture remained unchanged. Due to the ubiquitous occurrence of ICNs in several species, we suggest intrinsic brain activity as an integrative mechanism reflecting accumulated experiences.

© 2011 Elsevier Inc. All rights reserved.

#### Introduction

Traditionally, functional magnetic resonance imaging (fMRI) studies have investigated changes of brain activity in response to sensory, motor or cognitive tasks that subjects performed in the MR scanner. Only recently, colleagues have revealed networks of distributed brain regions that are characterized by coherent ongoing activity in subjects at rest, in the absence of any observable behavior (Biswal et al., 1995; Greicius et al., 2003; Laufs et al., 2003; Damoiseaux et al., 2006; Fox and Raichle, 2007). These resting-state or intrinsic connectivity networks (ICNs) strongly resemble previously described task-activation patterns (Smith et al., 2009). However, the relevance of ICNs for human behavior remains a controversial issue.

ICNs transcend levels of consciousness and consistently occur in humans, monkeys and rats (Lu et al., 2007; Vincent et al., 2007; Greicius et al., 2008; Larson-Prior et al., 2009; Biswal et al., 2010). The ubiquity and robustness of the intrinsic functional architecture strongly supports the notion of ICNs reflecting underlying structural connectivity (Fox and Raichle, 2007; Hagmann et al., 2008; Honey et al., 2009). But there have also been reports of immediate variations in the coherence of ICNs associated with task performance of humans (Fox et al., 2007; Seely et al., 2007; Albert et al., 2009; Lewis et al., 2009). We therefore hypothesize that at least portions of ICN activity continuously adapt with ongoing experiences and that intrinsic brain activity reflects past and anticipates future experiences.

In this study, we focused on repeated pain experiences and their relation to ICN activity before and after pain. More concretely, we asked whether recurring pain modulates functional connectivity (FC) within pain-relevant ICNs in a way that reflects recent pain and enables the prediction of future pain experiences. FC is a measure to quantify the strength of covarying activity between distributed voxels or brain regions. We derived ICNs by applying Independent Component Analysis (ICA) to resting state fMRI (rs-fMRI) data. Acute pain is

\* Corresponding author at: Dept. of Neurology, Klinikum Rechts der Isar der Technischen Universität München, Ismaningerstrasse 22, 81675 München, Germany.  
Fax: +49 89 4140 7665.

E-mail address: valentin.riedl@mytum.de (V. Riedl).

consistently associated with neuronal activity in a distinct network of subcortical and cortical brain regions (Apkarian et al., 2005; Tracey and Mantyh, 2007). Among these, somatosensory cortices (SSC) process sensory aspects of pain, while the ventromedial prefrontal cortex (vmPFC) has been associated with its modulation (Koyama et al., 2005; Seymour et al., 2005). Despite our knowledge about activating these brain regions by acute pain, less is known about their role in encoding past and future pain. Yet, understanding how the brain processes pain beyond an immediate experience might help to explain the development of chronic pain conditions.

## Materials and methods

### Participants

Thirteen healthy male volunteers without any history of neurological, psychiatric or pain disease participated in this study. All participants received detailed information about the experimental procedures, were free to withdraw from the study at any time, and gave written informed consent. The Ethics Committee of the university hospital "Klinikum Rechts der Isar" (Technische Universität Muenchen) approved the protocols of the study. The data of an additional group of 16 healthy subjects that were scanned on the same scanner twice within a 14-day interval while participating in another study of our department were re-examined as a control group (Sorg et al., 2007).

### Experimental design

Volunteers received a daily series of 8 painful and 8 non-painful alternating heat stimuli (40 s each, followed by 20 s baseline) on 11 consecutive working days. On the first and last day of the study we acquired resting-state functional MRI (rs-fMRI) data during 6 min before (PREpain) and after (POSTpain) painful stimulation. At the beginning of each fMRI session we collected an anxiety score (5-point Likert scale) from each subject in order to control for an overall level of arousal or anxiety to the study. The thermal stimulation protocol has previously been implemented in our group and described in detail (Valet et al., 2004). On the first day the pain threshold was assessed for each subject individually. Painful stimuli (1 °C above the pain threshold) were then applied via a thermode to the inner side of the right forearm in an undulating way and to one of three possible positions on the forearm to prevent skin sensitization. For each subject the stimulation temperature was kept constant during the 11 days of painful stimulation and the absolute temperature only varied slightly within the group (median:  $44.0 \pm 1$  °C). After the stimulation period the volunteers rated the perceived pain intensity (PAIN) on an 11-point numerical rating scale (NRS). Differences in PAIN-ratings between days 1 and 11 were tested nonparametrically using the Wilcoxon signed-rank test ( $p < 0.05$ ).

### Imaging data

We collected functional neuroimaging data on a 1.5 Tesla Siemens Symphony magnetic resonance system (Erlangen, Germany) using a gradient-echo EPI sequence (TE = 50 ms, TR = 3000 ms, flip angle = 90°, FoV = 230 mm<sup>2</sup>, matrix = 64 × 64, 28 slices, slice thickness = 5 mm). Subjects were instructed to think of nothing particular and keep their eyes closed. Each rs-fMRI run comprised 117 functional volumes (~ 6 min) of which the first 3 volumes were discarded due to T1 saturation effects. Structural MRI data (TE = 3.93 ms, TR = 1500 ms, TI = 760 ms, flip angle = 5°, FoV = 256 mm<sup>2</sup>, matrix = 256 × 256, 160 slices, voxel size = 1 × 1 × 1 mm<sup>3</sup>) were acquired at the end of each session.

### Processing of imaging data

Data preprocessing and ICA were performed as previously applied to rs-fMRI data in our group (Sorg et al., 2007).

### Preprocessing

Functional MRI data were pre-processed using the SPM software package (SPM5, Wellcome Department of Cognitive Neurology, London) and in-house code for Matlab 7.1 (MathWorks, Natick, MA). Data were motion corrected, spatially normalized into the stereotactic space of the Montreal Neurological Institute (MNI) and spatially smoothed with an 8x8x8 mm Gaussian kernel. Before the volumes were entered into the ICA analysis we applied a voxel-wise z-transformation on the time-course data  $y_{ijk}(t)$  by subtracting the mean  $\langle y_{ijk} \rangle$  and dividing by the standard deviation  $\sigma_{ijk}$ :  $\hat{y}_{ijk}(t) = (y_{ijk}(t) - \langle y_{ijk} \rangle) / \sigma_{ijk}$  ( $t$  being the time, indices  $i, j, k$  represent the three directions in space). The sensitivity of the multivariate ICA algorithm for correlation of variance between voxels, i.e. functional connectivity, was thereby rendered independent of the original BOLD signal magnitude across subjects.

### ICA

We used the Group ICA toolbox (GIFT 1.3d; icatb.sourceforge.net) established for independent component analyses of fMRI data (Calhoun et al., 2001, 2009, 2004). The toolbox performed the analysis in four stages on a concatenated data set comprising the 4 rs-fMRI runs of all subjects: first the GIFT dimensionality tool estimated 18 independent components (IC) based upon the MDL criteria (Li et al., 2007). The aggregated data set was then reduced using principal component analysis (PCA) before the Infomax ICA algorithm (Bell and Sejnowski, 1995) calculated the ICs. For each individual GIFT finally reconstructed independent spatial maps of each rs-fMRI run (Calhoun et al., 2001) converted to z-scores. Hence individual maps are normalized with respect to variance in the component timecourse and the between-subject analyses are then performed on the maps of spatial weights (REF calhoun 2004). From the group spatial maps, we selected functionally relevant ICNs in a fully automated manner. On the basis of previous descriptions of brain regions covered by each ICN (Brodmann areas in Damoiseaux et al., 2008; Sorg et al., 2007), we created spatial templates representing each ICN using the marsbar toolbox (<http://marsbar.sourceforge.net/>). We then calculated the spatial regression of these templates against the ICA-derived maps as implemented in the GIFT toolbox and selected the best-fit ICNs from our analysis. From this set of ICNs we selected those networks that covered at least one brain region previously described in task-activation studies of pain processing in humans (Bingel et al., 2007; Gundel et al., 2008): primary and secondary somatosensory cortices, medial and lateral prefrontal cortices, insula, cingulate cortex and thalamus; see Table S2 for peak coordinates. Before we entered the individual's spatial maps into second-level statistics we reintegrated the initially calculated scaling factor  $\sigma_{ijk}$  into the data by voxel-wise multiplication in order to preserve each individual's profile of variance magnitude while leaving the normalized timecourse component unchanged (Sorg et al., 2007).

### Second-level statistics

Group analyses were performed on the back-reconstructed spatial maps of all 13 subjects using SPM5 (Wellcome Trust Centre for Neuroimaging, UCL, London). We first evaluated the consistency of each ICN across sessions by calculating a repeated-measures ANOVA on the spatial maps of all 4 runs that we projected on a mean anatomical image of all subjects ( $p < 0.05$ , FDR-corrected)(see Fig. S1). We then tested the five ICNs comprising pain related brain regions (maps B, C, F, G, J/K of Fig. S1) for plastic changes in response to the 11 days of repeated pain and entered the four spatial maps of each subject into within-subject ANOVAs (factors "subject," "session PRE/

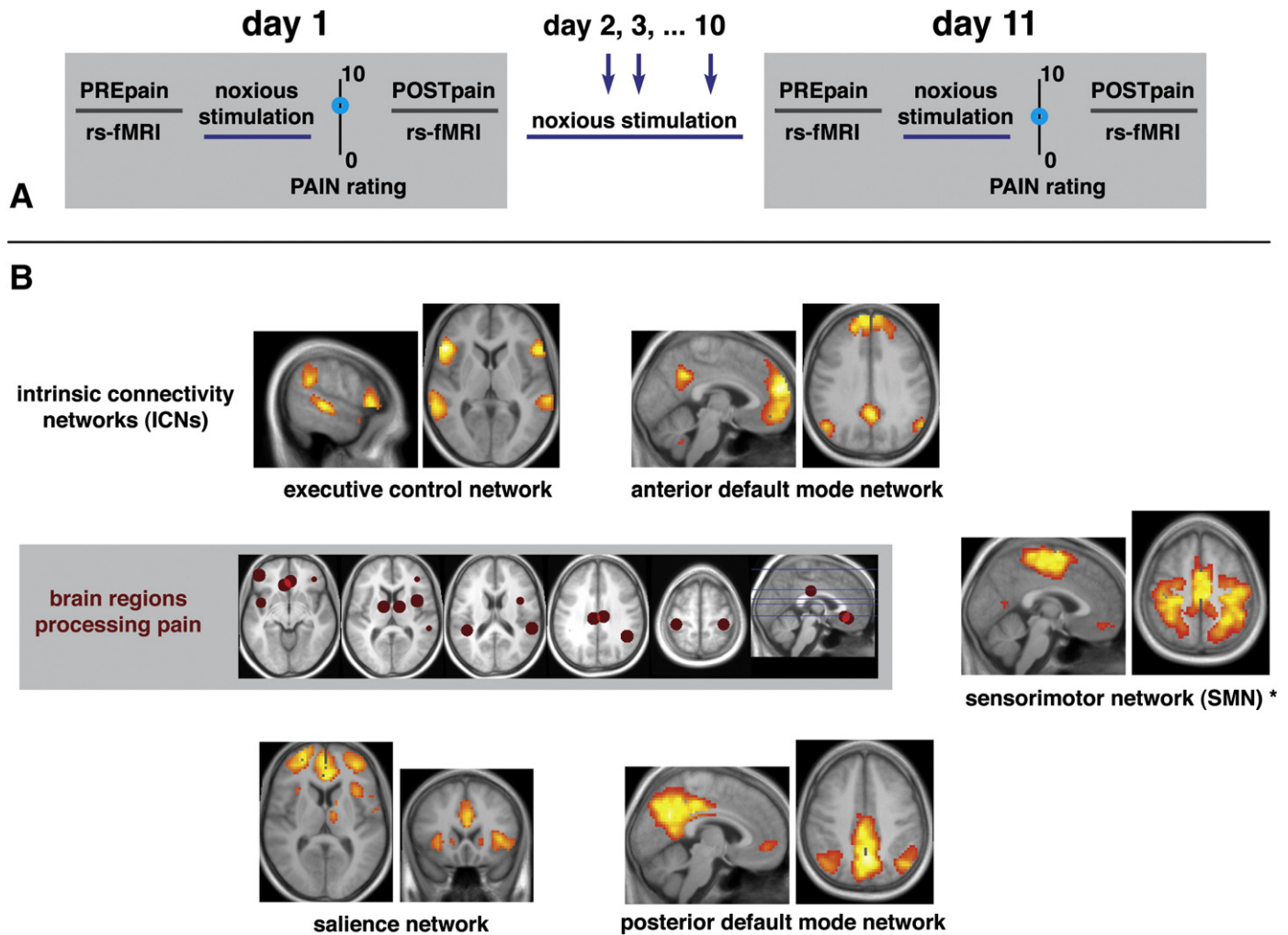


**Fig. 1.** Study design and brain network analysis. (A) Healthy volunteers received a short episode of noxious heat stimuli to their right forearm on 11 consecutive days and subsequently rated the perceived pain intensity (PAIN) on a numerical rating scale (0–10). Before (PREpain) and after (POSTpain) stimulation on the initial and last day of the study, we measured intrinsic brain activity in subjects at rest with resting-state functional magnetic resonance imaging (rs-fMRI). (B) Intrinsic connectivity networks (ICNs) covering brain regions known to process pain. We extracted ICNs representing the functional connectivity (FC) between brain regions with independent component analysis (ICA). We then tested ICNs including brain regions known to process pain for short-term (within day) and long-term (across 11 days) changes in response to the repeated pain. \*Only the sensorimotor ICN (SMN) revealed changes of coherent intrinsic activity during rest in response to repeated pain (see Fig. 2).

POST,"“day 1/11”). The resulting SPMs were masked with the average effect of conditions and FDR-corrected on the voxel level ( $p<0.05$ ).

#### Regression analysis of behavioral and network scores

For the regression analyses of behavioral and functional imaging data we used each individual's PAIN rating and FC scores representing a brain region's participation in an ICN. For each individual we calculated the FC-score as the mean z-score of all voxels within a regions-of-interest (ROI) from the ICA-derived spatial map. The coordinates for a combined SSC/PPC and a vmPFC ROI ( $r=10$  mm) were taken from two independent fMRI studies on pain processing (Bingel et al., 2007; Gundel et al., 2008) listed in Table S2. In case multiple clusters have been reported for a region, those coordinates were chosen that maximally covered grey matter in our dataset as validated with the grey matter segmentation masks from SPM5. On day 11, behavioral and neuroimaging data strongly depend on the subject's initial experience of the noxious stimulation. All scores on day 11 are therefore referenced to the status of day 1 and calculated as

$\Delta$ NRS ( $NRS_{day11} - NRS_{day1}$ ) for PAIN and  $\Delta$ z-score ( $z_{day11} - z_{day1}$ ) for FC. The correlations were tested for significance using nonparametric Spearman's rho measure ( $p<0.05$ ) and FDR-corrected for the 8 correlations tested.

#### Results

Healthy volunteers received a short episode of noxious heat stimulation to their right forearm and subsequently rated the perceived pain intensity. We repeated this procedure on 11 consecutive days and recorded 6 min of rs-fMRI before (PREpain) and after (POSTpain) painful stimulation on the initial and last day of the study (Fig. 1A).

#### Long-term adaptations of behavior and functional connectivity to repeated pain

We observed long-term adaptations to 11 days of experimentally induced pain both in behavioral and functional imaging data. Following each stimulation period, subjects rated the level of

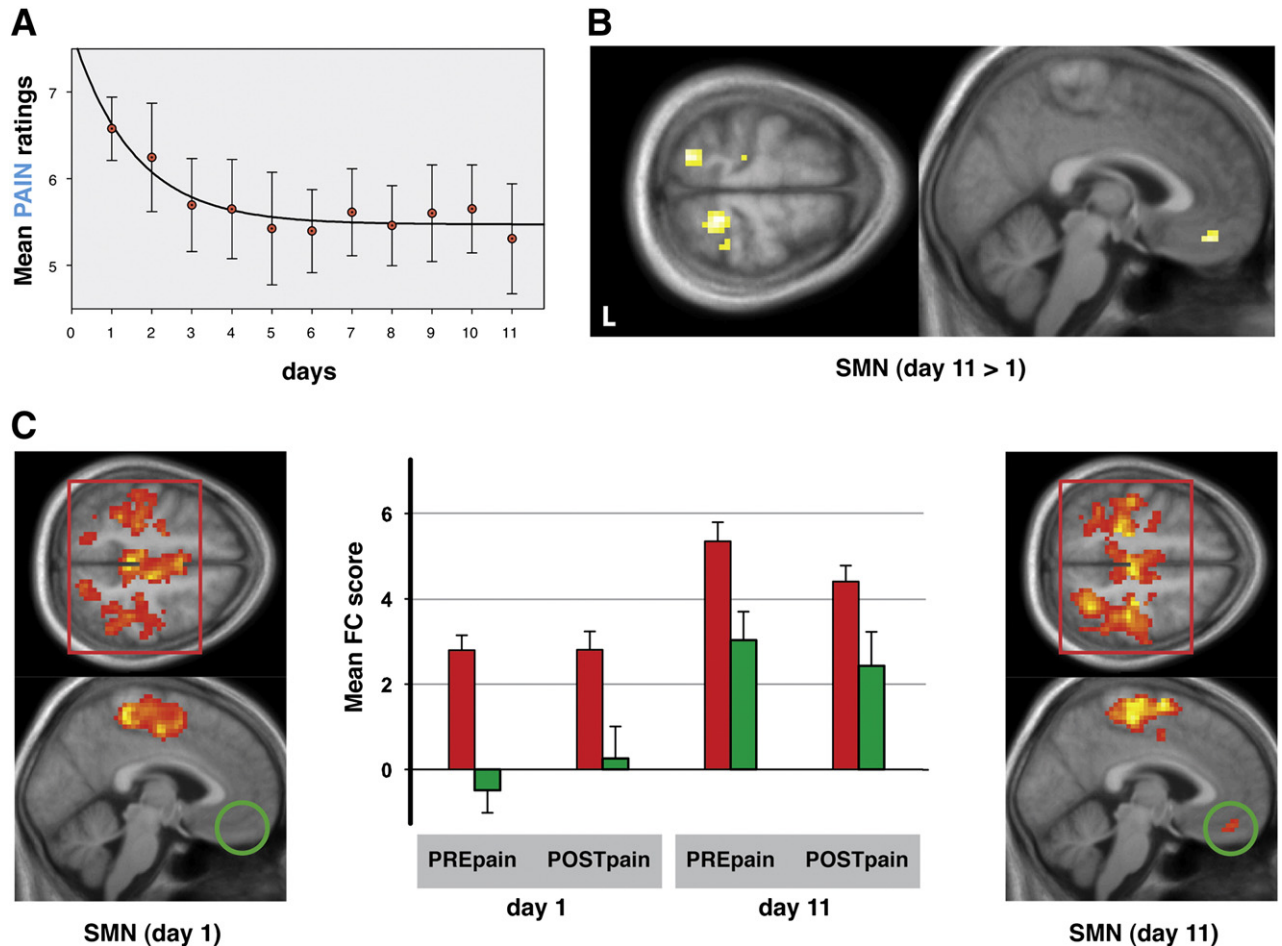


**Fig. 2.** Long-term adaptations of behavior and intrinsic SMN activity to repeated pain. (A) Mean PAIN ratings across 11 days of noxious stimulation with significantly lower PAIN between days 1 and 11 ( $p=0.012$ , two-tailed Wilcoxon test,  $n=13$ ). Error bars indicate standard error of mean. (B) Network plasticity in the SMN after 11 days of noxious stimulation. The statistical parametric map (SPM) shows brain regions with increased FC in the SMN at the group level rendered on a mean anatomical image of all subjects ( $p<0.05$ , FDR-corrected,  $z_{\max}=4.20$ ). The analysis revealed significantly higher FC in bilateral somatosensory (SSC), left posterior parietal (PPC) and ventromedial prefrontal (vmPFC) cortices. Peak-voxel coordinates in MNI space [x y z]: SSC left/right (BA 2,3) [ $-21 -30 66$ ]/[ $36 -30 57$ ], PPC left (BA 5) [ $-18 -60 66$ ], [ $-27 -51 69$ ], vmPFC (BA 11/12) [ $0 42 -18$ ]. BA, Brodmann area. (C) The SMN on day 1 (left) and day 11 (right). Conjunction maps are overlaid on a mean anatomical image of all subjects ( $p<0.05$ , FDR-corrected,  $z_{\max}=7.90$ ). Additionally, average FC-scores of the two SPM clusters (red: medial and lateral parts of SSC/PPC, green: vmPFC cluster) are plotted for illustration purposes. The FC-score encodes the participation of a brain region within an ICN and was calculated as the mean z-score of all voxels within this cluster. Error bars indicate standard error of mean.

perceived pain intensity. Fig. 2A shows the exponential decay of experienced pain over 11 days (averaged data of all 13 volunteers) resulting in significantly lower PAIN ratings between days 1 and 11 ( $p=0.012$ ), a finding supported by previous reports (Bingel et al., 2007). From the imaging data, we identified five ICNs covering brain regions known for pain processing (Fig. 1B and Table S2) by applying network-sensitive group-ICA to a concatenated data set of the 4 rs-fMRI runs of all subjects (Fig. S1) (Albert et al., 2009; Calhoun et al., 2009; Beckmann et al., 2005; Damoiseaux et al., 2006; Greicius, 2008; Sorg et al., 2007). We then tested these ICNs in SPM for FC changes in response to the painful stimulation. The within-subject ANOVA revealed long-term plasticity in two pain related brain regions of the sensorimotor ICN (SMN) (Fig. 2B,  $p<0.05$  FDR-corrected): after 11 days of painful stimulation, coherent intrinsic activity significantly increased between bilateral somatosensory (SSC)/posterior parietal (PPC) cortices. Additionally, the ventromedial prefrontal cortex (vmPFC) was recruited into the SMN by coherent activity (Fig. 2B, C right). Initially, the SMN encompasses somatosensory, posterior parietal and motor cortices (Fig. 2C left). Tests for “within-day” and interaction effects in the ANOVA revealed no significance in the SPM at  $p<0.01$  uncorrected at the voxel level ( $k>10$  voxel/mm $^3$ ).

The vmPFC has been described in several different ICNs of resting state fMRI analyses (Baliki et al., 2008; Damoiseaux et al., 2006; Dhond et al., 2008; Seeley et al., 2007; Smith et al., 2009; Sorg et al., 2007). It is therefore crucial to distinguish an additional recruitment of a brain region into an ICN from a simple shift of connectivity for this brain region from one ICN into another. The latter can be ruled out from our data, as we found no significant short- and long-term adaptations ( $p<0.01$  uncorrected at the voxel level;  $k>10$  voxel/mm $^3$ ) in other ICNs that covered the vmPFC. Therefore, FC changes after 11 days occurred selectively in the SMN.

To prove the consistency of intrinsic networks and to exclude any artificial fMRI scanning drifts or habituation effects of repetitive fMRI scanning of the SMN across several days we chose rs-fMRI data from a control group of healthy subjects ( $n=16$ ). This control group was scanned twice with identical scanning parameters on the same scanner in a 2-week interval while participating in another study (Sorg et al., 2007). The SMN was identified and analyzed as described in the methods section. We found no changes in the SMN of this control group ( $p<0.01$  uncorrected) which demonstrates the consistency and robustness of intrinsic networks across days and which is in accordance with other test-retest studies (Albert et al., 2010; Biswal

et al., 2010; Damoiseaux et al., 2006; Meindl et al., 2010; Shehzad et al., 2009). Therefore, we attribute the long-term FC changes in the SMN of our study group to the effects of repetitive painful stimulation.

#### *Activity of distinct brain regions in the intrinsic SMN reflects past and future pain*

Brain imaging studies have found increased electrical or BOLD signal activity in primary sensory cortices immediately following tactile or painful stimulation (Albanese et al., 2007; Ohara et al., 2006). We hypothesized that a short episode of pain might also affect the intrinsic FC of the somatosensory system. We therefore tested whether the level of pain that a subject experienced correlates with the coherent intrinsic activity of the SSC/PPC region during POSTpain rest. We extracted the FC of the SSC/PPC by calculating the mean z-score of all voxels within a region of interest (ROI) that we independently derived from task-fMRI studies (Table S2). The regression analysis between PAIN and POSTpain FC (day 1) (Fig. 3A) of the first day shows that higher pain perception is associated with increased FC in SSC/PPC minutes after stimulation ( $r = 0.57, p = 0.02$ ). In contrast, we found no correlation between PAIN and FC during rest prior to painful stimulation ( $r = -0.03, p = 0.80$ ). This means that a recent painful experience substantially modulates coherent activity in somatosensory cortices of the SMN. Notably, this effect was also present in the resting state data from day 11. The significant correlation between PAIN and POSTpain FC (day 11) in SSC/PPC ( $r = 0.52, p = 0.03$ ) supports the notion of retrospective coding in the SMN also to repeatedly processed noxious stimuli.

We then investigated behavioral correlates for the intrinsic coupling of vmPFC into the SMN that we observed after 11 days of stimulation. fMRI data acquired during pain processing have revealed a modulating role of vmPFC in pain perception (Apkarian et al., 2005; Bingel et al., 2007; Ohara et al., 2006; Seymour et al., 2005). Hence the vmPFC might already fulfill an anticipatory role in the SMN prior to the re-occurrence of previously experienced and learned perceptions. We extracted the vmPFC's FC-score from the ICA spatial maps prior to stimulation and correlated it with each subject's PAIN rating. As our subjects adapted from a broad range of initial PAIN ratings across the study period, we entered difference values (day 11 – day 1) for the data from the last day of the study. After 11 days of repeated exposure, a significant correlation between PREpain FC of vmPFC and PAIN exists ( $r = 0.65, p = 0.015$ ) (Fig. 3B, top). This plot also revealed that three subjects sensitized with repeated stimulation resulting in the strongest increase in FC of the vmPFC with the SMN.

To further substantiate the specificity of adapted vmPFC connectivity for upcoming pain, we also evaluated data from the initial day of the study as well as the somatosensory system of the SMN. PAIN ratings were indeed exclusively related to vmPFC activity on day 11. We found neither correlation between PAIN and PREpain FC of the vmPFC on the initial day of the study ( $r = 0.36, p = 0.23$ ), nor with PREpain FC of the SSC/PPC region on day 11 ( $r = -0.003, p = 0.99$ ). Additionally, we aimed at controlling for a potential "session effect" that might account for the increased FC in the vmPFC. We therefore entered the anxiety score that we collected at the beginning of each fMRI session as an additional parameter into a partial correlation analysis of PREpain FC in vmPFC and PAIN rating. The analysis revealed that the correlation between adapted PAIN and intrinsic FC of the vmPFC before stimulation remains significant, even when controlling for the habituation parameter of anxiety ( $r = 0.60, p = 0.043$ ).

Finally, we tested intra-network dependencies between long-term changes in vmPFC and the somatosensory system. We correlated the FC-score of vmPFC before painful stimulation with the FC-score of SSC/PPC after stimulation. Fig. 3B (bottom) shows the significant correlation between PREpain FC in vmPFC and POSTpain FC in SSC/PPC ( $r = 0.70, p = 0.007$ ). Importantly, autocorrelation effects between regions and scanning sessions were ruled out ( $p > 0.40$ ). This means that the extent

of POSTpain encoding in the somatosensory system adapts with the level of PREpain activity in the vmPFC within the same ICN.

#### **Discussion**

In this study, we found that coherent ongoing activity between pain processing brain regions in the resting state changes with repeatedly experienced pain. Within the SMN, FC of the somatosensory system reflected retrospective coding of recent pain, while activity in the vmPFC anticipated forthcoming pain of a repeatedly experienced episode.

#### *Repeated pain leads to increased coherent activity of pain regions in the resting state*

After 11 days of pain sensation, bilateral somatosensory cortices exhibited increased intrinsic brain activity within the SMN. Additionally, vmPFC was recruited into the SMN on day 11. The FC of remaining brain regions in this and four other ICNs did not change. Notably, the two brain regions that adapted to repeated pain play a fundamental role in the processing of acute pain (Apkarian et al., 2005; Tracey and Mantyh, 2007). While somatosensory cortices process sensory discriminatory information of a pain sensation, the vmPFC has been ascribed a modulatory role in pain perception (Ploghaus et al., 2003; Apkarian et al., 2005; Bingel et al., 2007; Seymour et al., 2005). Hence, our data show that repeated pain selectively alters intrinsic connectivity between brain regions initially involved in processing acute pain sensations.

Our data suggest that pain processing is not restricted to the immediate experience but continues during the resting state. While no study so far revealed long-term dynamics of ICNs in response to pain, two recent studies demonstrated an immediate interaction of pain with ICNs. Acupuncture modulates connectivity between pain regions in the default mode and sensorimotor ICN during the minutes after treatment (Dhond et al., 2008). Baliki et al. found that task-related deactivations of the DMN were diminished in patients with chronic back pain, especially in the vmPFC (Baliki et al., 2008). It is important to note that the ensemble of brain regions processing acute pain does not form a single pain ICN during rest. These brain areas are rather synchronized with various ICNs, such as the sensorimotor, default mode or salience network (Fig. 1B). In our study, only the sensorimotor ICN showed functional plasticity in response to repeated pain with increased coherent activity between somatosensory regions and an additionally recruited vmPFC. This implies that ICNs do not form a rigid architecture but adapt with continuous experiences. In the following, we will discuss a potential role of the two SMN subsystems for distinctive coding of past and future aspects of repeated pain.

#### *Activity in distinct parts of the SMN support learning and anticipation of pain*

The resting-state connectivity of the SMN increased following the intervention (Fig. 3A). Before stimulation, however, FC in these regions did not indicate any behavioral relevance. Our finding is in accordance with electrophysiological data indicating that short-term memory encoding of incoming sensory information (Pasternak and Greenlee, 2005), and specifically of pain (Albanese et al., 2007; Ohara et al., 2006), involves primary sensory brain regions. Furthermore, learning related plasticity of the intrinsic functional architecture has recently been shown for the visual and motor system (Albert et al., 2009; Lewis et al., 2009). Here, we show that intrinsic brain activity in a subsystem of the SMN retrospectively encodes an individual pain experience. Moreover, we found that behavioral adaptations to the same sensation (pain rating on day 11) are also reflected in adapted FC of the somatosensory system. Together, these studies and our data

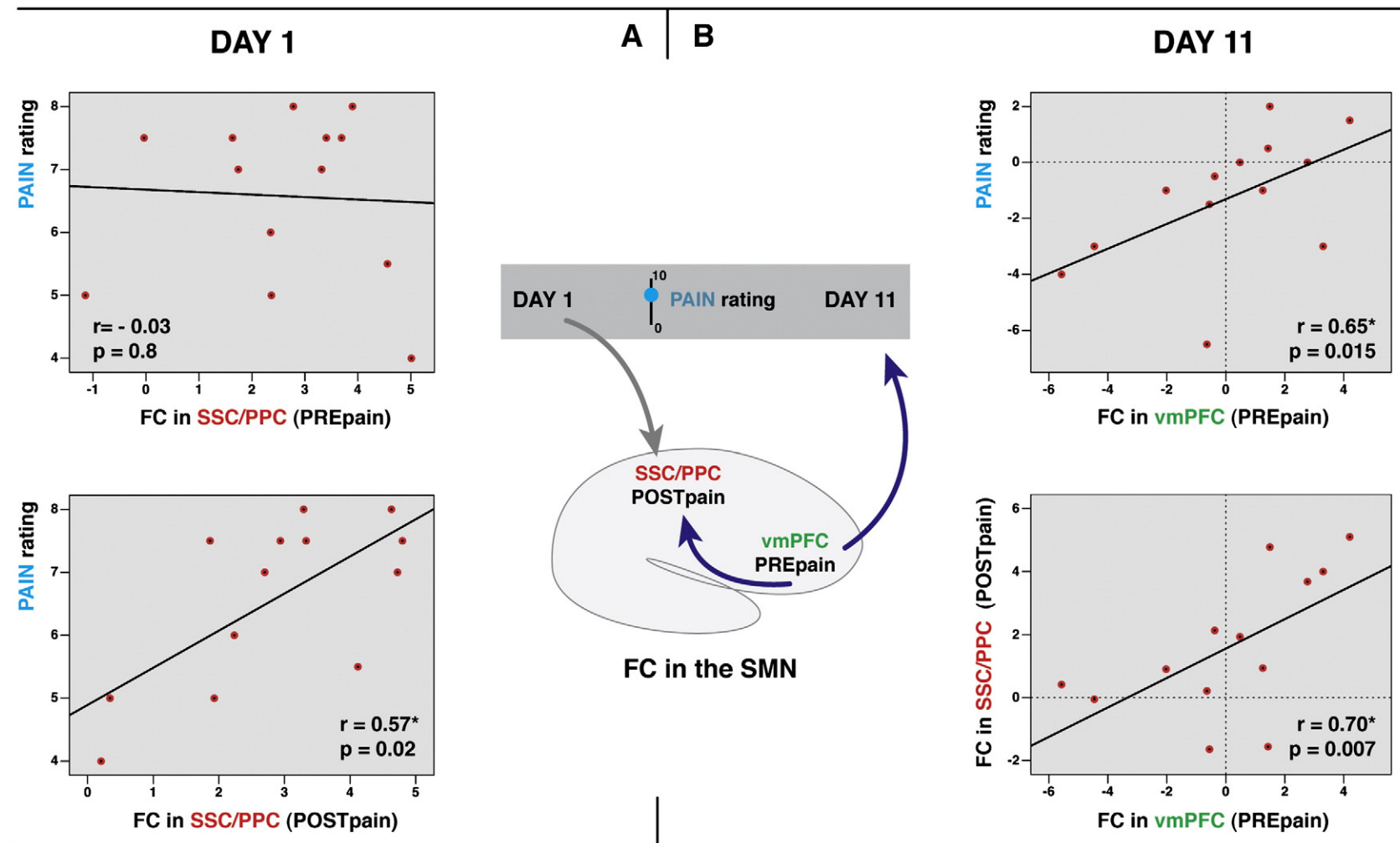


**Fig. 3.** Distinct coding of learning and anticipation of pain in the SMN. (A) During the POSTpain resting state, FC in SSC/PPC correlates with the individual PAIN rating (lower graph:  $r = 0.57, p = 0.02, n = 13$ ), while no correlation was found during PREpain resting state (upper graph:  $r = -0.03, p = 0.80, n = 13$ ). (B) After 11 days of pain, the change in resting state FC in the vmPFC before stimulation already predicts the change in PAIN rating and in FC of the SSC/PPC. Upper graph: FC in PREpain vmPFC correlates with subsequent PAIN ratings ( $r = 0.65, p = 0.015, n = 13$ ). Lower graph: FC in PREpain vmPFC correlates with POSTpain FC in the somatosensory system ( $r = 0.70, p = 0.007, n = 13$ ).

suggest that intrinsic brain activity is involved in memory coding of past experiences in various sensory modalities and continuously adapts with learning.

Intrinsic brain activity in the vmPFC predicted subjective pain intensity of a noxious stimulation minutes before the actual sensation. Importantly, predictive coding only evolved after subjects had repeatedly experienced, or learned, this particular situation. While most subjects habituated, three subjects rated the identical stimulation as being more painful than on the first day of the study. The sensitization of these individuals was predicted by the strongest coupling between vmPFC and the somatosensory system within the SMN. However, the prefrontal cortex is a heterogeneous brain region subserving various cognitive and regulatory functions. Therefore, further data are needed to concretize the cognitive processes underlying the “anticipatory coding” after repeated experiences suggested here. While we already corrected for several experimental parameters and anxiety as a potential confounding factor, a mixture of bodily and cognitive processes might account for the effect observed in the vmPFC. A limitation of this study is that we could not compare subjects perceiving repeated pain to subjects perceiving a different sensory sensation. Still, the circumscribed long-term effects in somatosensory and medial prefrontal regions fit well with the literature on brain activations during repeated acute pain and during chronic pain conditions (see following paragraph).

“Chronic pain is a state of continuous learning” (Apkarian et al., 2009). The anticipatory role we observed in vmPFC during the resting state might account for this learning effect. The literature on pain processing points to opposite brain activity in prefrontal regions between healthy subjects and patients suffering from chronic pain (Apkarian et al., 2005; Baliki et al., 2006; Bingel et al., 2007; Gundel et al., 2008). Healthy subjects that habituate to repeated pain show decreased activation in mPFC during pain processing (Bingel et al., 2007). In chronic pain patients, however, mPFC is the only region within the pain network being more strongly involved in pain processing as compared to normal subjects (Apkarian et al., 2005; Baliki et al., 2006). Drawing from these observations in pain activation studies, we suggest that intrinsic brain activity in the vmPFC anticipates upcoming pain on the basis of previous experiences and might ultimately indicate if an individual tends to pathological pain sensitization.

#### *Two layers of processing in the intrinsic functional architecture of ICNs*

Our finding of a dynamic intrinsic architecture across several days integrates two layers of processing currently discussed for ICNs (Fox and Raichle, 2007). On the one hand, immediate changes in the coherence of spontaneous activity are related to fluctuations in cognitive functions (Kelly et al., 2008; Mason et al., 2007; Seeley et al., 2007) and motor behavior (Fox et al., 2007, 2006). This suggests a volatile layer of intrinsic brain fluctuations influencing behavior in the range of seconds. On the other hand, intrinsic brain activity forms highly consistent patterns of synchronized brain regions in humans (Biswal et al., 2010; Smith et al., 2009), various species (Lu et al., 2007; Vincent et al., 2007) and even reduced states of vigilance (Boly et al., 2008; Horovitz et al., 2009). The intrinsic functional architecture might therefore reflect a rather robust layer of anatomical connections (Fox and Raichle, 2007; Vincent et al., 2007; Hagmann et al., 2008). We suggest that coherent intrinsic activity stabilizes networks of brain regions that are commonly activated together across the life span but continuously adapts to interactions with the environment to prepare the organism for what may happen. The intrinsic brain state might therefore have more impact on human behavior than does the brain's immediate response to an event (Fox and Raichle, 2007).

Supplementary materials related to this article can be found online at doi:10.1016/j.neuroimage.2011.04.011.

#### Acknowledgments

Valentin Riedl wishes to thank Karl Friston, Olaf Sporns, Walter Zieglaensberger, Tom Eichele, Christopher Honey and Markus Ploner for advice and discussions and Christine Vogg for technical assistance. Supported by the O1EV0710 grant and the “German Research Network on Neuropathic Pain” (DFNS) of the Federal Ministry of Education and Research (Bundesministerium für Bildung und Forschung, BMBF) and by the SFB391C9 grant of the German Research Foundation (Deutsche Forschungsgemeinschaft, DFG).

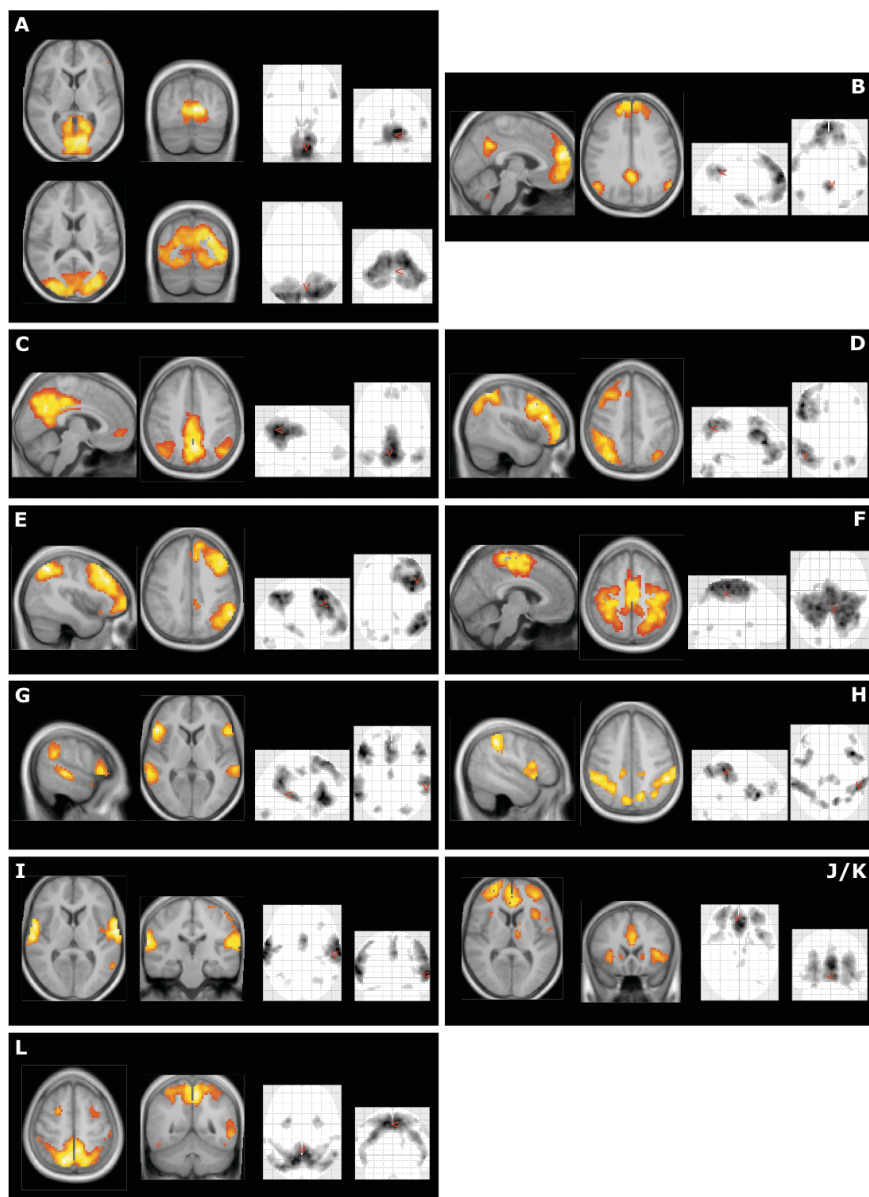
V.R., M.V. and A.W. equally contributed to this work.

#### References

- Albanese, M.C., Duerden, E.G., Rainville, P., Duncan, G.H., 2007. Memory traces of pain in human cortex. *J. Neurosci.* 27, 4612–4620.
- Albert, N.B., Robertson, E.M., Miall, R.C., 2009. The resting human brain and motor learning. *Curr. Biol.* 19, 1023–1027.
- Apkarian, A.V., Bushnell, M.C., Treede, R.D., Zubieta, J.K., 2005. Human brain mechanisms of pain perception and regulation in health and disease. *Eur. J. Pain* 9, 463–484.
- Apkarian, A.V., Baliki, M.N., Geha, P.Y., 2009. Towards a theory of chronic pain. *Prog. Neurobiol.* 87, 81–97.
- Baliki, M.N., Chialvo, D.R., Geha, P.Y., Levy, R.M., Harden, R.N., Parrish, T.B., Apkarian, A.V., 2006. Chronic pain and the emotional brain: specific brain activity associated with spontaneous fluctuations of intensity of chronic back pain. *J. Neurosci.* 26, 12165–12173.
- Baliki, M.N., Geha, P.Y., Apkarian, A.V., Chialvo, D.R., 2008. Beyond feeling: chronic pain hurts the brain, disrupting the default-mode network dynamics. *J. Neurosci.* 28, 1398–1403.
- Beckmann, C.F., DeLuca, M., Devlin, J.T., Smith, S.M., 2005. Investigations into resting-state connectivity using independent component analysis. *Philos. Trans. R. Soc. Lond. B Biol. Sci.* 360, 1001–1013.
- Bell, A.J., Sejnowski, T.J., 1995. An information-maximization approach to blind separation and blind deconvolution. *Neural Comput.* 7, 1129–1159.
- Bingel, U., Schoell, E., Herken, W., Büchel, C., May, A., 2007. Habituation to painful stimulation involves the antinociceptive system. *Pain* 131, 21–30.
- Biswal, B., Yetkin, F.Z., Haughton, V.M., Hyde, J.S., 1995. Functional connectivity in the motor cortex of resting human brain using echo-planar MRI. *Magn. Reson. Med.* 34, 537–541.
- Biswal, B.B., Mennes, M., Zuo, X.N., Gohel, S., Kelly, C., Smith, S.M., Beckmann, C.F., Adelstein, J.S., Buckner, R.L., Colcombe, S., et al., 2010. Toward discovery science of human brain function. *Proc. Natl. Acad. Sci. U. S. A.* 107, 4734–4739.
- Boly, M., Phillips, C., Tshibanda, L., Vanhaudenhuyse, A., Schabus, M., Dang-Vu, T.T., Moonen, G., Hustinx, R., Maquet, P., Laureys, S., 2008. Intrinsic brain activity in altered states of consciousness: how conscious is the default mode of brain function? *Ann. N.Y. Acad. Sci.* 1129, 119–129.
- Calhoun, V.D., Adali, T., Pearson, G.D., Pekar, J.J., 2001. A method for making group inferences from functional MRI data using independent component analysis. *Hum. Brain Mapp.* 14, 140–151.
- Calhoun, V.D., Adali, T., Pekar, J.J., 2004. A method for comparing group fMRI data using independent component analysis: application to visual, motor and visuomotor tasks. *Magn. Reson. Imaging* 22, 1181–1191.
- Calhoun, V.D., Liu, J., Adali, T., 2009. A review of group ICA for fMRI data and ICA for joint inference of imaging, genetic, and ERP data. *Neuroimage* 45, S163–S172.
- Damoiseaux, J.S., Rombouts, S.A., Barkhof, F., Scheltens, P., Stam, C.J., Smith, S.M., Beckmann, C.F., 2006. Consistent resting-state networks across healthy subjects. *Proc. Natl. Acad. Sci. U. S. A.* 103, 13848–13853.
- Damoiseaux, J.S., Beckmann, C.F., Arigita, E.J., Barkhof, F., Scheltens, P., Stam, C.J., Smith, S.M., Rombouts, S.A., 2008. Reduced resting-state brain activity in the “default network” in normal aging. *Cereb. Cortex* 18, 1856–1864.
- Dhond, R.P., Yeh, C., Park, K., Kettner, N., Napadow, V., 2008. Acupuncture modulates resting state connectivity in default and sensorimotor brain networks. *Pain* 136, 407–418.
- Fox, M.D., Raichle, M.E., 2007. Spontaneous fluctuations in brain activity observed with functional magnetic resonance imaging. *Nat. Rev. Neurosci.* 8, 700–711.
- Fox, M.D., Snyder, A.Z., Zacks, J.M., Raichle, M.E., 2006. Coherent spontaneous activity accounts for trial-to-trial variability in human evoked brain responses. *Nat. Neurosci.* 9, 23–25.
- Fox, M.D., Snyder, A.Z., Vincent, J.L., Raichle, M.E., 2007. Intrinsic fluctuations within cortical systems account for intertrial variability in human behavior. *Neuron* 56, 171–184.
- Greicius, M., 2008. Resting-state functional connectivity in neuropsychiatric disorders. *Curr. Opin. Neurol.* 21, 424–430.
- Greicius, M.D., Krasnow, B., Reiss, A.L., Menon, V., 2003. Functional connectivity in the resting brain: a network analysis of the default mode hypothesis. *Proc. Natl. Acad. Sci. U. S. A.* 100, 253–258.
- Greicius, M.D., Kiviniemi, V., Tervonen, O., Vainionpää, V., Alahuhta, S., Reiss, A.L., Menon, V., 2008. Persistent default-mode network connectivity during light sedation. *Hum. Brain Mapp.* 29, 839–847.
- Gundel, H., Valet, M., Sorg, C., Huber, D., Zimmer, C., Sprenger, T., Tolle, T.R., 2008. Altered cerebral response to noxious heat stimulation in patients with somatoform pain disorder. *Pain* 137, 413–421.

- Hagmann, P., Cammoun, L., Gigandet, X., Meuli, R., Honey, C.J., Wedeen, V.J., Sporns, O., 2008. Mapping the structural core of human cerebral cortex. *PLoS Biol.* 6, e159.
- Honey, C.J., Sporns, O., Cammoun, L., Gigandet, X., Thiran, J.P., Meuli, R., Hagmann, P., 2009. Predicting human resting-state functional connectivity from structural connectivity. *Proc. Natl. Acad. Sci. U. S. A.* 106, 2035–2040.
- Horovitz, S.G., Braun, A.R., Carr, W.S., Picchioni, D., Balkin, T.J., Fukunaga, M., Duyn, J.H., 2009. Decoupling of the brain's default mode network during deep sleep. *Proc. Natl. Acad. Sci. U. S. A.* 106, 11376–11381.
- Kelly, A.M., Uddin, L.Q., Biswal, B.B., Castellanos, F.X., Milham, M.P., 2008. Competition between functional brain networks mediates behavioral variability. *Neuroimage* 39, 527–537.
- Koyama, T., McHaffie, J.G., Laurienti, P.J., Coghill, R.C., 2005. The subjective experience of pain: where expectations become reality. *Proc. Natl. Acad. Sci. U. S. A.* 102, 12950–12955.
- Larson-Prior, L.J., Zempel, J.M., Nolan, T.S., Prior, F.W., Snyder, A.Z., Raichle, M.E., 2009. Cortical network functional connectivity in the descent to sleep. *Proc. Natl. Acad. Sci. U. S. A.* 106, 4489–4494.
- Laufs, H., Krakow, K., Sterzer, P., Eger, E., Beyerle, A., Salek-Haddadi, A., Kleinschmidt, A., 2003. Electroencephalographic signatures of attentional and cognitive default modes in spontaneous brain activity fluctuations at rest. *Proc. Natl. Acad. Sci. U. S. A.* 100, 11053–11058.
- Lewis, C.M., Baldassarre, A., Committeri, G., Romani, G.L., Corbetta, M., 2009. Learning sculpts the spontaneous activity of the resting human brain. *Proc. Natl. Acad. Sci. U. S. A.* 106, 17558–17563.
- Li, Y.O., Adali, T., Calhoun, V.D., 2007. Estimating the number of independent components for functional magnetic resonance imaging data. *Hum. Brain Mapp.* 28, 1251–1266.
- Lu, H., Zuo, Y., Gu, H., Waltz, J.A., 2007. Synchronized delta oscillations correlate with the resting-state functional MRI signal. *Proc. Natl. Acad. Sci. U. S. A.* 104, 18265–18269.
- Mason, M.F., Norton, M.J., Van Horn, J.D., Wegner, D.M., Grafton, S.T., Macrae, C.N., 2007. Wandering minds: the default network and stimulus-independent thought. *Science* 315, 393–395.
- Meindl, T., Teipel, S., Elmouden, R., Mueller, S., Koch, W., Dietrich, O., Coates, U., Reiser, M., Glaser, C., 2010. Test-retest reproducibility of the default-mode network in healthy individuals. *Hum. Brain Mapp.* 31 (2), 237–246.
- Ohara, S., Crone, N.E., Weiss, N., Lenz, F.A., 2006. Analysis of synchrony demonstrates "pain networks" defined by rapidly switching, task-specific, functional connectivity between pain-related cortical structures. *Pain* 123, 244–253.
- Pasternak, T., Greenlee, M.W., 2005. Working memory in primate sensory systems. *Nat. Rev. Neurosci.* 6, 97–107.
- Ploghaus, A., Becerra, L., Borras, C., Borsook, D., 2003. Neural circuitry underlying pain modulation: expectation, hypnosis, placebo. *Trends Cogn. Sci.* 7, 197–200.
- Seeley, W.W., Menon, V., Schatzberg, A.F., Keller, J., Glover, G.H., Kenna, H., Reiss, A.L., Greicius, M.D., 2007. Dissociable intrinsic connectivity networks for salience processing and executive control. *J. Neurosci.* 27, 2349–2356.
- Seymour, B., O'Doherty, J.P., Koltzenburg, M., Wiech, K., Frackowiak, R., Friston, K., Dolan, R., 2005. Opponent appetitive-aversive neural processes underlie predictive learning of pain relief. *Nat. Neurosci.* 8, 1234–1240.
- Shehzad, Z., Kelly, A.M., Reiss, P.T., Gee, D.G., Gotimer, K., Uddin, L.Q., Lee, S.H., Margulies, D.S., Roy, A.K., Biswal, B.B., et al., 2009. The resting brain: unconstrained yet reliable. *Cereb. Cortex* 19, 2209–2229.
- Smith, S.M., Fox, P.T., Miller, K.L., Glahn, D.C., Fox, P.M., Mackay, C.E., Filippini, N., Watkins, K.E., Toro, R., Laird, A.R., et al., 2009. Correspondence of the brain's functional architecture during activation and rest. *Proc. Natl. Acad. Sci. U. S. A.* 106, 13040–13045.
- Sorg, C., Riedl, V., Muhlau, M., Calhoun, V.D., Eichele, T., Laer, L., Drzezga, A., Forstl, H., Kurz, A., Zimmer, C., et al., 2007. Selective changes of resting-state networks in individuals at risk for Alzheimer's disease. *Proc. Natl. Acad. Sci. U. S. A.* 104, 18760–18765.
- Tracey, I., Mantyh, P.W., 2007. The cerebral signature for pain perception and its modulation. *Neuron* 55, 377–391.
- Valet, M., Sprenger, T., Boecker, H., Willoch, F., Rummey, E., Conrad, B., Erhard, P., Tolle, T.R., 2004. Distraction modulates connectivity of the cingulo-frontal cortex and the midbrain during pain—an fMRI analysis. *Pain* 109, 399–408.
- van de Ven, V.G., Formisano, E., Prvulovic, D., Roeder, C.H., Linden, D.E., 2004. Functional connectivity as revealed by spatial independent component analysis of fMRI measurements during rest. *Hum. Brain Mapp.* 22, 165–178.
- Vincent, J.L., Patel, G.H., Fox, M.D., Snyder, A.Z., Baker, J.T., Van Essen, D.C., Zempel, J.M., Snyder, L.H., Corbetta, M., Raichle, M.E., 2007. Intrinsic functional architecture in the anaesthetized monkey brain. *Nature* 447, 83–86.

## Supplementary Material



### Supplementary Figure S1 Legend

**ICNs derived from the group ICA.** We identified 12 spatial maps covering previously described resting state or intrinsic connectivity networks from our own group and others (Damoiseaux et al., 2006, 2008; Sorg et al., 2007; van de Ven et al., 2004). We ordered the spatial maps following the most recent description by Damoiseaux and colleagues (Damoiseaux et al., 2008). The ICNs show spatial patterns of distinct brain regions previously known to be involved in A: visual processing, B/C: anterior and posterior parts of the default mode network, D: ventral/reorienting attention network, E: working memory, F: somatosensory and motor functions, H: dorsal/executive attention network, I: auditory processing, G: executive control network, J/K: salience network and L: spatial attention network. Conjunction maps ( $z_{\max}=7.5$ ) are overlaid on a mean structural image of all subjects. The left hemisphere of the brain corresponds to the right side of the image.

**Supplementary Table S2**

<b>Brain region</b>	<b>Peak coordinates [x,y,z] in MNI space. Left / Right</b>
Pain processing brain regions from a previous task-fMRI study of our group (Gundel et al., 2008)	
Primary somatosensory cortex (SSC)	-36, -30, 66 / 36, -30, 66
Secondary somatosensory cortex	-42, -39, 21 / 57, -36, 18
Posterior parietal cortex (PPC)	-57, -48, 51 / 45, -48, 30
Insula	-42, 3, -3 / 39, 6, 9
Lateral prefrontal cortex	-45, 45, -9 / 39, 39, 0
Anterior cingulate cortex	-6, -21, 30 / 9, -18, 33
Thalamus	-12, -3, 6 / 12, -3, 6
Brain regions from a task-activation study on habituation to repeated pain (Bingel et al., 2007)	
Ventromedial prefrontal cortex (vmPFC)	-6, 30, -9 / 3, 36, -12

**Pain processing brain regions.** Regions of interest (ROI) ( $r=10\text{mm}$ ) reflecting pain processing brain regions were independently derived from two previous task-fMRI studies on immediate and repeated pain processing in humans. In case multiple coordinates have been reported, those were chosen that maximally covered grey matter in our dataset as validated with the grey matter segmentation masks from SPM5. These ROIs were then used to select those ICNs for further analyses that covered at least one pain processing ROI. Furthermore, the vmPFC-ROI and a combined SSC/PPC-ROI were used in the correlation analyses.

## 9 Paper 3: Intrinsic network connectivity reflects consistency of synesthetic experiences

(J Neurosci 2012)

7614 • The Journal of Neuroscience, May 30, 2012 • 32(22):7614–7621

Behavioral/Systems/Cognitive

# Intrinsic Network Connectivity Reflects Consistency of Synesthetic Experiences

Anna Dovern,<sup>1,2</sup> Gereon R. Fink,<sup>1,2</sup> A. Christina B. Fromme,<sup>1</sup> Afra M. Wohlschläger,<sup>3</sup> Peter H. Weiss,<sup>1,2\*</sup> and Valentin Riedl<sup>3\*</sup>

<sup>1</sup>Cognitive Neuroscience, Institute of Neuroscience and Medicine, Research Centre Jülich, 52425 Jülich, Germany, <sup>2</sup>Department of Neurology, University Hospital Cologne, 50937 Cologne, Germany, and <sup>3</sup>Departments of Neuroradiology, Neurology, Klinikum Rechts der Isar, Technische Universität München, 81675 Munich, Germany

Studying cognitive processes underlying synesthesia, a condition in which stimulation of one sensory modality automatically leads to abnormal additional sensory perception, allows insights into the neural mechanisms of normal and abnormal cross-modal sensory processing.

Consistent with the notion that synesthesia results from hyperconnectivity, functional connectivity analysis (adopting independent component analysis and seed-based correlation analysis) of resting-state functional magnetic resonance imaging data of 12 grapheme–color synesthetes and 12 nonsynesthetic control subjects revealed, in addition to increased intranetwork connectivity, both a global and a specific (medial and lateral visual networks to a right frontoparietal network) increase of intrinsic internetwork connectivity in grapheme–color synesthesia. Moreover, this increased intrinsic network connectivity reflected the strength of synesthetic experiences. These findings constitute the first direct evidence of increased functional network connectivity in synesthesia.

In addition to this significant contribution to the understanding of the neural mechanisms of synesthesia, our results have important general implications. In combination with data derived from clinical populations, our data strongly suggest that altered differences in intrinsic network connectivity are directly related to the phenomenology of human experiences.

## Introduction

Numbers or letters evoke additional color perceptions in grapheme–color synesthesia, one of the most common forms of synesthesia. Although to date the underlying neural mechanisms remain elusive, it has often been hypothesized that the concomitant perception of a sensation not inherent to the stimulus is caused by an increased connectivity (or hyperconnectivity) between the relevant brain regions (Hubbard and Ramachandran, 2005). During synesthetic experience, neural activity increases in occipital and temporal brain regions involved in grapheme and color processing, but also in parietal and frontal areas involved in binding processes (Weiss et al., 2001, 2005; Nunn et al., 2002; Hubbard and Ramachandran, 2005; Hubbard et al., 2005). In addition to these findings from functional activation studies,

morphometric data revealed structural changes in similar brain regions (Rouw and Scholte, 2007, 2010; Jäncke et al., 2009; Weiss and Fink, 2009; Hänggi et al., 2011). These morphometric changes suggest altered connectivity in brain networks of primary sensory and higher cognitive integration areas already in the resting state, i.e., when no synesthesia-inducing stimulus is present. However, the hypothesized hyperconnectivity in synesthesia has so far been mainly explored at the structural level. For example, a recent diffusion tensor imaging study revealed regionally increased structural connectivity in inferior temporal, parietal, and frontal cortices of grapheme–color synesthetes (Rouw and Scholte, 2007).

In this study, we tested whether similar differences also occur in the functional network architecture of the resting synesthetic brain. We therefore investigated intrinsic functional connectivity (FC) of brain networks with resting-state functional magnetic resonance imaging (rs-fMRI). Spontaneous low-frequency fluctuations of the blood-oxygen level-dependent (BOLD) signal can be temporally correlated across functionally related brain areas (Biswal et al., 1995; Fox and Raichle, 2007) and may thereby form intrinsic connectivity networks (ICN). ICNs consistently occur in healthy subjects and show strong correspondence to structural networks (Damoiseaux et al., 2006; Honey et al., 2007). However, deviations from this consistent architecture of intrinsic connectivity networks also occur. Neuropsychiatric patients with altered experiences or impaired cognitive functions, like in schizophrenia or Alzheimer's disease, show characteristic changes of intrinsic FC in several ICNs (Greicius et al., 2004; Jafri et al., 2008;

Received Oct. 26, 2011; revised April 5, 2012; accepted April 10, 2012.

Author contributions: A.D., G.R.F., A.C.B.F., A.M.W., P.H.W., and V.R. designed research; A.D., A.C.B.F., and P.H.W. performed research; A.D., A.C.B.F., P.H.W., and V.R. analyzed data; A.D., G.R.F., A.M.W., P.H.W., and V.R. wrote the paper.

\*P.H.W. and V.R. contributed equally to this work.

This work was supported by Grant 8762754 of the Kommission fuer Klinische Forschung at the Klinikum Rechts der Isar (to V.R.). We are grateful to our subjects and our colleagues at the Institute of Neuroscience and Medicine, Research Centre Jülich.

The authors declare no competing financial interests.

Correspondence should be addressed to either of the following: Peter H. Weiss, Cognitive Neurology Section, Institute of Neuroscience and Medicine, Research Centre Jülich, Leo-Brandt-Strasse 5, 52425 Jülich, Germany. E-mail: P.H.Weiss@fz-juelich.de; or Valentin Riedl, Department of Neuroradiology, Klinikum Rechts der Isar, Technische Universität München, Ismaningerstrasse 22, 81675 Munich, Germany, E-mail: valentin.riedl@mytum.de.

DOI:10.1523/JNEUROSCI.5401-11.2012

Copyright © 2012 the authors 0270-6474/12/327614-08\$15.00/0

Vercammen et al., 2010; Gour et al., 2011). In analogy, the additional (abnormal) experiences of synesthetes may be reflected in an altered intrinsic FC. Thus, we hypothesized that (1) grapheme–color synesthetes show specific patterns of functional hyperconnectivity at rest and (2) this hyperconnectivity correlates with the consistency of synesthetic experiences. To test these hypotheses, we investigated the intrinsic FC of synesthesia-related brain networks of coherent ongoing neuronal activity with independent component analysis (ICA) (Fox and Raichle, 2007; Biswal et al., 2010; Schölvinck et al., 2010) and with an additional seed-based FC approach for the cytoarchitectonically defined color area V4.

## Materials and Methods

**Subjects.** In the current study, 12 grapheme–color synesthetes and 12 control subjects without a history of neurological or psychiatric disease were investigated. The two groups were matched for gender (10 female in each group), age [synesthetes:  $32.6 \pm 9.9$  years (mean  $\pm$  SD); controls:  $30.6 \pm 5.7$  years;  $t_{(22)} = 0.611$ ,  $p = 0.55$ ], handedness as assessed by the Oldfield handedness inventory (Oldfield, 1971) (3 subjects with left-hand and 9 subjects with right-hand preference in each group; laterality quotient: synesthetes:  $38.7 \pm 77.6$ ; controls:  $41.3 \pm 74$ ;  $t_{(22)} = -0.084$ ,  $p = 0.93$ ), and IQ as assessed by the Mehrfachwahl-Wortschatz Intelligence Test type B (Lehr et al., 1995) (synesthetes:  $117.6 \pm 10.3$ ; controls:  $113.9 \pm 11.1$ ;  $t_{(20)} = 0.817$ ,  $p = 0.42$ ).

Authenticity of synesthesia was verified by applying a test of consistency (Baron-Cohen et al., 1993) in which synesthetic color experiences for 129 items were retested without warning after at least 6 months ( $15.2 \pm 12.4$  months) in all synesthetes (Weiss et al., 2005). This test confirmed the high consistency of the synesthetic color experiences in the 12 grapheme–color synesthetes (rate of consistent responses:  $84.8 \pm 14.5\%$ ). All but one grapheme–color synesthete reported also having phoneme–color synesthesia, i.e., sounds of single phonemes also trigger synesthetic color experiences. The local ethics committee of the Medical Faculty of the Rheinisch-Westfälische Technische Hochschule Aachen University approved the study and all subjects gave written informed consent.

**fMRI data acquisition.** Subjects were instructed to keep their eyes closed but remain alert and awake during the resting-state measurements in the scanner. Resting-state data were acquired on a 3-tesla MRI System (Trio; Siemens) using a standard echo-planar imaging (EPI) sequence to obtain standard T2\*-weighted EPI images with BOLD contrast (field of view, 200 mm; matrix size,  $64 \times 64$ ; voxel size,  $3.1 \times 3.1 \times 3.0$  mm $^3$ ). A total of 280 functional volumes of 36 3-mm-thick axial slices were collected sequentially with a 0.3 mm gap for each subject within a single scanning session (repetition time, 2.2 s; echo time, 30 ms; total duration,  $\sim 10$  min). The first six EPI volumes were discarded to allow for T1 equilibration effects. Standard preprocessing procedures were applied to the remaining 274 EPI images using Statistical Parametric Mapping software (SPM5; Wellcome Department of Imaging Neuroscience, London, UK; <http://www.fil.ion.ucl.ac.uk/spm/software/spm5/>).

**Independent component analysis.** ICA is a method that can be used to decompose fMRI data into spatially independent components, each comprising a spatial map of functionally connected brain regions and an associated time course. In the current study, ICA was used to identify synesthesia-relevant ICNs and to assess differential functional intranetwork and internetwork connectivity in grapheme–color synesthetes and control subjects.

Before the volumes were entered into the ICA, we applied a voxelwise  $z$ -transformation ( $\hat{y}_{ijk}(t)$ ) on the time course data  $y_{ijk}(t)$  by subtracting the mean  $\langle y_{ijk} \rangle$  and dividing by the standard deviation  $\sigma_{ijk}$ :  $\hat{y}_{ijk}(t) = (y_{ijk}(t) - \langle y_{ijk} \rangle) / \sigma_{ijk}$  ( $t$  is time; indices  $i$ ,  $j$ ,  $k$  represent the three directions in space). The sensitivity of the multivariate ICA algorithm for correlation of variance between voxels, i.e., functional connectivity, was thereby rendered independent of the original BOLD signal magnitude across subjects (Sorg et al., 2007).

To obtain the most robust and comparable set of independent components from the resting-state fMRI dataset, we performed a spatial group ICA on the combined, concatenated dataset of synesthetes and controls ( $n = 24$ ) using GIFT software (<http://icatb.sourceforge.net/>,

version 2.0 d) and iteratively ran 30 ICAs using the ICASSO procedure (Himberg et al., 2004). We calculated 25 independent components according to the minimum description length criteria that can be implemented in GIFT (Calhoun et al., 2001). The analysis was performed in three steps (Calhoun et al., 2001): data reduction with principal component analysis (PCA), ICA using the Infomax algorithm on the concatenated dataset of all subjects (including both synesthetes and controls), and finally back-reconstruction of the group independent components into the single-subject space using GICA3 (Erhardt et al., 2011). Each independent component was composed of a spatially independent brain map and an associated time course of ongoing fMRI fluctuations during rest. We selected functionally relevant ICNs from the whole set of independent components by applying a multiple spatial regression analysis against brain templates comprising synesthesia-related brain regions that were created with the anatomy toolbox (Eickhoff et al., 2005). The brain regions assumed to be critically involved in synesthetic experiences were derived from previous functional and structural imaging studies (Nunn et al., 2002; Hubbard et al., 2005; Weiss et al., 2005; Rouw and Scholte, 2007; Weiss and Fink, 2009; Rouw and Scholte, 2010) and covered the visual, auditory, and intraparietal cortices. The anatomy toolbox by Eickhoff and colleagues (2005) was used to build spatial masks covering these three brain regions. The visual mask included area 17, area 18, hOC3v (V3v), hOC4 (V4), and hOC5 (V5); the auditory mask included areas TE 1.0, TE 1.1, and TE 1.2; and the intraparietal mask comprised the areas hIP1, hIP2, and hIP3. A threshold of beta  $> 1$  for at least one of the three spatial variables was determined to select synesthesia-relevant ICNs. In addition, a separate group ICA was applied to each of the two groups using identical parameters as in the combined (controls and synesthetes) approach. This procedure validated the presence of all synesthesia-relevant ICNs in both the synesthetes and the control subjects in independent analyses.

To analyze group differences of within-network connectivity, we entered spatial maps of individual ICNs of the combined group ICA into an ANOVA with the factors subject, group, component, and a group  $\times$  component interaction using SPM5. Contrasts were masked by conjunction maps of the one-sample  $t$  test (FWE corrected,  $p < 0.05$ ; Fig. 1, left) of the respective network and thresholded at  $p < 0.05$ , FWE corrected at the voxel level. Finally, each individual subject's FC between the synesthesia-relevant ICNs was derived by calculating pairwise zero-lag correlation coefficients between the BOLD signal time courses of the synesthesia-relevant ICNs. We performed this functional network connectivity (FNC) analysis using the FNC Matlab toolbox (version 2.3) (Jafri et al., 2008).

**Seed-based correlation analysis for the cytoarchitectonically defined color area V4.** To complement the ICA results by an independent approach, we performed a seed-based correlation analysis by calculating the FC from cytoarchitectonically defined color area V4 to all other voxels of the brain. The bilateral V4 seed regions were created using the Anatomy Toolbox (Eickhoff et al., 2005). The REST toolkit (Song et al., 2011) was used for removing the linear trend of time courses from the data, temporal bandpass filtering of the data (0.01–0.1 Hz), and calculating the individual FC maps. Finally, a Fisher's  $z$  transformation was used to normalize the individual correlation maps to  $z$  maps. Then, for each group, the Fisher's  $z$  maps were entered into a separate one-sample  $t$  test (using SPM5) to identify regions showing significant FC with color area V4. A height threshold of  $p < 0.05$  (FWE corrected) and an extent threshold of 50 voxels were applied to the one-sample  $t$  tests. Moreover,  $z$  maps were entered into a two-sample  $t$  test to detect significant group differences between synesthetes and controls. The two-sample  $t$  test was masked by the conjunction map of the one-sample  $t$  tests (FWE corrected; height threshold,  $p < 0.05$ ; extent threshold, 50 voxels) of synesthetes and control subjects. Again, a height threshold of  $p < 0.05$  (FWE corrected) was applied.

## Results

### Independent component analysis

We identified seven synesthesia-relevant ICNs in a multiple spatial regression analysis using three spatial priors (visual cortex, auditory cortex, and intraparietal cortex): medial and lateral vi-

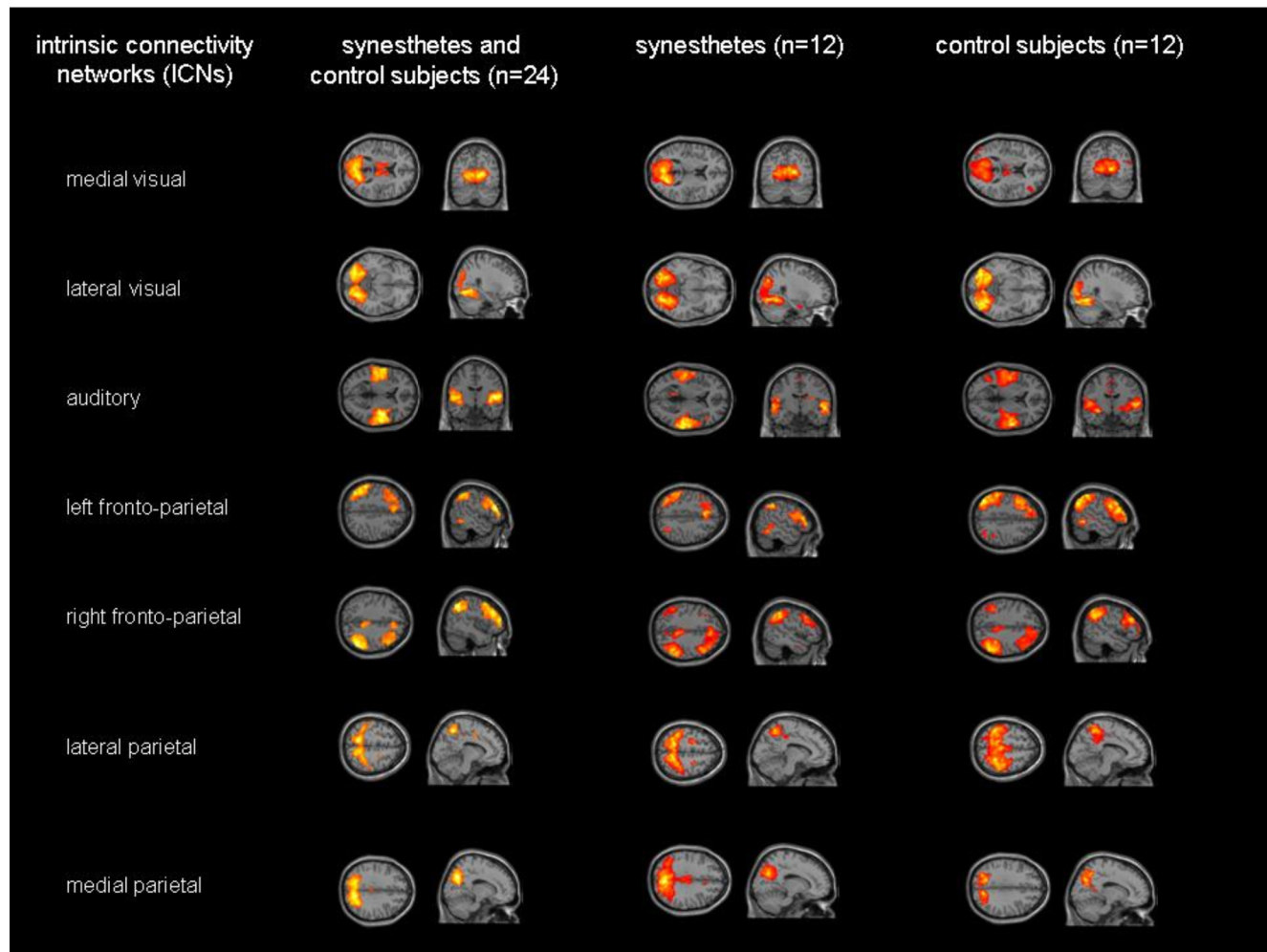


**Figure 1.** Illustration of the seven synesthesia-relevant ICNs revealed by the combined and separate group ICAs. Seven synesthesia-relevant ICNs were identified by ICA and spatial regression analysis (for further details, see Materials and Methods). Results of the one-sample  $t$  tests on the individual subjects ICN patterns are visualized on axial, sagittal, or coronal sections of the standard brain template provided by SPM5. Due to differences in statistical power, a threshold of  $p < 0.05$ , FWE corrected, was applied for the combined group ICA, while the within-group ICA results for both groups are shown for a height threshold of  $p < 0.05$ , FDR corrected, and an extent threshold of 50 voxels.

sual network, auditory network, left and right frontoparietal network, and medial and lateral parietal network (Fig. 1; Tables 1, 2). These ICNs strongly resemble previously described ICNs involved in sensory and cognitive processing (Smith et al., 2009). Figure 1 illustrates that all synesthesia-relevant ICNs from the combined group analysis were also detected by separate ICAs of each group. In addition to this qualitative assessment, we also quantified group differences of within-network connectivity in an ANOVA between grapheme–color synesthetes and control subjects. This ANOVA revealed regions with significantly stronger functional connectivity for synesthetes compared with controls for all networks of interest, while only the left and right frontoparietal networks also included regions showing stronger functional connectivity in the control subjects (Table 3). Note that the within-network differences between groups were limited to rather small clusters.

We next investigated group differences of network connectivity between the seven synesthesia-relevant ICNs. This FNC analysis revealed clear differences in the intrinsic network architecture between grapheme–color synesthetes and control subjects. For the control group, only five significant connections emerged (as indexed by significant correlations between the time courses of the seven ICNs, one-sample  $t$  tests, two-sided,  $p <$

**Table 1.** Results of the multiple spatial regression analysis conducted to identify synesthesia-relevant ICNs to be included in the FNC analysis

ICN number	Label of ICNs	Betas			Multiple regression value
		Auditory mask	Intraparietal mask	Visual mask	
1	Medial visual network	−0.12433	−0.00555	<b>1.81960</b>	0.30953
18	Auditory network	<b>3.53987</b>	0.01085	−0.18998	0.13207
12	Lateral visual network	−0.11789	−0.01240	<b>1.02344</b>	0.09962
16	Left frontoparietal network	−0.06476	<b>1.70691</b>	−0.05126	0.05326
25	Lateral parietal network	−0.01792	<b>1.06765</b>	−0.02037	0.02193
19	Medial parietal network	−0.02189	<b>1.07975</b>	0.08141	0.02109
21	Right frontoparietal network	−0.03788	<b>1.01988</b>	−0.03213	0.01828
3		0.01709	0.03890	−0.24333	0.00560
—		—	—	—	—
—		—	—	—	—
—		—	—	—	—
11		−0.00122	−0.02028	−0.01598	0.00003

Only components with a beta  $> 1$  (bold) on at least one of the three spatial variables were subjected to the FNC analysis to ensure that only ICNs that covered at least one of the synesthesia-relevant brain regions (visual cortex, auditory cortex, and intraparietal cortex) were included. This threshold is represented in the table by the line. Note that already the betas of the next ICN in the table (arbitrarily numbered “3”) are far from the critical value 1, indicating that this and all the other ICNs (with even lower betas) do not contain significant parts of the synesthesia-relevant brain regions.

**Table 2.** Brain regions belonging to the seven synesthesia-relevant ICNs

Region	Hemisphere	Cluster size (voxels)	t value	MNI coordinates		
				x	y	z
<b>Medial visual network</b>						
Calcarine gyrus	R	2217*	23.5	12	-69	6
Calcarine gyrus	L		21.7	-3	-72	9
Thalamus	R	261*	12.6	12	-21	12
Thalamus	L		10.7	-6	-15	9
Superior medial gyrus	M	180	11.4	0	36	45
<b>Lateral visual network</b>						
Fusiform gyrus	R	2677*	24.1	27	-69	-9
Fusiform gyrus	L		19.6	-21	-78	-9
Insula	R	61	9.2	42	9	6
<b>Auditory network</b>						
Superior temporal gyrus; TE 1.2	R	1697	19.0	54	-3	0
Superior temporal gyrus; TE 1.2	L	1521	17.6	-54	-9	0
Middle cingulate cortex	L	78	10.2	-9	3	39
<b>Left frontoparietal network</b>						
Inferior frontal gyrus	L	1591	20.4	-48	30	18
Inferior parietal lobule	L	721	18.4	-51	-39	45
Insula	L	69	17.0	-33	18	0
Posterior cingulate cortex	L	67	11.9	-3	-36	33
Inferior temporal gyrus	L	67	9.5	-51	-54	-9
Thalamus	L	65	10.2	-6	-15	9
Middle frontal gyrus	R	50	8.6	48	36	21
Precuneus	L	40	9.1	-6	-51	15
<b>Right frontoparietal network</b>						
Inferior frontal gyrus	R	1909	14.5	45	33	27
Inferior parietal lobule	R	756	18.6	51	-54	39
Precuneus	R	151	12.4	6	-42	45
Superior parietal lobule	R	48	7.5	15	-72	54
Middle temporal gyrus	R	33	9.7	63	-27	-9
Insula	R	30	6.6	39	21	-3
Thalamus	R	29	9.3	9	-24	12
Inferior parietal lobule	L	17	7.6	-42	-51	42
<b>Lateral parietal network</b>						
Supramarginal gyrus	L	2615*	19.1	-54	-27	33
Supramarginal gyrus	R		13.6	57	-30	33
Middle cingulate cortex	L	122	12.0	-6	0	42
Insula	R	108	10.1	42	-3	6
Insula	L	100	9.3	-42	-3	9
Inferior temporal gyrus	L	30	10.6	-54	-63	-12
Inferior temporal gyrus	R	25	10.0	54	-54	-6
Inferior frontal gyrus	L	27	9.2	-54	9	24
Inferior frontal gyrus	R	14**	8.0	54	9	24
<b>Medial parietal network</b>						
Cuneus	R	2445*	20.8	15	-69	33
Cuneus	L		15.5	-15	-69	36
Posterior cingulate cortex	R	210*	8.3	6	-42	24
Posterior cingulate cortex	L		8.0	-6	-45	18
Midbrain	M	22	8.4	0	-27	-9

One-sample t test,  $p < 0.05$ , FWE corrected. Note that only clusters including at least 15 voxels are listed. Anatomical locations and terms were derived from the Anatomy toolbox (Eickhoff et al., 2005). \*These voxels belong to a contiguous bilateral cluster. \*\*Although this cluster just missed the predefined threshold of 15 voxels, it was included in the table as it reflects the bilateral organization of the lateral parietal ICN.

0.05, FDR corrected; Fig. 2A). In stark contrast, 15 significant connections between the seven ICNs were present in the synesthetes (one-sample t tests, two-sided,  $p < 0.05$ , FDR corrected; Fig. 2B). Note that all significant connections observed in controls were also present in the synesthetes (Fig. 2A, B, black lines). Thus, the global functional network architecture in synesthesia consisted of the intrinsic nonsynesthetic network connectivity plus additional intrinsic connections (Fig. 2B, double lines). Specifically, the integration of the two visual ICNs into the network architecture was clearly different between controls and synesthetes: while the visual networks were only interconnected (and

**Table 3.** Within-network differences between synesthetes and controls

	Hemisphere	Cluster size (voxels)	Max. t value	MNI coordinates		
				x	y	z
<b>Synesthetes &gt; controls</b>						
Lateral visual network	R	5	4.46	15	-60	-3
Auditory network	L	3	5.47	-57	-9	3
Left frontoparietal network	L	2	4.62	-39	-27	18
	L	37	7.5	-6	21	45
	L	5	5.38	-33	0	60
	L	3	4.39	-39	33	15
Right frontoparietal network	R	17	6.4	42	12	39
Medial parietal network	R	13	5.25	24	6	54
Lateral parietal network	L	2	4.61	18	-57	33
	L	12	5.82	-33	-36	42
	L	2	5.02	-33	-39	48
<b>Controls &gt; synesthetes</b>						
Left frontoparietal network	L	6	4.91	-39	6	48
Right frontoparietal network	R	37	8.06	39	-42	36
	R	2	4.66	6	39	45

Please note that single voxels are not listed in the table. Also note that there was a higher significant FC in the medial visual network in synesthetes compared to controls, although limited to two single voxels. All reported results are significant at  $p < 0.05$  (FWE corrected).

not connected to any other ICN) in controls, these two networks were highly interconnected with the other ICNs in the grapheme–color synesthetes.

In addition to these global differences of the intrinsic network architecture between synesthetes and control subjects (i.e., three times more significant connections in the synesthetes), the direct group comparison revealed that two specific network connections were significantly stronger in the grapheme–color synesthetes (two-sample t tests, two-sided,  $p < 0.05$ , FDR corrected): these were the connections between the medial ( $p = 0.0024$ ) and lateral ( $p = 0.0022$ ) visual networks and the right frontoparietal network (Fig. 2B, gray lines). In addition, the connection between the lateral visual and auditory network showed a trend toward significance ( $p = 0.05$ ).

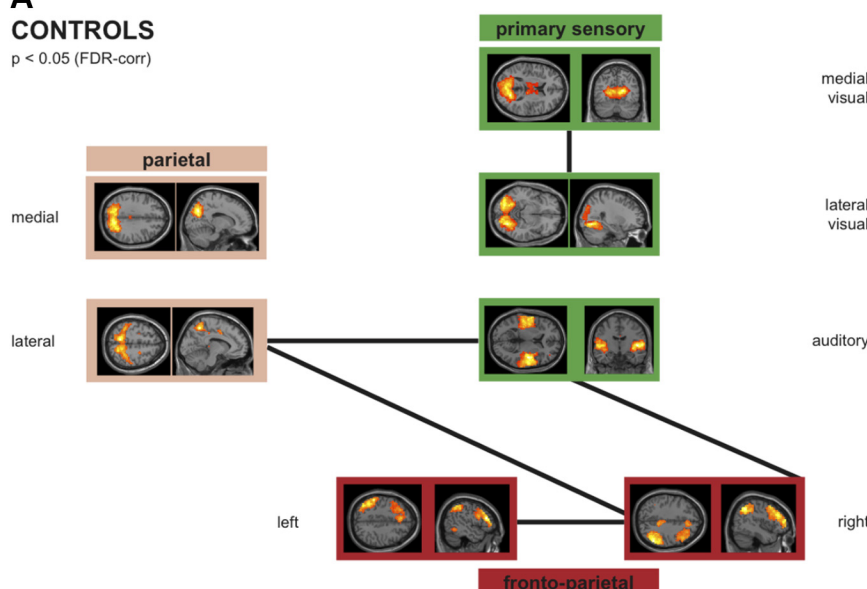
To test whether the increased FNC determined the consistency of synesthetic experiences, correlation analysis was performed with the individual consistency scores and the strength of the three functional network connections that differed between synesthetes and controls. In synesthetes, the connection strength of the lateral visual ICN with both the auditory ICN ( $p = 0.006$ ) and the right frontoparietal ICN ( $p = 0.03$ ) significantly correlated with the consistency scores (Fig. 2C). No significant correlation was found for the connection between the medial visual and right frontoparietal ICNs ( $p = 0.10$ ).

### Seed-based correlation analysis for the cytoarchitectonically defined color area V4

One-sample t tests based on the z-transformed individual FC maps revealed that in grapheme–color synesthetes, color area V4 showed a significant FC with other synesthesia-relevant regions, namely primary and secondary visual areas, auditory cortex bilateral, and right parietal cortex, while in control subjects, V4 was also functionally connected to primary and secondary visual areas but showed no FC with the auditory cortices and the right parietal cortex (Fig. 3; Table 4). Thus, the seed-based correlation analysis confirmed the FNC analysis results of a significantly increased intrinsic FC between the lateral visual network (including the color area V4) and the bilateral auditory network as well as the right frontoparietal network in synesthetes compared with controls (Fig. 2B). However, the differences in the seed-based correlation patterns between synesthetes and controls did not survive

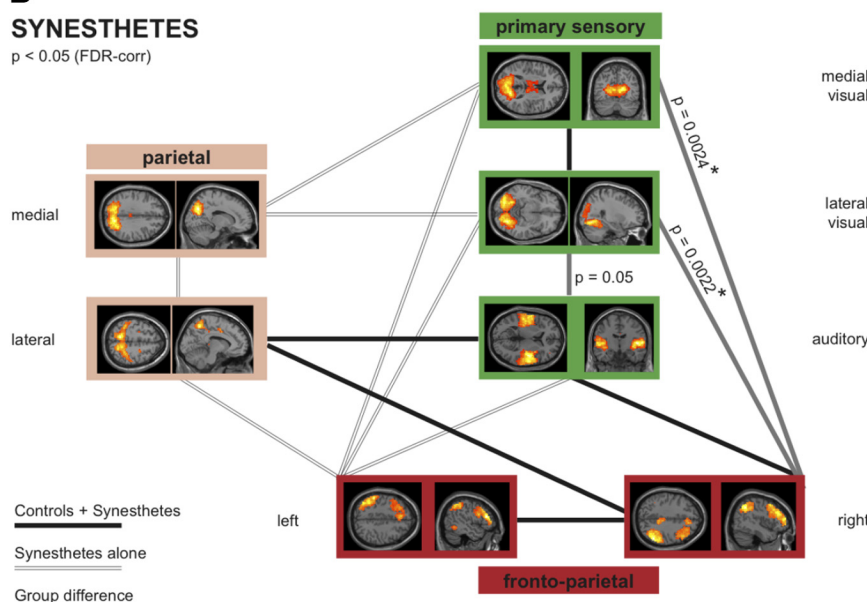
### A CONTROLS

$p < 0.05$  (FDR-corr)

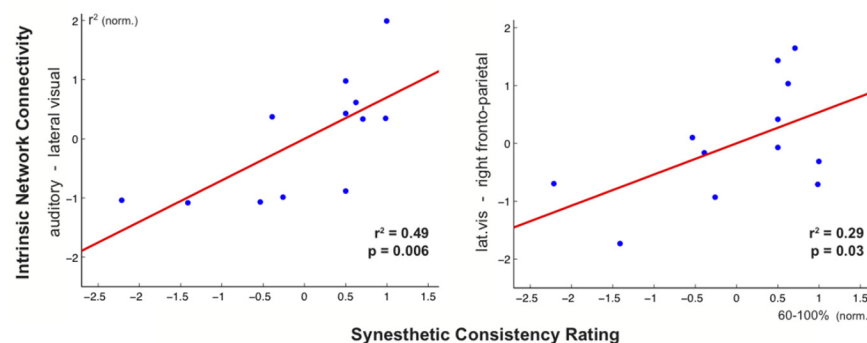


### B SYNESTHETES

$p < 0.05$  (FDR-corr)



### C Correlation between network connectivity and consistency of synesthesia



the predefined statistical threshold ( $p < 0.05$ , FWE corrected) when assessed by a two-sample  $t$  test.

### Discussion

Supporting neurobiological models of synesthesia that hypothesize increased connectivity in grapheme–color synesthetes (Hubbard and Ramachandran, 2005), the current rs-fMRI study reveals increased intrinsic functional connectivity in grapheme–color synesthetes, complementing earlier findings of increased structural connectivity in synesthesia (Rouw and Scholte, 2007). Our results thus complement the findings of previous studies in nonsynesthetes showing the structural correlates of intrinsic FC networks (Honey et al., 2007; Vincent et al., 2007). Moreover, our results are in line with a recent resting-state electroencephalography (EEG) study in which several synesthesia-relevant brain regions revealed stronger functional connectivity in lower frequencies of the theta and alpha band in colored–hearing synesthetes compared with nonsynesthetic control subjects (Jäncke and Langer, 2011). Such connectivity changes in the low-frequency band may well constitute the electrophysiological correlate for the low-frequency BOLD fluctuations in resting state fMRI data as suggested by simultaneous EEG–fMRI studies (Laufs et al., 2003; Van de Ville et al., 2010).

Applying a multiple spatial regression analysis to the combined group ICA,

←

consistency of synesthetic experiences. By means of multiple spatial regression analysis, the following seven synesthesia-relevant ICNs were selected for further correlation analyses in an automated manner: three primary sensory ICNs (medial and lateral visual network, auditory network), the right and left frontoparietal ICN, and the medial and lateral parietal ICNs. **A**, Significant pairwise correlations between the time courses of the ICNs in both groups are represented by thick black lines connecting the respective ICNs (one-sample  $t$  tests, two-sided,  $p < 0.05$ , FDR corrected). **B**, Additional significant connections in synesthetes are indicated by double lines (one-sample  $t$  tests, two-sided,  $p < 0.05$ , FDR corrected). Gray lines represent significant group differences, i.e., additional connections in synesthetes that are significantly stronger compared with the control group (two-sample  $t$  test, two-sided,  $p < 0.05$ , uncorrected; \* indicates group differences surviving FDR correction). **C**, Correlation analyses between the functional connectivity and the consistency of synesthetic experiences (using the normalized scores for the three functional connections that were significantly stronger in grapheme–color synesthetes and the normalized consistency scores) revealed a significant correlation between the synesthetic consistency scores and the intrinsic connectivity strength between the lateral visual and the auditory ICNs ( $r^2 = 0.49, p = 0.006$ , left) and the lateral visual and the right frontoparietal ICNs ( $r^2 = 0.29, p = 0.03$ , right).

**Figure 2.** **A, B**, Illustration of the intrinsic network architecture in controls (A) and synesthetes (B) composed of coherent, ongoing neuronal activity between seven synesthesia-relevant ICNs. **C**, Intrinsic network connectivity correlates with the

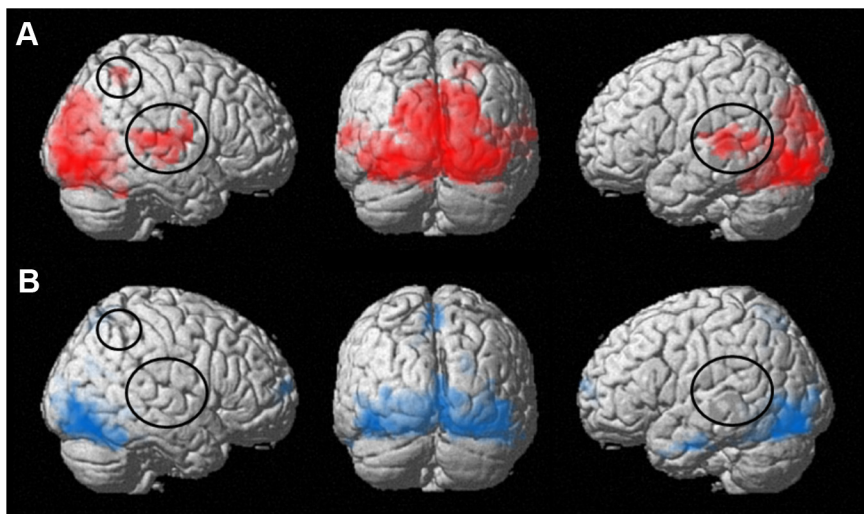


**Figure 3.** *A, B*, Surface renderings of brain regions functionally connected with bilateral color area V4 in grapheme–color synesthetes (*A*) and control subjects (*B*). The synesthesia-relevant brain regions (right parietal cortex and bilateral auditory cortices) that are functionally connected to color area V4 in synesthetes (*A*) but not control subjects (*B*) are circled. Please note that also the functional connectivity of V4 with other primary and secondary visual areas was more pronounced in synesthetes. All shown regions reached significance at  $p < 0.05$  (FWE corrected, extent threshold 50 voxels).

**Table 4. Regions functionally connected with bilateral color area V4 in synesthetes and controls**

	Hemi-sphere	Cluster size (voxels)	Max. t value	MNI coordinates		
				X	y	z
<b>Synesthetes</b>						
Primary and secondary visual cortex	L	4573*	32.67	-27	-87	-9
	R			27	-84	-9
Auditory cortex	L	250	17.74	-63	-36	3
	R	336	16.55	66	-21	6
Parietal cortex	R	58	13.40	24	-54	57
<b>Controls</b>						
Primary and secondary visual cortex	R	3506*	30.70	21	-87	-18
	L			-27	-66	-21
Medial frontal cortex	M	88	15.96	6	63	12
Inferior temporal cortex	L	136	15.49	-57	-9	-27
Cuneus	R	52	14.84	21	-72	27
Superior parietal cortex	M	132	14.37	0	-72	54

\*These voxels belong to a contiguous bilateral cluster. Note that the clusters in grapheme–color synesthetes are more extensive than in controls (Fig. 3). In contrast, control subjects show smaller, separable clusters.

we identified seven synesthesia-relevant ICNs whose intranetwork and internetwork connectivity was investigated. These seven ICNs were also identified in the separate within-group ICAs, indicating a homogenous distribution of the ICNs in synesthetes and controls. Consistent with the notion of functional hyperconnectivity in grapheme–color synesthesia, the direct group comparison of intranetwork connectivity differences revealed regions showing significantly stronger intrinsic FC in synesthetes than control subjects for all seven synesthesia-relevant ICNs. In contrast, only two ICNs (i.e., the left and right frontoparietal networks) contained regions with stronger FC in controls compared with synesthetes.

The finding of increased intranetwork connectivity in synesthetes is consistent with the results of a recent study by Hupé et al. (2011) that suggests that the joint coding of real and synesthetic colors is distributed rather than localized in the visual cortex. In fact, our findings are direct support for the assumption of Hupé et al. (2011) that “... if synesthetic experience relies on connecting regions together, it does not necessarily involve a stronger

BOLD response in any region but maybe subtle coactivations in distributed regions.” Thus, the current study strongly supports Hupé et al.’s hypothesis that “network analysis of brain connectivity appears then as a promising approach to elucidate principles underlying synesthesia” (Hupé et al., 2011, page 11).

With respect to the internetwork connectivity, the current study revealed increased global and specific intrinsic functional network connectivity in synesthetic subjects. Here, “global” refers to the overall increased amount of significant connections between the seven investigated ICNs in the group of synesthetic subjects compared with the nonsynesthetes. In contrast, “specific” refers to those connections for which a significant group difference was revealed, emphasizing the relevance of these specific connections in processing synesthetic experiences. With respect to the increased global intrinsic network connectivity in

grapheme–color synesthesia, it is remarkable that all (five) significant connections between the ICNs found in the control group were also present in the synesthetic subjects. This observation is in line with the notion that synesthetes are healthy subjects without any neurological or psychiatric disease (Hubbard, 2007), but are endowed with additional competences. The finding that the additional experiences of synesthetic subjects are associated with an increased functional network connectivity is also in line with a study by Jafri and colleagues (2008), who revealed an increased functional network connectivity of the default mode network in schizophrenic patients and speculated that this increased functional network connectivity was linked to their hallucinatory experiences. In contrast, reduced functional connectivity has been shown in patients with psychiatric deficits resulting in limited experiences [as in dementia (Greicius et al., 2004)]. However, with respect to this notion, the findings in the ICA literature are inconclusive as the opposite pattern, i.e., decreased functional connectivity in schizophrenia (Vercammen et al., 2010) and increased functional connectivity in dementia (Gour et al., 2011), has also been reported. Grapheme–color synesthetes showed not only a threefold increase of global intrinsic network connectivity compared with controls, but also specific (quantitative) differences in the intrinsic network connectivity: the two visual ICNs were significantly more strongly connected to the right-lateralized frontoparietal ICN in synesthetes compared with non-synesthetes. This is in accordance with the known role of frontoparietal networks in color-form binding for normal perception (Donner et al., 2002) and previous studies reporting attenuation of synesthetic binding following transcranial magnetic stimulation of the right parietal cortex (Esterman et al., 2006; Muggleton et al., 2007).

Moreover, the strength of the functional connectivity in the resting state between the lateral visual, auditory, and right frontoparietal ICN were associated with the individual consistency of the synesthetic experiences. Recently, different patterns of effective connectivity were shown to be associated with the type of grapheme–color synesthesia (van Leeuwen et al., 2011). In projectors, i.e., synesthetes experiencing the appearance of the synesthetic color in external space (colocalized with the induc-

ing grapheme), the cross-activation of V4 was elicited by a bottom-up pathway in the fusiform gyrus. In contrast, V4 cross-activation was evoked by a top-down process via the parietal lobe in associators, i.e., synesthetes who experience the synesthetic color internally, in their mind's eye. Together, these data suggest that the stability and characteristics of synesthetic experiences are reflected by the degree of functional connectivity at rest and effective connectivity during the performance of tasks inducing synesthetic color perceptions.

The seed-based correlation analysis revealed a significant functional connectivity of bilateral color area V4 with the auditory cortex bilaterally and the right parietal cortex in synesthetes but not in controls. Constituting an independent approach, the seed-based correlation analysis confirmed our findings of the FNC analysis of the seven synesthesia-relevant ICNs, as this analysis also revealed an increased internetwork connectivity between the lateral visual network (including color area V4) with the auditory network and the right frontoparietal network.

Although the converging results of the seed-based correlation and the FNC analyses show the potential of resting-state fMRI for assessing functional connectivity by different approaches, there are also limitations to this method. For example, some authors related the connectivity of networks covering midline and brainstem structures, at least in part, to pulsation artifacts (Birn et al., 2008). Moreover, it needs to be noted that during resting-state fMRI, sensory input (e.g., scanner noise) is present. Nevertheless, as our main findings are unrelated to midline or brainstem structures and our synesthetes did not report synesthetic experiences triggered by the scanner noise, it is unlikely that these aspects have confounded the current results.

Our data, together with previous data showing structural differences and differences in functional network characteristics between synesthetes and nonsynesthetes at rest (Rouw and Scholte, 2007, 2010; Jäncke et al., 2009; Weiss and Fink, 2009; Hänggi et al., 2011; Jäncke and Langer, 2011), indicate that there are general differences between the brains of synesthetes and nonsynesthetes even when no synesthesia-inducing stimuli are present. We suggest that these structural and functional differences predispose the synesthetes' brains to elicit synesthetic experience in response to particular inducer stimuli. One should keep in mind, however, that these structural and functional differences might occur as a result of the synesthetic experiences rather than causing them. The latter possibility can only be examined by longitudinal studies preferentially performed in synesthetic and nonsynesthetic children (Simner et al., 2009).

A further important step is to investigate the functional network architecture during the actual perception of synesthetic experiences. First evidence for increased functional connectivity in this context is provided by Specht and Laeng (2011), who showed an increased coherence of the color area V4 with a perceptual network during a single letter stroop task in two grapheme–color synesthetes (compared with 10 control subjects). Such task-related ICA analysis should be replicated in a larger group of synesthetes and should be complemented with an FNC analysis.

Our data on globally and specifically increased intrinsic network connectivity in grapheme–color synesthetes may help to inform the current debate whether hyperconnectivity in synesthesia occurs either locally, i.e., within circumscribed anatomical regions (Hubbard, 2007), or globally, i.e., widespread throughout the brain (Bargary and Mitchell, 2008). Previous studies investigating structural alterations in grapheme–color synesthetes provided (equivocal) evidence for either type of (structural) hyperconnectivity in synesthesia: structural differences between

synesthetes and controls emerged either at the local (Rouw and Scholte, 2007, 2010; Weiss and Fink, 2009) or at the global (Jäncke et al., 2009; Hänggi et al., 2011) level. Our functional connectivity data suggest that a combination of both models most appropriately characterizes grapheme–color synesthetes since they differ functionally from nonsynesthetes at both levels, i.e., at a global level (i.e., overall increased number of significant ICNs in synesthetes compared with controls) and a specific level (i.e., significantly increased FC between some specific ICNs). Furthermore, the current finding stress the importance of investigating both global and specific functional network connectivity in clinical populations to properly characterize the pathophysiological changes in the network architecture caused by schizophrenia, dementia, or other systemic diseases.

## References

- Bargary G, Mitchell KJ (2008) Synesthesia and cortical connectivity. *Trends Neurosci* 31:335–342.
- Baron-Cohen S, Harrison J, Goldstein LH, Wyke M (1993) Coloured speech perception: is synesthesia what happens when modularity breaks down? *Perception* 22:419–426.
- Birn RM, Murphy K, Bandettini PA (2008) The effect of respiration variations on independent component analysis results of resting state functional connectivity. *Hum Brain Mapp* 29:740–750.
- Biswal B, Yetkin FZ, Haughton VM, Hyde JS (1995) Functional connectivity in the motor cortex of resting human brain using echo-planar MRI. *Magn Reson Med* 34:537–541.
- Biswal BB, Mennes M, Zuo XN, Gohel S, Kelly C, Smith SM, Beckmann CF, Adelstein JS, Buckner RL, Colcombe S, Dogonowski AM, Ernst M, Fair D, Hampson M, Hoptman MJ, Hyde JS, Kiviniemi VJ, Kötter R, Li SJ, Lin CP, et al. (2010) Toward discovery science of human brain function. *Proc Natl Acad Sci U S A* 107:4734–4739.
- Calhoun VD, Adali T, Pearlson GD, Pekar JJ (2001) A method for making group inferences from functional MRI data using independent component analysis. *Hum Brain Mapp* 14:140–151.
- Damoiseaux JS, Rombouts SA, Barkhof F, Scheltens P, Stam CJ, Smith SM, Beckmann CF (2006) Consistent resting-state networks across healthy subjects. *Proc Natl Acad Sci U S A* 103:13848–13853.
- Donner TH, Kettermann A, Diesch E, Ostendorf F, Villringer A, Brandt SA (2002) Visual feature and conjunction searches of equal difficulty engage only partially overlapping frontoparietal networks. *Neuroimage* 15:16–25.
- Eickhoff SB, Stephan KE, Mohlberg H, Grefkes C, Fink GR, Amunts K, Zilles K (2005) A new SPM toolbox for combining probabilistic cytoarchitectonic maps and functional imaging data. *Neuroimage* 25:1325–1335.
- Erhardt EB, Rachakonda S, Bedrick EJ, Allen EA, Adali T, Calhoun VD (2011) Comparison of multi-subject ICA methods for analysis of fMRI data. *Hum Brain Mapp* 32:2075–2095.
- Esterman M, Verstynen T, Ivry RB, Robertson LC (2006) Coming unbound: disrupting automatic integration of synesthetic color and graphemes by transcranial magnetic stimulation of the right parietal lobe. *J Cogn Neurosci* 18:1570–1576.
- Fox MD, Raichle ME (2007) Spontaneous fluctuations in brain activity observed with functional magnetic resonance imaging. *Nat Rev Neurosci* 8:700–711.
- Gour N, Ranjeva JP, Ceccaldi M, Confort-Gouny S, Barbeau E, Soulier E, Guye M, Didic M, Felician O (2011) Basal functional connectivity within the anterior temporal network is associated with performance on declarative memory tasks. *Neuroimage* 58:687–697.
- Greicius MD, Srivastava G, Reiss AL, Menon V (2004) Default-mode network activity distinguishes Alzheimer's disease from healthy aging: evidence from functional MRI. *Proc Natl Acad Sci U S A* 101:4637–4642.
- Hänggi J, Wotruska D, Jäncke L (2011) Globally altered structural brain network topology in grapheme-color synesthesia. *J Neurosci* 31:5816–5828.
- Himberg J, Hyvärinen A, Esposito F (2004) Validating the independent components of neuroimaging time series via clustering and visualization. *Neuroimage* 22:1214–1222.
- Honey CJ, Kötter R, Breakspear M, Sporns O (2007) Network structure of cerebral cortex shapes functional connectivity on multiple time scales. *Proc Natl Acad Sci U S A* 104:10240–10245.

- Hubbard EM (2007) Neurophysiology of synesthesia. *Curr Psychiatry Rep* 9:193–199.
- Hubbard EM, Ramachandran VS (2005) Neurocognitive mechanisms of synesthesia. *Neuron* 48:509–520.
- Hubbard EM, Arman AC, Ramachandran VS, Boynton GM (2005) Individual differences among grapheme-color synesthetes: brain-behavior correlations. *Neuron* 45:975–985.
- Hupé JM, Bordier C, Dojat M (2011) The neural bases of grapheme-color synesthesia are not localized in real color-sensitive areas. *Cereb Cortex*. Advance online publication. Retrieved March 31, 2012. doi:10.1093/cercor/bhr236.
- Jafri MJ, Pearson GD, Stevens M, Calhoun VD (2008) A method for functional network connectivity among spatially independent resting-state components in schizophrenia. *Neuroimage* 39:1666–1681.
- Jäncke L, Langer N (2011) A strong parietal hub in the small-world network of coloured-hearing synaesthetes during resting state EEG. *J Neuropsychol* 5:178–202.
- Jäncke L, Beeli G, Eulig C, Hänggi J (2009) The neuroanatomy of grapheme–color synesthesia. *Eur J Neurosci* 29:1287–1293.
- Laufs H, Krakow K, Sterzer P, Eger E, Beyerle A, Salek-Haddadi A, Kleinschmidt A (2003) Electroencephalographic signatures of attentional and cognitive default modes in spontaneous brain activity fluctuations at rest. *Proc Natl Acad Sci U S A* 100:11053–11058.
- Lehrer S, Triebig G, Fischer B (1995) Multiple choice vocabulary test MWT as a valid and short test to estimate premorbid intelligence. *Acta Neurol Scand* 91:335–345.
- Muggleton N, Tsakanikos E, Walsh V, Ward J (2007) Disruption of synesthesia following TMS of the right posterior parietal cortex. *Neuropsychologia* 45:1582–1585.
- Nunn JA, Gregory LJ, Brammer M, Williams SC, Parslow DM, Morgan MJ, Morris RG, Bullmore ET, Baron-Cohen S, Gray JA (2002) Functional magnetic resonance imaging of synesthesia: activation of V4/V8 by spoken words. *Nat Neurosci* 5:371–375.
- Oldfield RC (1971) The assessment and analysis of handedness: the Edinburgh inventory. *Neuropsychologia* 9:97–113.
- Rouw R, Scholte HS (2007) Increased structural connectivity in grapheme–color synesthesia. *Nat Neurosci* 10:792–797.
- Rouw R, Scholte HS (2010) Neural basis of individual differences in synthetic experiences. *J Neurosci* 30:6205–6213.
- Schölvicck ML, Maier A, Ye FQ, Duyn JH, Leopold DA (2010) Neural basis of global resting-state fMRI activity. *Proc Natl Acad Sci U S A* 107:10238–10243.
- Simner J, Harrold J, Creed H, Monro L, Foulkes L (2009) Early detection of markers for synesthesia in childhood populations. *Brain* 132:57–64.
- Smith SM, Fox PT, Miller KL, Glahn DC, Fox PM, Mackay CE, Filippini N, Watkins KE, Toro R, Laird AR, Beckmann CF (2009) Correspondence of the brain's functional architecture during activation and rest. *Proc Natl Acad Sci U S A* 106:13040–13045.
- Song XW, Dong ZY, Long XY, Li SF, Zuo XN, Zhu CZ, He Y, Yan CG, Zang YF (2011) REST: a toolkit for resting-state functional magnetic resonance imaging data processing. *PLoS One* 6:e25031.
- Sorg C, Riedl V, Mühlau M, Calhoun VD, Eichele T, Läer L, Drzezga A, Förstl H, Kurz A, Zimmer C, Wohlschläger AM (2007) Selective changes of resting-state networks in individuals at risk for Alzheimer's disease. *Proc Natl Acad Sci U S A* 104:18760–18765.
- Specht K, Laeng B (2011) An independent component analysis of fMRI data of grapheme-colour synesthesia. *J Neuropsychol* 5:203–213.
- Van de Ville D, Britz J, Michel CM (2010) EEG microstate sequences in healthy humans at rest reveal scale-free dynamics. *Proc Natl Acad Sci U S A* 107:18179–18184.
- van Leeuwen TM, den Ouden HE, Hagoort P (2011) Effective connectivity determines the nature of subjective experience in grapheme-color synesthesia. *J Neurosci* 31:9879–9884.
- Vercammen A, Knegteling H, den Boer JA, Liemburg EJ, Aleman A (2010) Auditory hallucinations in schizophrenia are associated with reduced functional connectivity of the temporo-parietal area. *Biol Psychiatry* 67:912–918.
- Vincent JL, Patel GH, Fox MD, Snyder AZ, Baker JT, Van Essen DC, Zempel JM, Snyder LH, Corbetta M, Raichle ME (2007) Intrinsic functional architecture in the anaesthetized monkey brain. *Nature* 447:83–86.
- Weiss PH, Fink GR (2009) Grapheme-colour synesthetes show increased grey matter volumes of parietal and fusiform cortex. *Brain* 132:65–70.
- Weiss PH, Shah NJ, Toni I, Zilles K, Fink GR (2001) Associating colours with people: a case of chromatic-lexical synesthesia. *Cortex* 37:750–753.
- Weiss PH, Zilles K, Fink GR (2005) When visual perception causes feeling: enhanced cross-modal processing in grapheme–color synesthesia. *Neuroimage* 28:859–868.

**10 Paper 4: Selective changes of resting-state networks in individuals at risk for Alzheimer's disease**  
**(PNAS 2007)**

## Selective changes of resting-state networks in individuals at risk for Alzheimer's disease

Christian Sorg<sup>\*†</sup>, Valentin Riedl<sup>‡§</sup>, Mark Mühlau<sup>‡</sup>, Vince D. Calhoun<sup>¶||</sup>, Tom Eichele<sup>\*\*</sup>, Leonhard Läer<sup>††</sup>, Alexander Drzezga<sup>††</sup>, Hans Förstl<sup>\*</sup>, Alexander Kurz<sup>\*</sup>, Claus Zimmer<sup>††</sup>, and Afra M. Wohlschläger<sup>††††</sup>

Departments of <sup>\*</sup>Psychiatry, <sup>†</sup>Neurology, <sup>‡</sup>Nuclear Medicine, <sup>§</sup>Neuroradiology, and <sup>¶</sup>Nuclear Medicine, Klinikum Rechts der Isar, Technische Universität München, Ismaningerstrasse 22, 81675 Munich, Germany; <sup>||</sup>MIND Institute, 1101 Yale Boulevard, Albuquerque, NM 87131; <sup>\*\*</sup>Department of Electrical and Computer Engineering, University of New Mexico, Albuquerque, NM 87131; <sup>\*\*</sup>Cognitive Neuroscience Group, Faculty of Psychology, University of Bergen, Jonas Lies Vei 91, 5011 Bergen, Norway; and <sup>††</sup>Munich Center for Neurosciences, Brain and Mind, Ludwig-Maximilians Universität; Grosshadernerstrasse 2, 82152 Martinsried, Germany

Edited by Leslie G. Ungerleider, National Institutes of Health, Bethesda, MD, and approved September 25, 2007 (received for review September 17, 2007)

**Alzheimer's disease (AD) is a neurodegenerative disorder that prominently affects cerebral connectivity.** Assessing the functional connectivity at rest, recent functional MRI (fMRI) studies reported on the existence of resting-state networks (RSNs). RSNs are characterized by spatially coherent, spontaneous fluctuations in the blood oxygen level-dependent signal and are made up of regional patterns commonly involved in functions such as sensory, attention, or default mode processing. In AD, the default mode network (DMN) is affected by reduced functional connectivity and atrophy. In this work, we analyzed functional and structural MRI data from healthy elderly ( $n = 16$ ) and patients with amnestic mild cognitive impairment (aMCI) ( $n = 24$ ), a syndrome of high risk for developing AD. Two questions were addressed: (i) Are any RSNs altered in aMCI? (ii) Do changes in functional connectivity relate to possible structural changes? Independent component analysis of resting-state fMRI data identified eight spatially consistent RSNs. Only selected areas of the DMN and the executive attention network demonstrated reduced network-related activity in the patient group. Voxel-based morphometry revealed atrophy in both medial temporal lobes (MTL) of the patients. The functional connectivity between both hippocampi in the MTLs and the posterior cingulate of the DMN was present in healthy controls but absent in patients. We conclude that in individuals at risk for AD, a specific subset of RSNs is altered, likely representing effects of ongoing early neurodegeneration. We interpret our finding as a proof of principle, demonstrating that functional brain disorders can be characterized by functional-disconnectivity profiles of RSNs.

default mode network | intrinsic brain activity | mild cognitive impairment

**A**lzheimer's disease (AD) is a neurodegenerative disorder clinically characterized by progressive dementia and neuropsychiatric symptoms (1). AD is neuropathologically defined by tau pathology and amyloid aggregations (2). Tau pathology starts in regions of the medial temporal lobe (MTL) and is well correlated with cell loss and atrophy; amyloid deposition primarily affects distributed neocortical regions but is not especially prominent in the MTL (2, 3). Atrophy of the MTL is correlated with the degree of dementia and also the extent of temporoparietal hypometabolism; both results are assumed to reflect changes in cerebral connectivity, especially between the MTL and the neocortex (3–5). In non-human primates, prominent structural connectivity between the MTL and neocortical regions as well as broad neocortical hypometabolism after ablation of parts of the MTL were demonstrated (6, 7). Evidence for disrupted structural and functional connectivity (FC) further suggests that AD includes a disconnection syndrome (5, 8–10).

Mild cognitive impairment (MCI) is a syndrome with cognitive decline greater than expected for an individual's age and educational level but not interfering notably with activities of daily living; prevalence of MCI is  $\approx 15\%$  in adults older than 65 years; more than half of patients with MCI progress to dementia within 5 years; the amnestic subtype of MCI has a high risk of

progression to AD constituting a prodromal stage of AD (1, 11, 12). Previous results of task-related functional MRI (fMRI) in patients with MCI (13, 14) indicate that FC seems to be already impaired in prodromal stages of AD (15). Reduced white matter volumes of the MTL in amnestic MCI (aMCI) point at changed MTL–neocortex connectivity (16). Very recent fMRI studies in AD reported on FC changes especially during rest (5, 9, 17). Together, these findings suggest that the functional integration of brain areas in the cerebral resting state in individuals at risk for AD is disturbed and that functional changes are related to MTL atrophy.

The study of intrinsic brain activity may be central for understanding the physiology of functional brain disorders (5, 18–20). Functional brain disorders such as AD, schizophrenia, or autism are characterized by structural alterations that are subtle or have an uncertain relationship to clinical symptoms (21). Such structural lesions might be functionally related to alterations of intrinsic brain activity that are reflected by changes of connectivity (18, 19). Here, the study of spontaneous coherent fluctuations of the blood oxygen level-dependent (BOLD) signal at rest by fMRI is of special interest. Synchronized BOLD fluctuations overlap with brain systems that are involved in functions such as motor, sensory, language, attention, or default mode processing (22–28). Evidence for the neuronal nature of so-called resting state networks (RSNs) comes from studies that employ simultaneous fMRI and electroencephalograms (EEGs) (29, 30), from the observation of altered connectivity caused by neurological diseases (5), and from the existence of homologous RSNs in non-human primates that overlap with neuroanatomically defined systems (31).

Regions including the posterior cingulate, inferior parietal, and medial prefrontal cortex, constitute a RSN called default mode network (DMN) (32, 33). The areas of the DMN show consistently greater BOLD activity during rest than during any attention-demanding task, a phenomenon called deactivation; the same regions are prominently involved in episodic memory processes together with the MTL; their spontaneous fluctuations at rest are anticorrelated to the spontaneous fluctuations of a widely distributed neocortical system that largely overlaps with attention-related RSNs (5, 22, 27, 28, 32, 34–36). In AD, parietal

---

Author contributions: C.S. and V.R. contributed equally to this work; C.S., A.D., H.F., A.K., and A.M.W. designed research; C.S., L.L., H.F., A.K., C.Z., and A.M.W. performed research; V.D.C. and T.E. contributed new reagents/analytic tools; C.S., V.R., M.M., and A.M.W. analyzed data; and C.S., V.R., and A.M.W. wrote the paper.

The authors declare no conflict of interest.

This article is a PNAS Direct Submission.

Freely available online through the PNAS open access option.

<sup>†</sup>To whom correspondence should be addressed. E-mail: c.sorg@lrz.tum.de.

This article contains supporting information online at [www.pnas.org/cgi/content/full/0708803104/DC1](http://www.pnas.org/cgi/content/full/0708803104/DC1).

© 2007 by The National Academy of Sciences of the USA

**Table 1. Subject demographic information**

Parameter	NC	MCI
n	16	24
Age, years	68.1 ± 3.8	69.3 ± 8.1
Sex, male/female	10/6	13/11
Education, </>12 years	10/6	14/10
CDR, sum of boxes	0 ± 0	2.2 ± 0.9*
MMSE	29.6 ± 0.5	27.7 ± 1.1*
CERAD (delayed recall)	7.4 ± 1.3	4.3 ± 2.1*

Data are presented as mean ± SD. NC, normal control; CDR, Clinical Dementia Rating scale; MMSE, Mini-Mental State Exam; CERAD, Consortium to Establish a Registry for Alzheimer's Disease. \*, P < 0.05 difference between groups.

regions of the DMN demonstrate altered functional connectivity at rest within the DMN itself, to the MTL, and to neocortical areas that are involved in attention processes (5, 9, 17). Accounting for these findings, the hypothesis suggested above of altered FC at rest in individuals at high risk for AD can be specified in terms of RSNs with a focus on FC changes in the DMN and attention-related RSNs. In general, the finding of RSNs allows for a broadened perspective on functional brain disorders in the field of neuroimaging: the brain shows rich intrinsic dynamics in absence of tasks, with external stimuli more modulating than determining brain activity (19, 20, 27, 31, 37); the plurality of RSNs reflects this structured intrinsic activity, and selective changes of RSNs may characterize traits and states of functional brain disorders such as AD (18, 19, 21, 26).

Most previous studies investigating RSNs have used region-of-interest (ROI)-based correlation analyses (9, 17, 22–24). The signal time course of a selected ROI is correlated with remaining brain areas, resulting in a ROI specific correlation map. More recently, instead of defining *a priori* spatial hypotheses, a number of studies used model-free approaches involving independent component analysis (ICA) to describe RSNs in rest-fMRI data (5, 25, 26, 30). ICA allows for the extraction of distinct spatiotemporal patterns by identifying spatially independent and temporally synchronous brain regions (38).

In the present work, we combined ICA and ROI-based correlation methods to investigate RSNs in patients with aMCI. We focused on the following questions: (i) Are any RSNs changed in aMCI compared with healthy elderly? (ii) Are there any volumetric changes in the patient group pointing at possible ongoing neurodegeneration? (iii) How are potential functional and structural changes related with respect to their spatial extent?

We examined 24 patients and 16 healthy elderly (Table 1). Participants were instructed to close their eyes and relax during 4 min of fMRI scanning. Rest-fMRI data were analyzed by using a group ICA approach involving subject-wise concatenation of the individual fMRI data sets and subsequent back-projection into subject space (15, 39). Voxel-based morphometry (VBM) of additional structural MRI data and ROI-based correlation analyses of the rest-fMRI data were performed to analyze possible causes of altered functional connectivity.

## Results

**RSNs in Healthy Elderly and Patients with aMCI.** The ICA was performed employing a group ICA model for fMRI data (GIFT).<sup>§§</sup> After the IC estimation on the subject-wise concatenated data, the toolbox performs the analysis in three stages: data reduction through principal component analysis (PCA),

ICA decomposition of aggregate data, and subsequent back-reconstruction of individual subject maps and time courses (39, 40). Results of the separate analyses for each study group are depicted in Fig. 1 [see also *Supporting Information (SI) Table 2*]. Each group IC image contains a pair of two spatial IC patterns that are correlated (red) or anticorrelated (blue) with the time course of the component (data not shown). In the corresponding glass brain projection, the result of a one-sample *t* test for the back-reconstructed individual subject IC patterns across both groups is shown [ $P < 0.05$  false discovery rate (FDR) corrected for multiple comparisons]. Eight IC patterns represented functionally relevant RSNs as described previously (26). Both IC patterns of Fig. 1e/E and f/F were pairwise anticorrelated within one IC. The first two IC patterns of Fig. 1 partly coincide with the visual cortex: a/A covers inferior parts of the occipital cortex such as the striate area [Brodmann area (BA) 17/18]; b/B shows lateral and dorsal parts of the occipital gyrus (BA 19). The transverse (BA 41) and superior temporal gyrus (BA 22/42) of the auditory cortex are depicted in Fig. 1c/C. Fig. 1d/D represents a right lateralized frontoparietal network comprising the supramarginal gyrus (BA 39/40), middle temporal gyrus (BA 21), and middle frontal gyrus (BA 8) on the right side as well as bilateral frontal areas covering middle and inferior frontal gyrus (BA 8/9/46). This network is consistent with a ventral/reorienting attention network (34).

In Fig. 1e/E the upper IC pattern covers medial and lateral parts of the superior parietal lobe as well as the precuneus (BA 7). This network is constituted by areas well known to be active during spatial attention (41). The anticorrelated network of Fig. 1e/E (blue) includes a number of areas relevant for sensorimotor coordination in pre- and postcentral gyri (BA 3/4), the caudal zone of the cingulate motor cortex (BA 24), and parts of the superior frontal gyrus (BA 8) (41). The upper IC pattern of Fig. 1f/F includes medial prefrontal areas (BA 9/10/11), anterior (BA 12/32), and posterior cingulate cortex (PCC) (BA 23/31), the inferior temporal gyrus (BA 21), and bilateral supramarginal gyrus (BA 39) in the parietal lobe. This pattern corresponds to the DMN (26, 32, 42). Involvement of the hippocampus (HC), as seen by Greicius *et al.* (5), was not observed here. The anticorrelated network of Fig. 1f/F covers the superior parietal lobe (BA 7/40), V5/MT, and inferior temporal gyrus (BA 37), as well as parts of the inferior frontal gyrus mainly on the right side. These areas comprise a dorsal/executive attention network (34).

**Altered RSNs in Patients with aMCI.** The second analysis aimed at between-group differences in corresponding RSNs. We performed a two-sample *t* test on each of the eight RSNs contrasting the individual, back-reconstructed IC patterns of both groups. The only contrasts revealing any group difference concerned both IC patterns of Fig. 1f/F and are shown in Fig. 2 ( $P < 0.05$ , FDR corrected). None of the two-sample *t* tests on the five remaining components revealed significant group difference at  $P < 0.001$ , uncorrected for multiple comparisons (cluster extent threshold, 15 voxels). The following areas of the DMN associated IC pattern demonstrated reduced component time course-related activity in the patient group (see also *SI Table 3*): left PCC (BA 31), right medial prefrontal cortex (BA 10), and two small clusters in parietal cortex bilaterally (BA 39). Accordingly, we found reduced activity in the patient group in bilateral superior parietal lobes (BA 7, 40) and in the right prefrontal cortex, namely precentral (BA 4) and inferior frontal gyrus (BA 9) of the anticorrelated IC pattern of Fig. 1f/F.

**Patients with aMCI Have Reduced Gray Matter Volume in the Medial Temporal Lobes.** To assess possible causes of reduced functional connectivity, we analyzed our data for structural differences between both study groups. Neither the analyses of global volumes of gray matter (GM) and white matter (WM) nor the

<sup>§§</sup>Correa, N., Adali, T., Li, Y., and Calhoun, V. D. (2005) in Proceedings of the IEEE Conference on Acoustics, Speech, Signal Processing, Philadelphia, PA, pp. 401–404.

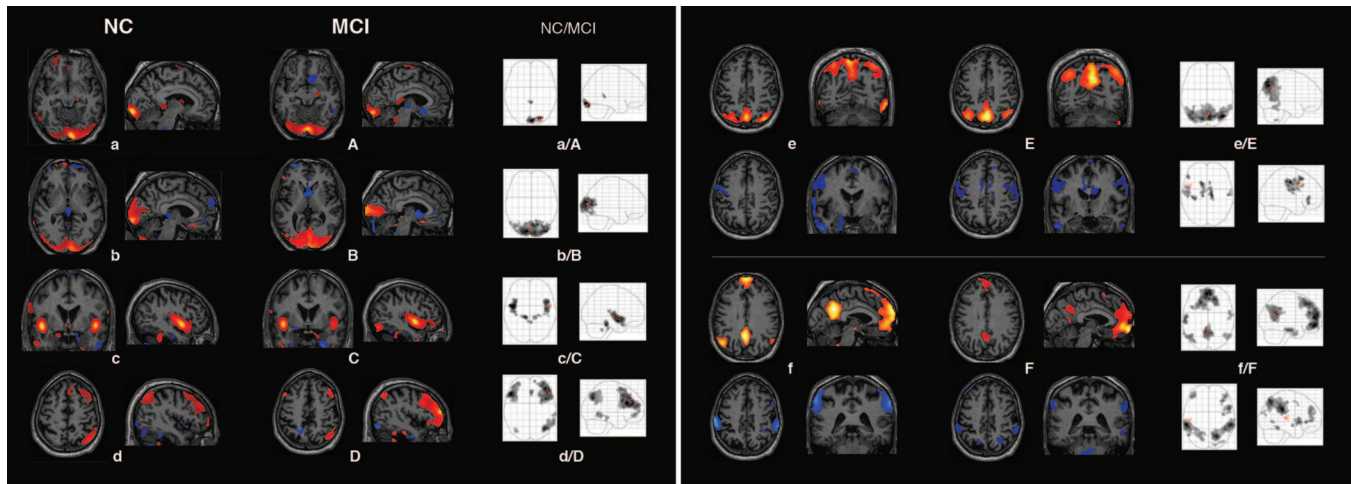


**Fig. 1.** RSNs of normal controls (a–f) and patients with aMCI (A–F). Each group IC image contains a pair of two spatial IC patterns that are correlated (red) or anticorrelated (blue) with the time course of the component (data not shown). (a/A–d/D) Each pair of IC patterns is shown within one brain image. (e/E and f/F) Each upper row represents the correlated IC pattern, each lower row the anticorrelated one. IC patterns are superimposed on a single-subject high-resolution T1 image. The black to yellow/light blue color scale represents z values, ranging from 1.8 to 8.0. Glass brain projections illustrate results of one-sample *t* tests on the individual back-reconstructed subject IC patterns across both groups ( $P < 0.05$ , FDR-corrected). (a/A–d/D) One-sample *t* test on the anticorrelated individual subject IC patterns provided no significant results. In axial view the right hemisphere is displayed on the right. NC, normal controls.

voxel-wise analysis of WM revealed significant differences. However, the voxel-wise analysis of GM revealed GM loss bilaterally in the MTL including the HC, the thalamus, the insular cortex, as well as in patches within the inferior parietal lobe (Fig. 3). These findings comply with previous reports on subtle abnormalities in structural brain images of patients with aMCI (16, 43). These areas did not overlap with those regions found to be altered in RSNs of the patient group.

**At-Rest Coactivation of HC and PCC Is Absent in Patients with aMCI.** To examine the relation of neocortical disconnectivity and MTL atrophy we investigated the functional connectivity between the

HC and the RSNs with ROI correlation analyses. We hypothesized reduced coactivation of HC and PCC of the DMN in the patient group. The PCC is the central region of the posterior DMN that is primarily affected by AD-associated alterations such as hypometabolism or elevated atrophy rate; impaired PCC–MTL connectivity is assumed to be the main cause for prominent metabolic PCC changes in AD (3–7, 17). We computed the pairwise correlations between the time courses from each HC and the PCC cluster which was identified by ICA. The average correlation between left/right HC and PCC was  $z = 0.37/0.30$ , SE = 0.08/0.08 in the control group and  $z = -0.03/-0.09$ , SE = 0.10/0.08 in the patient group. We found significant group differences for each HC ( $P = 0.04/0.02$ , Bonferroni-

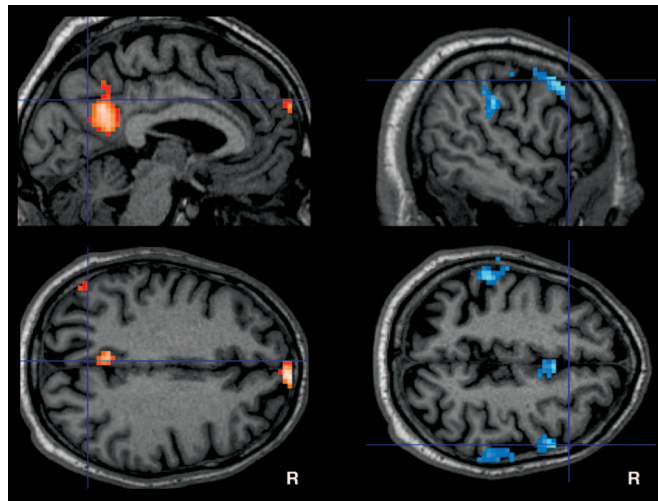


**Fig. 2.** Contrasts of RSNs between normal controls and patients with aMCI. (Left) Maps corresponding to DMNs of Fig. 1f/F, *Upper*. (Right) Maps corresponding to executive attention networks of Fig. 1f/F, *Lower*. Color maps represent significant ( $P < 0.05$ , FDR-corrected) voxels of higher component-related activity in controls compared with patients. Corresponding *t* values are color-coded with black to yellow (from 0 to 5.0) to light blue (from 0 to 6.2). Maps are superimposed on a single-subject high-resolution T1 image. The patient group did not show any significant higher activation for DMN and executive attention network. For all remaining RSNs of Fig. 1, two-sample *t* tests did not reveal any significant difference between the two groups. R, right hemisphere.

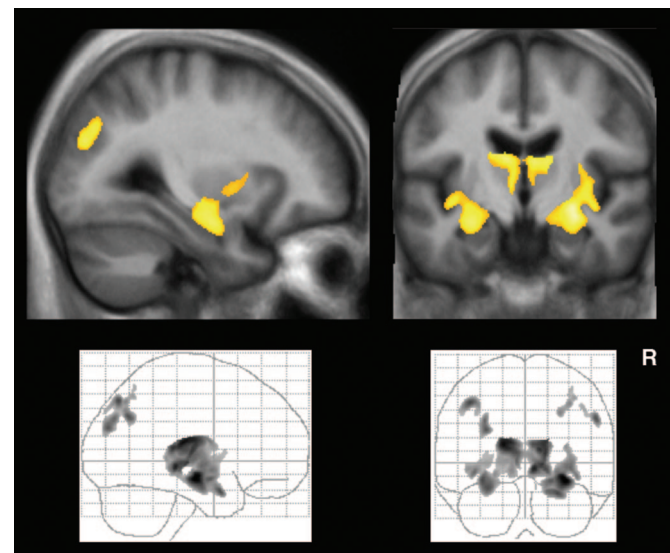


**Fig. 3.** Color maps showing significant ( $P < 0.05$ , FDR-corrected) voxels of decreased GM in aMCI compared with controls superimposed on sagittal and coronal slices transformed in standard MNI space. Corresponding *t* values are color-coded with black to yellow (from 0 to 6.3). The distribution of the complete regional pattern of decreased GM in patients is represented by glass brain projections.

corrected) by applying an analyses of covariance, which included corresponding HC volume as covariate. The correlation between left and right HC did not differ significantly between healthy controls ( $z = 0.76$ , SE = 0.10) and patients ( $z = 0.62$ , SE = 0.08) in a two-sample  $t$  test. To evaluate the degree of functional coactivation of the HCs and any RSN, we separately correlated the time courses of each HC with the time course of each RSN across all subjects. The strongest and only significant effect was found between left HC and the DMN ( $z = 0.13$ , SE = 0.06,  $P = 0.003$ , Bonferroni-corrected, one-sample  $t$  test), indicating relevant functional integration of the HC and the DMN during rest (5).

## Discussion and Conclusion

In this work we investigated spatiotemporal patterns of hemodynamic activity during relaxed wakefulness and underlying brain volumes in healthy elderly and patients with amnestic MCI. By applying ICA, VBM, and ROI-based correlation analyses, we characterized eight RSNs that were spatially consistent across subjects and corresponded with functionally relevant patterns. Areas of the DMN and the executive attention network showed diminished functional connectivity in patients, whereas the respective volumes remained unaffected. Atrophy was found for both MTLs, including HCs in the patient group. Functional connectivity between both HCs and left PCC of the DMN was absent in patients. These results suggest that in aMCI a selected subset of RSNs is affected by altered functional connectivity, likely representing effects of early neurodegeneration.

**Selectively Altered RSNs in Patients with aMCI.** Our data suggest that disconnection phenomena associated with prodromal stages of AD are specific to a subset of RSNs whereas other networks remain unaffected. By applying ICA in patients with aMCI, we found left PCC and right medial prefrontal cortex of the DMN as well as bilateral superior parietal lobes and bilateral inferior frontal gyri of the executive attention network to be selectively affected (Fig. 2). Regions of the affected RSNs did not differ significantly in volumetric aspects between the two groups, confirming the functional nature of the observed alterations (Fig. 3). Our finding concerning the DMN is consistent with previous results demonstrating altered deactivation in regions of the DMN in MCI (44). The areas constituting the DMN and the executive attention network also seem to be involved in early changes of AD: In patients at risk for AD activity of the PCC or superior parietal cortex is changed during memory or executive attention-related tasks, respectively (14, 15). In mild AD, these regions show changed functional connectivity at rest (5, 9) and overlap with regional patterns of atrophy, glucose hypometabolism, and hypoperfusion (for overview, see ref. 3). Also, regions showing early amyloid deposition overlap with posterior parts of the default mode and executive attention network (2, 3, 45). In summary, our result of selective changes of RSNs in individuals at risk for AD corresponds very well with changes that have previously only been described in AD.

Changes of the MTL are discussed as a possible factor causing neocortical disconnectivity in AD (2, 4, 5, 7). The HC and posterior parts of the DMN display coherent spontaneous activity at rest (36) and constitute an episodic memory network that is linked to successful recollection (35). Functional connectivity of the HC with neocortical areas, especially with the PCC, is reduced in AD during rest (17). The VBM analysis (Fig. 3) demonstrated reduced GM within the MTL in the patient group. This finding is in line with previous results for aMCI (16, 43) and points to MTL neurodegeneration (3) as well as impaired MTL—neocortex connectivity (16). Our ROI correlation analysis revealed that both HCs show significantly reduced functional connectivity with the left PCC of the DMN in patients compared with controls. Among all RSNs, the DMN was functionally most

strongly related to the HC at rest. This relation was demonstrated by the only significant correlation between left HC and DMN across all subjects, which is in line with previous results (5, 36). Taken together, the presented results indicate relevant functional integration of the HC in the DMN at rest as well as an impaired HC–parietal memory system in aMCI.

We conclude that the selectively changed functional connectivity of RSNs in individuals at high risk for AD reflects altered connectivity between the MTL and neocortical areas (4, 5, 7, 9, 15, 44). Apparently, MTL—neocortex disconnectivity is related to neurodegeneration, which is expressed by MTL atrophy (16). In addition to FC changes in the DMN, our result also points to relevant functional disconnectivity of the executive attention network, which is in line with observed attentional deficits in MCI and AD (9, 14, 15). This finding indicates impaired interaction between these two anticorrelated networks that prominently organize intrinsic brain activity (9, 22, 28). Finally, our work suggests that rest-fMRI has the potential for the evaluation of connectivity in patients at risk for AD for diagnostic purposes; one possible way would be to use ICA-derived patterns to define ROIs where FC analysis can classify patients from controls. We are currently in the process of assessing symptom progression in our patients in a two-year follow-up examination where FC analysis might provide a more accurate way to evaluate the risk of conversion to dementia for individual patients than neuropsychological testing and structural imaging alone.

**RSNs and Functional Brain Disorders.** In this work we identified spatially consistent RSNs across both study groups that match previous results (22, 24, 26, 46). Damoiseaux *et al.* (26) evaluated the spatial consistency of RSNs and found a set of 10 reliably detectable RSNs across subjects and sessions. Although we changed many parameters such as ICA model, age, and health condition of participants, the regional patterns of detected RSNs show large regional concordance with their findings. Identified RSNs can be divided into two groups. The spatial patterns of the first group (Fig. 1 a/A, b/B, c/C, and e/E) are associated with sensory or sensorimotor functions, characterized in several previous studies (23, 24, 46, 47). The remaining networks encompass regions involved in higher cognitive functions (34, 35, 41, 48, 49). The bilateral posterior parietal network of map e/E including precuneus and intraparietal sulcus is known to be associated with spatial attention processes (41). This network is anticorrelated to the RSN of map e/E representing regions normally involved in sensorimotor integration; areas of both networks are part of a functional system participating in goal-directed movement coordination (41). The spatial pattern of Fig. 1f/F (*Upper*) covers areas of the DMN; this network is suggested to support default mode function, such as maintaining a background level of attention for the detection of salient events by monitoring internal and external environment (49). Evidence increases that large parts of the posterior DMN together with the hippocampal system are associated with autobiographical and prospective memory processing (35, 36, 50). Both the network of Fig. 1f/F (*Lower*), involving bilateral superior parietal cortex, intraparietal sulcus, and inferior frontal gyrus, and the right lateralized frontoparietal network of Fig. 1d/D overlap with the regions of the dorsal/executive and ventral/reorienting attention systems (34). The dorsal attention system is assumed to be involved in top-down direction of attention, and the ventral system, lateraled to the right, supports reorienting of attention in response to salient stimuli (27). Rest fluctuations of the two systems, which are considered member of a group of areas routinely exhibiting task-related activation, are anticorrelated to spontaneous BOLD fluctuations of the DMN, demonstrated by ROI-based methods (22, 28). Using ICA, we found the anticorrelated coupling of the DMN limited to the dorsal attention network. Our result is supported by the finding that the two attention networks can be distinguished by their spontaneous rest activity (27); it seems plausible that a system concerned with attentional shifts in response to salient external

stimuli is less strongly connected to introspectively oriented default mode processing during rest than a system involved in goal-directed orienting of attention.

In summary, we identified eight distinct, partly anticorrelated, and spatially consistent RSNs in healthy elderly and patients with aMCI. The division of the rest-related BOLD signal into separate RSNs presumably reflects the functional organization of brain activity into stabilized functional-anatomical systems (18, 19, 31). Regarding the synchronicity of spontaneous BOLD fluctuations during rest, pathology-induced changes seem to exist also in patients with autism, schizophrenia, attention deficit hyperactivity disorder, or major depression (51–54). Taking into account these findings and our result of selective changes of RSNs in aMCI, we suggest that rest-fMRI and especially RSNs constitute very promising tools for the functional characterization of functional brain disorders, for intergroup comparisons, and possibly with some potential for assessing functional connectivity on a single-subject level.

## Materials and Methods

Subject data and ICA of rest-fMRI data are described below. Detailed information regarding ROI-based correlation analyses of fMRI data and VBM analysis of structural MRI data can be found in *SI Materials and Methods*.

**Subjects and Task.** Sixteen healthy controls (6 female, ages 63–73 years) and 24 patients (11 female, ages 58–80 years) diagnosed with aMCI participated in the study. All subjects provided informed consent in accordance with the Human Research Committee guidelines of the Klinikum Rechts der Isar, Technische Universität, München. Patients were recruited from the Memory Clinic of the Department of Psychiatry, controls by word-of-mouth advertising. Examination of every subject included medical history, neurological examination, informant interview (only for patients), neuropsychological assessment [CERAD battery, Consortium to Establish a Registry for AD (55)], structural MRI, and for patients additional blood tests. Patients met criteria for aMCI which contain reported and neuropsychologically assessed memory impairments, largely intact activities of daily living, and excluded dementia (Table 1) (11). Exclusion criteria for entry into the study were other neurological, psychiatric, or systemic diseases (e.g., stroke, depression, alcoholism), or clinically remarkable MRI (e.g., stroke lesions) which could be related to cognitive impairment. Five controls and nine patients were treated for hypertension ( $\beta$ -blockers, angiotensin-converting enzyme inhibitors, and calcium channel blockers), and six controls and eight patients were treated for hypercholesterolemia (statins). None of the subjects had diabetes mellitus. None of the subjects or patients received psychotropic medication, especially cholinesterase inhibitors.

All subjects underwent 4 min of resting-state scan first followed by an attention and a memory task, which are not discussed here. For the resting-state scan, subjects were instructed simply to keep their eyes closed, not to think of anything in particular, and not to fall asleep.

**Imaging Methods.** Imaging was performed on a 1.5T Siemens Symphony system. Functional data were collected by using a gradient echo EPI sequence (TE = 50 ms, TR = 3,000 ms, flip angle = 90°, FoV = 200 mm<sup>2</sup>, matrix = 64 × 64, 33 slices, slice thickness = 4 mm, and 0.4-mm interslice gap) (where TE is echo time, TR is repetition time, FoV is field of view, and T1 is inversion time) for a 4-min period resulting in a total of 80 volumes. The first three functional scans were discarded before the subsequent analysis. A T1-weighted anatomical dataset was obtained from each subject by using a magnetization-prepared rapid acquisition gradient echo sequence (TE = 3.93 ms, TR = 1,500 ms, TI = 760 ms, flip angle = 5°, FoV = 256 mm<sup>2</sup>, matrix = 256 × 256, 160 slices, voxel size = 1 × 1 × 1 mm<sup>3</sup>).

**Preprocessing.** Functional MRI data were preprocessed by using the Oxford Centre for Functional Magnetic Resonance Imaging of the Brain Software Library (FMRIB; FSL version 3.2), statistical parametric mapping (Wellcome Department of Cognitive Neurology; SPM5), and in-house software for Matlab (MathWorks).

In a first step, nonbrain structures were removed from the echo planar imaging volumes. Next we performed a mean-based intensity normalization of all slices within a volume by the same factor (56). Data were then motion-corrected, spatially normalized into the stereotactic space of the Montreal Neurological Institute (MNI), and spatially smoothed with an 8 × 8 × 8 mm Gaussian kernel with SPM5. Before they were entered into the ICA, a voxel-wise transformation was applied on the time course data  $y_{ijk}(t)$ ,  $\hat{y}_{ijk}(t) = [y_{ijk}(t) - \langle y_{ijk} \rangle] / \sigma_{ijk}$  (for each voxel:  $t$ , time;  $i, j, k$ , three directions in space;  $\langle y_{ijk} \rangle$ , mean;  $\sigma_{ijk}$  standard deviation). This procedure removed any systematic, between-group differences with respect to BOLD amplitudes from the four-dimensional data set  $\hat{y}_{ijk}(t)$ . Sensitivity for variance correlation was thereby rendered independently of variance magnitude.

**ICA.** We performed the ICA by using group ICA for fMRI toolbox (GIFT version 1.3b; icatb.sourceforge.net)<sup>§§</sup> established for the analysis of fMRI data (15, 39, 54). The toolbox supports a group ICA approach, which first concatenates the individual data across time, followed by the computation of the subject-specific components and time courses. For each of the two study groups the toolbox performed the analysis in three stages: (i) data reduction, (ii) application of the ICA algorithm, and (iii) back-reconstruction for each individual subject (39).

In the first step (i), data from each subject were reduced by using PCA, whereby computational complexity was reduced and most of the information content of the data was preserved. After concatenating the resulting volumes, the number of independent sources was estimated by the GIFT dimensionality estimation tool based on the aggregated data: 28/31 ICs for the control/patient group (57). The final reduction step according to the selected number of components was achieved by PCA again. In the second stage of the analysis (ii) we chose the Infomax algorithm for running the proper IC analysis and a GM mask based on all subjects. In the final stage of back-reconstruction (iii), time courses and spatial maps were computed for each subject. After back-reconstruction, the mean spatial maps of each group were transformed to z scores for display (39). Before any statistics were applied to the individual subject maps, the initially calculated scaling factor  $\sigma_{ijk}$  was reintegrated into the data by voxel-wise multiplication.

Each IC contains a pair of two spatial IC patterns that are correlated or anticorrelated to the time course of the component. Upon visual inspection, eight IC patterns were located in the cortex and represented functionally relevant RSNs as described previously (26, 46). The remaining IC patterns were attributed to two major forms of artifacts: IC patterns representing tissue border artifacts near the ventricular system, the skull, and cerebrospinal fluid space or IC patterns with main activation in midbrain structures below  $z = -20$  (MNI) in axial slices burdened by major vessel artifacts and lack of reliability in EPI scans. Individual subject IC patterns representing RSNs were entered into one- and two-sample random-effects analyses in SPM5. Results were thresholded at  $P < 0.05$ , FDR-corrected for multiple comparisons. The between-group two-sample  $t$  tests were masked with a within-group mask thresholded at  $P < 0.05$ , uncorrected.

We thank two reviewers for constructive suggestions. This work was supported by the German Federal Ministry of Education and Research Grant 01EV0710 and by Kommision für Klinische Forschung, Klinikum Rechts der Isar, München Grant 8765160.

1. Blennow K, de Leon MJ, Zetterberg H (2006) *Lancet* 368:387–403.
2. Braak H, Braak E (1991) *Acta Neuropathol* 82:239–259.
3. Buckner RL, Snyder AZ, Shannon BJ, LaRossa G, Sachs R, Fotenos AF, Sheline YI, Klunk WE, Mathis CA, Morris JC, et al. (2005) *J Neurosci* 25:7709–7717.
4. Meguro K, LeMestric C, Landeau B, Desgranges B, Eustache F, Baron JC (2001) *J Neurol Neurosurg Psychiatry* 71:315–321.
5. Greicius MD, Srivastava G, Reiss AL, Menon V (2004) *Proc Natl Acad Sci USA* 101:4637–4642.
6. Lavenex P, Suzuki WA, Amaral DG (2002) *J Comp Neurol* 447:394–420.
7. Blaizot X, Meguro K, Millien I, Baron JC, Chavoix C (2002) *J Neurosci* 22:9166–9170.
8. Van Hoesen GW (1997) *J Neuropsychiatry Clin Neurosci* 9:331–341.
9. Wang K, Liang M, Wang L, Tian L, Zhang X, Li K, Jiang T (2007) *Hum Brain Mapp* 28:967–978.
10. Delbeuck X, Van der Linden M, Collette F (2003) *Neuropsychol Rev* 13:79–92.
11. Gauthier S, Reisberg B, Zaudig M, Petersen RC, Ritchie K, Broich K, Belleville S, Brodaty H, Bennett D, Chertkow H, et al. (2006) *Lancet* 367:1262–1270.
12. Petersen RC, Smith GE, Waring SC, Ivnik RJ, Tangalos EG, Kokmen E (1999) *Arch Neurol* 56:303–308.
13. Dickerson BC, Salat DH, Greve DN, Chua EF, Rand-Giovannetti E, Rentz DM, Bertram L, Mullin K, Tanzi RE, Blacker D, et al. (2005) *Neurology* 65:404–411.
14. Dannhauser TM, Walker Z, Stevens T, Lee L, Seal M, Shergill SS (2005) *Brain* 128:1418–1427.
15. Celone KA, Calhoun VD, Dickerson BC, Atri A, Chua EF, Miller SL, DePeau K, Rentz DM, Selkoe DJ, Blacker D, et al. (2006) *J Neurosci* 26:10222–10231.
16. Stoub TR, DeToledo-Morrell L, Stebbins GT, Leurgans S, Bennett DA, Shah RC (2006) *Proc Natl Acad Sci USA* 103:10041–10045.
17. Wang L, Zang Y, He Y, Liang M, Zhang X, Tian L, Wu T, Jiang T, Li K (2006) *NeuroImage* 31:496–504.
18. Buckner RL, Vincent JL (2007) *NeuroImage* 37:1091–1096.
19. Fox MD, Raichle ME (2007) *Nat Rev Neurosci* 8:700–711.
20. Raichle ME, Mintun MA (2006) *Annu Rev Neurosci* 29:449–476.
21. Matthews PM, Honey GD, Bullmore ET (2006) *Nat Rev Neurosci* 7:732–744.
22. Fox MD, Snyder AZ, Vincent JL, Corbetta M, Van Essen DC, Raichle ME (2005) *Proc Natl Acad Sci USA* 102:9673–9678.
23. Hampson M, Peterson BS, Skudlarski P, Gatenby JC, Gore JC (2002) *Hum Brain Mapp* 15:247–262.
24. Biswal B, Yetkin FZ, Haughton VM, Hyde JS (1995) *Magn Reson Med* 34:537–541.
25. Beckmann CF, Smith SM (2004) *IEEE Trans Med Imaging* 23:137–152.
26. Damoiseaux JS, Rombouts SA, Barkhof F, Scheltens P, Stam CJ, Smith SM, Beckmann CF (2006) *Proc Natl Acad Sci USA* 103:13848–13853.
27. Fox MD, Corbetta M, Snyder AZ, Vincent JL, Raichle ME (2006) *Proc Natl Acad Sci USA* 103:10046–10051.
28. Fransson P (2005) *Hum Brain Mapp* 26:15–29.
29. Laufs H, Kleinschmidt A, Beyerle A, Eger E, Salek-Haddadi A, Preibisch C, Krakow K (2003) *NeuroImage* 19:1463–1476.
30. Mantini D, Perrucci MG, Del Gratta C, Romani GL, Corbetta M (2007) *Proc Natl Acad Sci USA* 104:13170–13175.
31. Vincent JL, Patel GH, Fox MD, Snyder AZ, Baker JT, Van Essen DC, Zempel JM, Snyder LH, Corbetta M, Raichle ME (2007) *Nature* 447:83–86.
32. Raichle ME, MacLeod AM, Snyder AZ, Powers WJ, Gusnard DA, Shulman GL (2001) *Proc Natl Acad Sci USA* 98:676–682.
33. Raichle ME, Snyder AZ (2007) *NeuroImage* 37:1083–1090.
34. Corbetta M, Shulman GL (2002) *Nat Rev Neurosci* 3:201–215.
35. Shannon BJ, Buckner RL (2004) *J Neurosci* 24:10084–10092.
36. Vincent JL, Snyder AZ, Fox MD, Shannon BJ, Andrews JR, Raichle ME, Buckner RL (2006) *J Neurophysiol* 96:3517–3531.
37. Buzsaki G, Draguhn A (2004) *Science* 304:1926–1929.
38. Calhoun VD, Adali T (2006) *IEEE Eng Med Biol Mag* 25:79–90.
39. Calhoun VD, Adali T, Pearlson GD, Pekar JJ (2001) *Hum Brain Mapp* 14:140–151.
40. Schmithorst VJ, Holland SK (2004) *J Magn Reson Imaging* 19:365–368.
41. Grefkes C, Fink GR (2005) *J Anat* 207:3–17.
42. De Luca M, Beckmann CF, De Stefano N, Matthews PM, Smith SM (2006) *NeuroImage* 29:1359–1367.
43. Whitwell JL, Petersen RC, Negash S, Weigand SD, Kantarci K, Ivnik RJ, Knopman DS, Boeve BF, Smith GE, Jack CR, Jr (2007) *Arch Neurol* 64:1130–1138.
44. Rombouts SA, Barkhof F, Goekoop R, Stam CJ, Scheltens P (2005) *Hum Brain Mapp* 26:231–239.
45. Klunk WE, Engler H, Nordberg A, Wang Y, Blomqvist G, Holt DP, Bergstrom M, Savitcheva I, Huang GF, Estrada S, et al. (2004) *Ann Neurol* 55:306–319.
46. Beckmann CF, Smith SM (2005) *NeuroImage* 25:294–311.
47. Xiong J, Parsons LM, Gao JH, Fox PT (1999) *Hum Brain Mapp* 8:151–156.
48. Alescio-Lautier B, Michel BF, Herrera C, Elahmadi A, Champon C, Touzet C, Paban V (2007) *Neuropsychologia* 45:1948–1960.
49. Gusnard DA, Raichle ME, Raichle ME (2001) *Nat Rev Neurosci* 2:685–694.
50. Addis DR, Wong AT, Schacter DL (2007) *Neuropsychologia* 45:1363–1377.
51. Cherckassky VL, Kana RK, Keller TA, Just MA (2006) *NeuroReport* 17:1687–1690.
52. Greicius MD, Flores BH, Menon V, Glover GH, Solvason HB, Kenna H, Reiss AL, Schatzberg AF (2007) *Biol Psychiatry* 62:429–437.
53. Liang M, Zhou Y, Jiang T, Liu Z, Tian L, Liu H, Hao Y (2006) *NeuroReport* 17:209–213.
54. Garrity AG, Pearlson GD, McKiernan K, Lloyd D, Kiehl KA, Calhoun VD (2007) *Am J Psychiatry* 164:450–457.
55. Morris JC, Heyman A, Mohs RC, Hughes JP, van Belle G, Fillenbaum G, Mellits ED, Clark C (1989) *Neurology* 39:1159–1165.
56. Manjaly ZM, Marshall JC, Stephan KE, Gurd JM, Zilles K, Fink GR (2003) *NeuroImage* 19:674–683.
57. Li YO, Adali T, Calhoun VD (2007) *Hum Brain Mapp* 28:1251–1266.

## Supporting Information

### Materials and Methods

#### *Data analysis: VBM*

For statistical comparison of the anatomical T1-weighted images VBM2 software (<http://dbm.neuro.uni-jena.de/vbm>), an extension of SPM2 software (<http://www.fil.ion.ucl.ac.uk/spm>), was used. VBM2 applies the “optimized” protocol (1, 2) and, additionally, a hidden Markov random field model (3). We used study-specific prior probability maps and a Gaussian kernel of 8 mm for smoothing. Global volumes of gray matter (GM), white matter (WM), and cerebrospinal fluid (CSF) were derived from the non-normalized segmented images as provided by SPM2 after the first segmentation process. Total intracranial volume (TIV) was approximated by the sum of the global volumes of GM, WM, and CSF. To correct for head size, brain tissue fractions of FGM, FWM, and FCSF were calculated by dividing the respective volumes by the TIV. For group comparisons of global values, 2-sided independent t-tests were performed. Differences between groups at a level of  $p < 0.05$  were regarded as significant. For the voxel-wise analysis of GM, we applied an analysis of covariance (ANCOVA) and included gender, age, and the global GM volume as nuisance variables. White matter reportedly is not dependent on these covariates therefore analysis was performed as Analysis of Variance (ANOVA) (1, 2) with  $p < 0.05$ . We included only voxels with a GM value greater than 0.1 (maximum value: 1) to avoid possible edge effects around the border between GM, WM, and CSF. We applied a height threshold of  $p < 0.05$ , FDR corrected, corresponding to a voxel level of  $p < 0.001$  uncorrected and an extent threshold of  $p < 0.05$  family wise error (FWE) corrected corresponding to a cluster extent of 542 contiguous voxels.

#### *Data analysis: ROI-based correlation analysis*

Data were preprocessed as described in Methods with two additional steps: After smoothing and before variance normalising data were low-pass filtered ( $f < 0.1$  Hz) and mean signal values which were calculated by averaging over the gray matter mask were removed for each group. These procedures eliminate any systematic fluctuations not involved in specific regional correlations. Three ROIs were created: The ROIs for the left and right HC were derived from the automated anatomical labeling ROI library (4); the most significant cluster from the between-group two-sample t-test of the DMN of our ICA approach which was centred in the left posterior cingulate provided the third ROI (see Results). For the correlation analysis between left/right HC and left posterior cingulate voxelwise BOLD time courses for each ROI were extracted and first eigenvectors of each ROI were computed. Then correlation coefficients for each pair of ROIs were calculated. Temporal correlation coefficients were converted to z values by using Fischer's r-to-z transformation. This transformation generates values that are approximately normally distributed. Afterwards data from patients and healthy controls concerning the HC-PCC correlation were entered into corresponding ANCOVAs with HC volumes as covariates and results were Bonferroni corrected. HC volumes were derived from the VBM analysis. The significance for the correlation between both HCs was tested in a two-sample t-test. For the analysis of the functional integration of the HC into any RSN the time courses of each IC representing a RSN were extracted using the group ICA for fMRI toolbox (GIFT, see Results). Correlation analyses for both HC and each RSN were performed separately as described above for pairwise ROI correlation analysis. After using Fischer's r-to-z transformation data of all subjects were entered into a one-sample random-effects analysis and results were Bonferroni corrected.

## References

1. Ashburner, J. & Friston, K. J. (2000) *Neuroimage* **11**, 805-821.
2. Good, C. D., Johnsrude, I. S., Ashburner, J., Henson, R. N., Friston, K. J., & Frackowiak, R. S. (2001) *Neuroimage* **14**, 21-36.
3. Cuadra, M. B., Cammoun, L., Butz, T., Cuisenaire, O., & Thiran, J. P. (2005) *IEEE Trans Med Imaging* **24**, 1548-1565.
4. Tzourio-Mazoyer, N., Landeau, B., Papathanassiou, D., Crivello, F., Etard, O., Delcroix, N., Mazoyer, B., & Joliot, M. (2002) *Neuroimage* **15**, 273-289.

**Table 2. Peak foci for ICs d/D to f/F corresponding to Figure 1**

lobe	voxels	anatomy	BA	L/R	z-score	peak x;y;z
<b>IC d/D</b>						
frontal	1524	middle frontal gyrus	8, 9, 46	R	5.85	[42;42;24]
				R	5.61	[42;12;30]
		inferior frontal gyrus		R	5.20	[45;48;-6]
	73	medial frontal gyrus	8	R	4.87	[3;30;42]
	655	middle frontal gyrus	9, 46	L	6.09	[-48;27;24]
					4.69	[-42;45;15]
					4.65	[-45;18;39]
temporal	126	middle temporal gyrus	21	R	4.67	[63;-54;-3]
					4.18	[66;-30;-15]
parietal	522	supramarginal gyrus	39, 40	R	5.60	[39;-69;39]
					4.28	[54;-57;27]
					3.96	[48;-48;54]
	30	supramarginal gyrus	39	L	3.93	[-36;-78;45]
					3.62	[-39;-69;39]
<b>IC e/E</b>						
<b>time-course correlated IC-pattern (red)</b>						
parietal	3454	superior parietal lobe, precuneus	7	L/R	6.10	[39;-72;42]
					5.73	[6;-75;48]
					5.54	[-12;-81;51]
	78	MT +	19	L	4.12	[-48;-60;-15]
	59		19	R	3.29	[54;-54;-18]
	22	cerebellum		R	4.01	[6;-54;-51]

<b>time-course anti-correlated IC-pattern (blue)</b>						
frontal	375	cingular motor cortex, caudal zone	24	L/R	5.39	[12;-15;42]
		superior frontal gyrus	8	L	4.87	[-15;15;51]
					4.67	[-12;-18;21]
	239	post- /precentral gyrus	3/4	L	4.67	[-33;-27;45]
					4.43	[-51;-9;39]
	51	post- /precentral gyrus	3/4	R	4.22	[57;-15;39]
					3.79	[63;-6;36]
	22	anterior cingulate cortex, caudal zone	24	R	4.13	[6;18;33]
	50	inferior frontal gyrus	47	L	4.67	[-51;33;0]
<b>IC f/F</b>						
<b>time-course correlated IC-pattern (red)</b>						
frontal	2510	orbital gyrus, superior frontal gyrus	11	L/R	6.53	[-3;51;-9]
		anterior cingulate	12			
		superior frontal gyrus	10		6.32	[6;51;12]
		anterior cingulate	32			
		superior frontal gyrus	9		5.96	[-18;27;48]
temporal	125	middle temporal gyrus	21	L	5.58	[-60;-15;-21]
					5.35	[-60;-24;-21]
	97			R	4.44	[57;-3;-30]
					4.10	[63;-6;-21]
parietal	805	posterior cingulate	31	L/R	6.09	[-6;-51;24]
		posterior cingulate	30		5.10	[-6;-57;6]
	253	supramarginal gyrus	39	L	4.71	[-45;-66;33]
					4.70	[-51;-66;24]
	137			R	4.33	[51;-69;30]
					4.19	[57;-60;21]
<b>time-course anti-correlated IC-pattern (blue)</b>						
frontal	173	inferior frontal gyrus, opercular part	44	R	5.18	[54;9;-3]
	178	inferior frontal gyrus, triangular part	9	R	5.00	[36;30;-3]
					4.57	[42;39;21]
					4.49	[45;45;0]
	130	inferior frontal gyrus		L	4.72	[-45;42;30]
					4.29	[-45;42;15]

	21	precentral gyrus	4	R	3.96	[54;9;45]
					3.60	[51;0;54]
temporal	47	inferior temporal gyrus	37	L	4.63	[-48;-48;-15]
	21	insula		R	4.22	[39;-9;-9]
	40	inferior temporal gyrus	37	R	3.91	[54;-51;-12]
					3.84	[42;-51;-15]
	28	V5/MT		L	4.26	[-54;-63;0]
parietal	1164	superior parietal lobe	7, 40	R	5.69	[18;-66;54]
		intraparietal sulcus			5.67	[57;-36;33]
					5.09	[42;-45;36]
	945	superior parietal lobe	7, 40	L	6.16	[-60;-33;33]
					5.42	[-54;-42;39]
					4.89	[-60;-45;30]

**Table 3. Peak foci of brain regions showing higher activation in the control group in the default mode and executive attention network (IC f/F in Fig.1) corresponding to Fig. 2**

lobe	voxels	anatomy	BA	L/R	z-score	peak x;y;z
<b>Default mode network</b>						
frontal	48	superior frontal gyrus	10	R	4.33	[6;63;27]
parietal	126	posterior cingulate	31	L	4.47	[-6;-54;24]
					3.92	[0;-54;15]
	45	supramarginal gyrus	39	L	3.76	[-45;-69;36]
	20	supramarginal gyrus		R	3.26	[51;-66;33]
<b>Executive attention network</b>						
frontal	59	precentral gyrus	4	R	4.11	[45;3;57]
					4.07	[54;9;45]
					3.22	[54;-3;48]
	34	inferior frontal gyrus (triangular part)	9	R	3.81	[36;45;33]
					3.52	[33;51;27]
					2.95	[33;42;24]
	10	inferior frontal gyrus (opercular part)		R	3.20	[57;12;-6]
parietal	245	superior parietal lobe	7, 40	R	5.31	[63;-30;30]
					3.67	[57;-21;51]
					3.41	[66;-24;18]
	237	superior parietal lobe		L	4.87	[-63;-30;24]
					4.12	[-54;-30;48]
					3.68	[-60;-18;42]
	63	anterior cingulate	24	R	4.17	[3;12;48]
					3.72	[6;6;36]
					3.67	[9;0;48]

## 11 Paper 5: Increased intrinsic brain activity in the striatum reflects symptom dimensions in schizophrenia (Schizophr Bull 2012)

Schizophrenia Bulletin  
doi:10.1093/schbul/sbr184

# Increased Intrinsic Brain Activity in the Striatum Reflects Symptom Dimensions in Schizophrenia

**Christian Sorg<sup>1-3,†</sup>, Andrei Manoliu<sup>1,2,†</sup>, Susanne Neufang<sup>2</sup>, Nicholas Myers<sup>2,4</sup>, Henning Peters<sup>2</sup>, Dirk Schwerthöffer<sup>1</sup>, Martin Scherr<sup>1</sup>, Mark Mühlau<sup>5</sup>, Claus Zimmer<sup>2</sup>, Alexander Drzezga<sup>3</sup>, Hans Förstl<sup>1</sup>, Josef Bäuml<sup>1</sup>, Tom Eichele<sup>6,7</sup>, Afra M. Wohlschläger<sup>2,5</sup>, and Valentin Riedl<sup>2-5,\*</sup>**

<sup>1</sup>Department of Psychiatry, Klinikum rechts der Isar, Technische Universität München, Munich, Germany; <sup>2</sup>Department of Neuroradiology, Klinikum rechts der Isar, Technische Universität München, Ismaninger strasse 22, 81675 Munich, Germany; <sup>3</sup>Department of Nuclear Medicine, Klinikum rechts der Isar, Technische Universität München, Munich, Germany; <sup>4</sup>Munich Center for Neurosciences Brain and Mind, Ludwig-Maximilians-Universität München, Martinsried, Germany; <sup>5</sup>Department of Neurology, Klinikum rechts der Isar, Technische Universität München, Munich, Germany; <sup>6</sup>Department of Biological and Medical Psychology, University of Bergen, Bergen, Norway; <sup>7</sup>The Mind Research Network, Albuquerque, NM

†Both the authors equally contributed to the study.

\*To whom correspondence should be addressed; tel: 49-89-4140-7631, fax: 49-89-4140-7665, e-mail: valentin.riedl@mytum.de

**Striatal dysfunction is thought to be a fundamental element in schizophrenia. Striatal dopamine dysfunction impacts on reward processing and learning and is present even at rest. Here, we addressed the question whether and how spontaneous neuronal activity in the striatum is altered in schizophrenia. We therefore assessed intrinsic striatal activity and its relation with disorder states and symptom dimensions in patients with schizophrenia. We performed resting-state functional (rs-fMRI) and structural magnetic resonance imaging as well as psychometric assessment in 21 schizophrenic patients during psychosis. On average 9 months later, we acquired follow-up data during psychotic remission and with comparable levels of antipsychotic medication. Twenty-one age- and sex-matched healthy controls were included in the study. Independent component analysis of fMRI data yielded spatial maps and time-courses of coherent ongoing blood-oxygen-level-dependent signal fluctuations, which were used for group comparisons and correlation analyses with scores of the positive and negative syndrome scale. During psychosis, coherent intrinsic activity of the striatum was increased in the dorsal part and correlated with positive symptoms such as delusion and hallucination. In psychotic remission of the same patients, activity of the ventral striatum was increased and correlated with negative symptoms such as emotional withdrawal and blunted affect. Results were controlled for volumetric and medication effects. These data provide first evidence that in schizophrenia intrinsic activity is changed in the striatum and corresponds to disorder states and symptom dimensions.**

**Key words:** schizophrenia/psychosis/intrinsic brain activity/resting-state fMRI/striatum

## Introduction

Striatal dysfunction is thought to be a fundamental element in schizophrenia.<sup>1</sup> Especially, dopamine transmission in the striatum is increased during prodromal and psychotic states.<sup>2,3</sup> Such elevated dopamine levels correlate with positive disease symptoms and antidopaminergic drugs reduce these symptoms in most patients.<sup>4</sup>

It is still unclear, how striatal dopamine relates to brain activity in humans, but animal experiments revealed that increased dopamine modulates spontaneous activity in the striatum.<sup>5,6</sup> Furthermore, theoretical accounts suggest that changed spontaneous brain activity contributes to psychotic symptoms by worsening the signal-to-noise ratio (SNR) of evoked and intrinsic activity.<sup>7,8</sup> In particular, noisy striatal signals are assumed to contribute to aberrant salience processing and disrupted reinforcement learning that both underlie positive symptoms in schizophrenia such as delusions.<sup>9-11</sup>

These data suggest that an investigation of intrinsic brain activity in humans might help to better understand the pathophysiology of schizophrenia. Few studies reported on global connectivity changes in the intrinsic functional architecture of schizophrenic patients.<sup>12</sup> Others have concentrated on cortical networks of intrinsic activity and found distributed changes in frontal, temporal, and parietal cortices.<sup>13-16</sup> However, in vivo evidence for specifically altered intrinsic activity in the resting-state signal of the striatum is missing.

In order to test for aberrant intrinsic striatal activity, we measured ongoing hemodynamic signal fluctuations with fMRI during a 10-minutes rest period (rs-fMRI) in

**Table 1.** Demographic and Clinical Characteristics

Measure	HC (n = 21)	SP (n = 21)	SPR (n = 13)	SP (n = 21) vs HC (n = 21) <sup>a</sup>		SPR (n = 13) vs HC (n = 13) <sup>a</sup>		SP (n = 13) vs SPR (n = 13) <sup>b</sup>	
	Mean (SD)	Mean (SD)	Mean (SD)	T Score	P Value	T Score	P Value	T Score	P Value
Age	33.57 (13.6)	34.05 (12.27)	33.69 (10.53)	-0.121	0.904	-0.330	0.745		
Sex (male/female)	10/11	10/11	9/4						
PANSS									
Total	30.14 (0.65)	80.76 (20.77)	52.75 (13.93)	8.96	.000*	3.240	.004*	6.466	.000*
Positive	7.05 (0.22)	19.4 (6.09)	11.92 (3.63)	9.091	.000*	4.801	.000*	3.212	.008*
Negative	7.10 (0.44)	21.14 (8.20)	13.58 (5.63)	7.84	.000*	4.102	.000*	3.345	.007*
General	16.05 (0.22)	39.81 (11.06)	27.25 (8.30)	9.846	.000*	4.858	.000*	4.473	.001*
GAF	99.76 (1.09)	39.62 (11.68)	59.25 (14.44)	-23.492	.000*	-10.046	.000*	-3.627	.004*
CPZ		388.61 (384.67)	206.95 (189.67)					1.281	.227

Note: HC, healthy control group; SP, group of patients with schizophrenia during psychosis; SPR, group of patients with schizophrenia during psychotic remission; PANSS, Positive and Negative Syndrome Scale; GAF, Global Assessment of Functioning Scale; CPZ, chlorpromazine equivalent dose.

<sup>a</sup>Two-sample *t* test.

<sup>b</sup>Paired *t* test.

\*Significant for *P* < .05 corrected for multiple comparisons.

patients with schizophrenia and healthy controls (HCs). Patients were assessed during psychosis and during psychotic remission. We decomposed the rs-fMRI data with independent component analysis (ICA) into spatially independent maps of intrinsically coupled brain regions with associated blood-oxygen-level-dependent (BOLD) signal fluctuations.<sup>17</sup> From these spatial maps, we selected a previously described basal ganglia resting-state network (BGN) including the striatum.<sup>18</sup> Additionally, we selected any further intrinsic cortical network with striatal contributions. The ICA approach allows the simultaneous exploration of intrinsic connectivity changes of the striatum within several networks.<sup>19</sup> We controlled our analyses of intrinsic functional connectivity for medication effects and structural changes.

We addressed the following questions: (1) is intrinsic striatal activity changed in schizophrenia; (2) are potential changes modulated by psychosis, which is characterized by hyperdopaminergia<sup>1</sup>; and (3) are changes related to symptom dimensions of schizophrenia.

## Methods

### Participants and Task

Twenty-one patients and 21 HCs participated in the study (table 1). All participants provided informed consent in accordance with the Human Research Committee guidelines of the Klinikum Rechts der Isar, Technische Universität München. Patients were recruited from the Department of Psychiatry, Klinikum Rechts der Isar, TU München, controls by word of mouth advertising. Participants' examination included medical history, psychiatric interview,

psychometric assessment, and blood tests for patients (all performed by D.S. and M.S.). Psychiatric diagnoses were based on *Diagnostic and Statistical Manual of Mental Disorders, Fourth Edition* (DSM-IV).<sup>20</sup> The Structured Clinical Interview for DSM-IV (SCID-I German version) was used to assess the presence of psychiatric diagnoses. The severity of clinical symptoms was measured with the positive and negative syndrome scale (PANSS)<sup>21</sup> on the day of scanning. D.S. and M.S. have been professionally trained for SCID and PANSS-based interviews with interrater reliability for diagnoses and scores of more than 95%. The global level of social, occupational, and psychological functioning was measured with the Global Assessment of Functioning Scale.<sup>22</sup>

All patients were diagnosed with schizophrenia. Further inclusion criteria were an age between 18 and 60 years, current psychotic symptoms for the fMRI-session during psychosis (SP) and remission of psychotic symptoms (indicated by significantly decreased PANSS scores) for the fMRI-session during psychotic remission (SPR). Patients were inpatient during SP and ambulatory during SPR. On average about 9 months after psychosis ( $t_{\text{mean}} = 285.84$  days,  $SD = 167.66$ ), 13 of 21 patients approved a second investigation during remission. The 8 remaining patients that also were diagnosed as remitted from psychosis by external psychiatrists could not be convinced of an additional reexamination and rescanning. Importantly, the subsample of patients that was reexamined did not differ from the initial patient group with respect to demographical or medication parameters (table 1) but had significantly reduced PANSS scores.

Patients were free of any current or past neurological or internal systemic disorder, current depressive or manic

episode, substance abuse (except nicotine), and cerebral pathology in MRI. Three of 21 patients during psychosis and 4 of 13 patients during psychotic remission were free of antipsychotic medication. All other patients received mono- or dual therapy with atypical antipsychotic medication, including Aripiprazole (2 cases during SP/1 case during SPR), Olanzapine (11/1), Clozapine (4/3), Quetiapine (2/3), Ziprasidone (1/0), Risperidone (5/2), Aripiprazole (2/1), and Paliperidone (3/1) (see online supplementary table S1 for individual medication protocols and dosage; see also table 1 for mean chlorpromazine (CPZ) equivalent dose<sup>23</sup>). Importantly, CPZ did not differ significantly between SP and SPR. All controls were free of any current or past psychiatric, neurological or systemic disorder, or psychotropic medication.

All participants underwent 10 minutes of rs-fMRI with the instruction to keep their eyes closed and not to fall asleep. We verified that subjects stayed awake by interrogating via intercom immediately after the rs-fMRI scan. Before and after scanning, a medical examination of patients validated their stable condition and investigated whether they had feelings of odd situations during the scanning. No patient dropped out during the first scanning session. HCs were scanned only once to define the range of normal BGN coherence; thus, it was not possible to directly test for schizophrenia-specific changes between first and second scan. However, several independent rs-fMRI studies in HCs confirmed the consistency of rs-fMRI networks across days and months.<sup>24,25</sup>

#### *FMRI Data Acquisition and Analysis*

MRI was performed on a 3 T whole-body MR scanner (Achieva; Philips, Netherland) using an 8-channel phased-array head coil. For coregistration and volumetric analysis, T1-weighted anatomical data were obtained from each subject by using a magnetization-prepared rapid acquisition gradient echo sequence (echo time [TE] = 4 ms, time of repetition [TR] = 9 ms, inversion time [TI] = 100 ms, flip angle = 5°, field of view [FoV] = 240 × 240 mm<sup>2</sup>, matrix = 240 × 240, 170 slices, voxel size = 1 × 1 × 1 mm<sup>3</sup>). FMRI data were collected using a gradient echo planar imaging sequence (TE = 35 ms, TR = 2000 ms, flip angle = 82°, FoV = 220 × 220 mm<sup>2</sup>, matrix = 80 × 80, 32 slices, slice thickness = 4 mm, and 0 mm interslice gap; 10 minutes of scanning result in 300 volumes).

For each participant, the first 3 functional scans of each fMRI-session were discarded due to magnetization effects. Statistical parametric mapping 8 (SPM8) (Wellcome Department of Cognitive Neurology, London) was used for motion correction, spatial normalization into the stereotactic space of the Montreal Neurological Institute and spatial smoothing with an 8 × 8 × 8 mm Gaussian kernel. None of the participants had to be excluded due to excessive head motion (linear shift <3 mm across run and on a frame-to-frame basis, rotation <1.5°). We also verified nonsignificant differences in the SNR ratio of the fMRI

data between healthy subjects (mean: 47.27, SD: 10.79) and patient group (mean: 46.21, SD: 11.6) with  $P = .76$ .

Preprocessed data were decomposed into 40 spatial independent components within a group ICA framework,<sup>17</sup> which is based on the infomax algorithm and implemented in the GIFT-software (<http://icatb.sourceforge.net>). Dimensionality estimation was performed by using the minimum description length criteria and resulted in 40 components representing the mean of all individual estimates. Before volumes were entered into ICA analysis, voxel-wise  $z$ -transformation on time course data  $y_{ijk}(t)$  was applied by subtracting the mean  $\langle y_{ijk} \rangle$  and dividing by the SD  $\sigma_{ijk}(t) = (y_{ijk}(t) - \langle y_{ijk} \rangle) / \sigma_{ijk}$ ,  $t$  time, i,j,k directions in space). The sensitivity of the multivariate ICA algorithm for correlation of variance between voxels, ie, functional connectivity, was thereby rendered independent of the original BOLD signal magnitude across subjects. Data were concatenated and reduced by 2-step principal component analysis, followed by independent component estimation with the infomax algorithm. We subsequently ran 40 ICA (ICASSO) to ensure stability of the estimated components. This results in a set of average group components, which are then back reconstructed into single-subject space. We then applied a multiple spatial regression with a mask containing caudate nucleus and putamen to the 40 independent components to automatically select those including the striatum (figure 1, supplementary figure S1 and tables S2 and S3). The mask was generated with the WFU-Pickatlas (<http://www.fmri.wfubmc.edu/>). Before we entered the individual's spatial maps into second-level statistics, we reintegrated the initially calculated scaling factor  $\sigma_{ijk}$  into the data by voxel-wise multiplication in order to preserve each individual's profile of variance magnitude while leaving the normalized time course component unchanged.<sup>26</sup>

To statistically evaluate spatial maps of selected independent components (ICs), we calculated voxel-wise one-sample  $t$  tests on participants' reconstructed spatial maps for each group and session, using SPM8 ( $P < .05$ , false discovery rate [FDR], figure 1). To analyze group effects, participants' spatial maps were entered into two-sample  $t$  tests with striatal volumes as covariate of no interest when comparing patients with HC ( $P < .05$  FDR-corrected, figure 2, supplementary table S4). To evaluate the temporal aspect of selected ICs, we investigated the frequency distribution of each IC's time course. The power spectral density of each participant's time course for each session was calculated and then averaged across frequencies ranging from 0.01 to 0.1 Hz. Differences across groups were assessed by using two-sample  $t$  tests (supplementary figure S2).

The relation between striatal activity and symptom dimensions was studied within a region of interest (ROI)-based approach. ROI-restricted  $z$  scores (derived from subjects' BGN-ICs) were partially correlated with PANSS scores in patients with striatal volume and antipsychotic medication CPZ as regressors of no interest

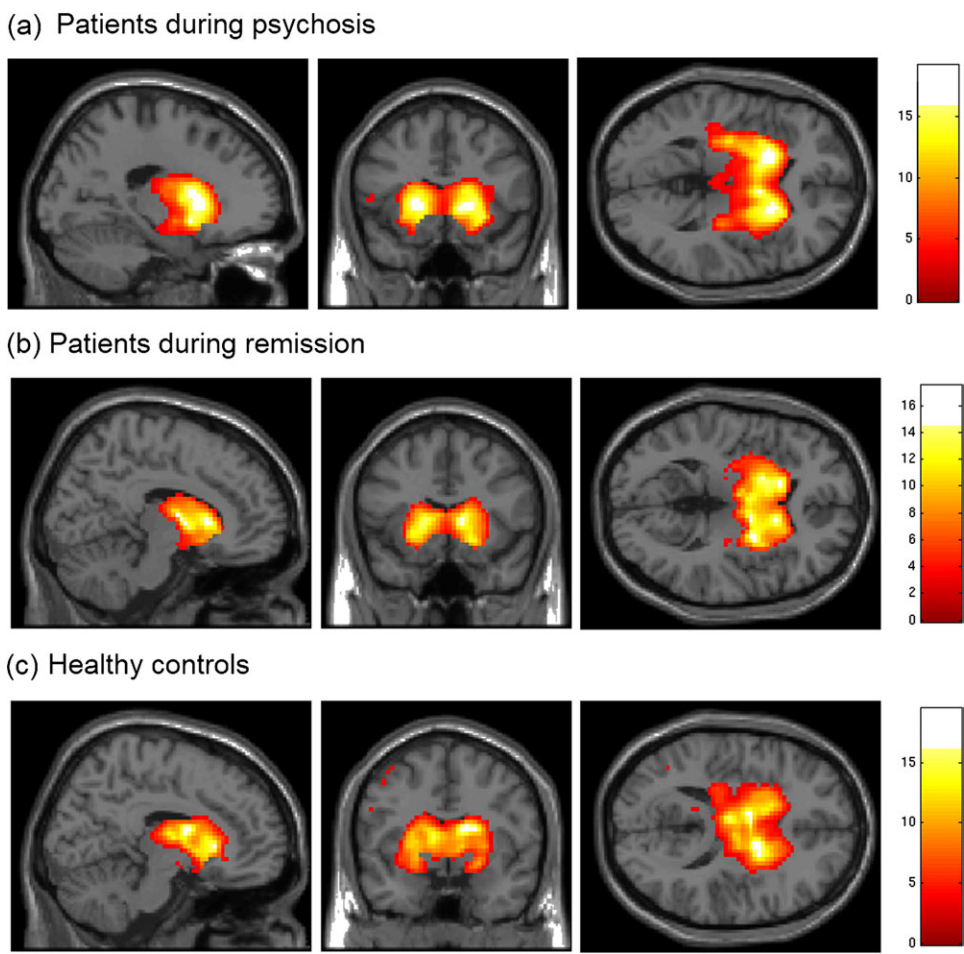


**Fig. 1.** Spatial maps of coherent intrinsic activity within the basal ganglia network (BGN). After independent component analysis of resting-state fMRI data, spatial maps of single-subject ICs representing the BGN were entered into voxel-wise one-sample  $t$  tests across individuals of each group and thresholded at  $P < .05$ , corrected for false discovery rate. Statistical parametric maps representing brain areas with significantly covarying activity were superimposed on a single-subject high-resolution T1 image (color scale representing  $z$  values from 0 to 16). The BGN includes the striatum, pallidum, and thalamus. (a) Patients during psychosis, (b) patients during psychotic remission, and (c) healthy controls.

(partial correlation,  $P < .05$ ; figure 3, table 1). Striatal ROIs were created by using the MARSBAR-toolbox (Release 0.42, <http://marsbar.sourceforge.net/>). Centers of spherical ROIs with 6 mm radius were derived from the study of Martinez and colleagues,<sup>27</sup> including left and right associative striatum ( $\pm 24, 12, 0$ ) and left and right limbic striatum ( $\pm 12, 9, -9$ ). For patients' BGN-IC of each session,  $z$  scores were extracted for each ROI and averaged across each bilateral ROI-pair.

#### Voxel-Based Morphometry Analysis

In order to control any functional connectivity results for potentially structural alterations, we calculated an averaged volumetric score for the striatum and included that as a covariate of no interest. For data preprocessing and analysis, the voxel-based morphometry 8 (VBM8) toolbox (<http://dbm.neuro.uni-jena.de/vbm.html>) was used. Images were corrected for bias-field inhomogeneity, registered using linear (12-parameter affine) and nonlinear transformations, and tissue classified into gray matter

(GM), white matter, and cerebrospinal fluid within the same generative model.<sup>28</sup> The resulting GM images were modulated to account for volume changes resulting from the normalization process. Here, we only considered non-linear volume changes so that further analyses did not have to account for differences in head size. Finally, images were smoothed with a Gaussian kernel of 8 mm (FWHM). We then calculated an averaged score for bilateral ventral and dorsal striatum and tested that for group differences. Additionally, we included this averaged VBM score as covariate of no interest in the above-described functional analysis of group differences across spatial IC maps.

## Results

### The Basal Ganglia Network Includes the Ventral and Dorsal Striatum

For each subject, ICA of fMRI data resulted in spatial maps, displayed in  $z$  scores, and associated time course values. Together, these measures represent the relative

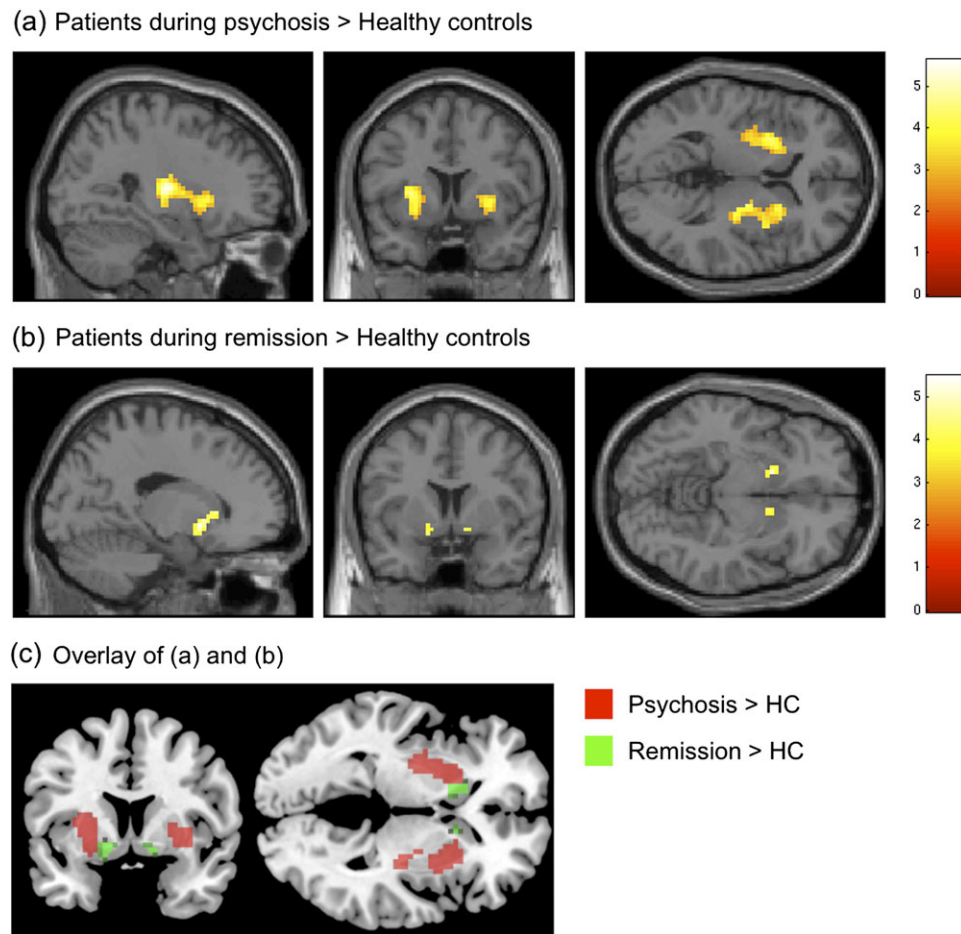


**Fig. 2.** Increasingly synchronized intrinsic activity in distinct locations of the striatum depends on disorder state. Statistical parametric maps (SPMs) of brain areas with significantly increased covarying activity in patients. (a) Two-sample  $t$  test between patients during psychosis and healthy controls (HCs), Montreal Neurological Institute (MNI)-coordinates [x,y,z] of the SPM: [27,12,4]; (b) Two-sample  $t$  test between patients during psychotic remission and HCs, MNI-coordinates: [17,5,−8]; (c) Overlay of (a) and (b) reveals spatially distinct subregions within the striatum, MNI-planes (y,z): [−7,−1]. Striatal volume was entered as covariate of no interest. All  $t$  tests were thresholded at  $P < .05$  and corrected for false discovery rate. SPMs were superimposed on a single-subject high-resolution T1 image (color scale representing  $z$  values from 0 to 6).

degree to which the component contributes to the overall BOLD signal at a given time point. Automated component selection by spatially regressing a striatum mask with all spatial maps revealed a subcortical basal ganglia network (BGN) in each individual (supplementary table S2). This BGN was spatially consistent across groups and sessions, matched previous results,<sup>18</sup> and included the striatum (nucleus caudatus, putamen), globus pallidus, and thalamus (figure 1, one-sample  $t$  test,  $P < .05$ , correction for false discovery rate). Additionally, 3 further ICs with cortical centers of mass had minor striatal contribution (supplementary figure S1 and tables S2 and S3).

#### *Spatial Maps of Coherent Intrinsic Brain Activity Reflect Psychosis and Psychotic Remission in Distinct Parts of the Striatum*

Compared with controls, psychotic patients showed increased activity in the associative and sensorimotor

striatum of the BGN (figure 2 and supplementary table S4, two-sample  $t$  test,  $P < .05$  FDR, corrected for striatal volume). During psychotic remission, the same patients showed stronger activity in bilateral limbic striatum (figure 2 and supplementary table S4, two-sample  $t$  test,  $P < .05$  FDR, corrected for striatal volume) when compared with HC. The 3 cortical ICs with striatal involvement did not differ across groups and sessions ( $P < .001$  uncorrected).

#### *Spectral Power of Time Courses of Synchronous Activity Was Changed During Psychotic Remission*

As a complementary measure to the spatial information provided by component maps, we estimated the spectral power of BGN-time courses, averaged for frequencies from 0.01 to 0.1 Hz, and compared them across groups and sessions (supplementary figure S2; two-sample  $t$  tests for comparisons with controls, paired  $t$  test for comparisons across sessions). Patients in psychotic remission

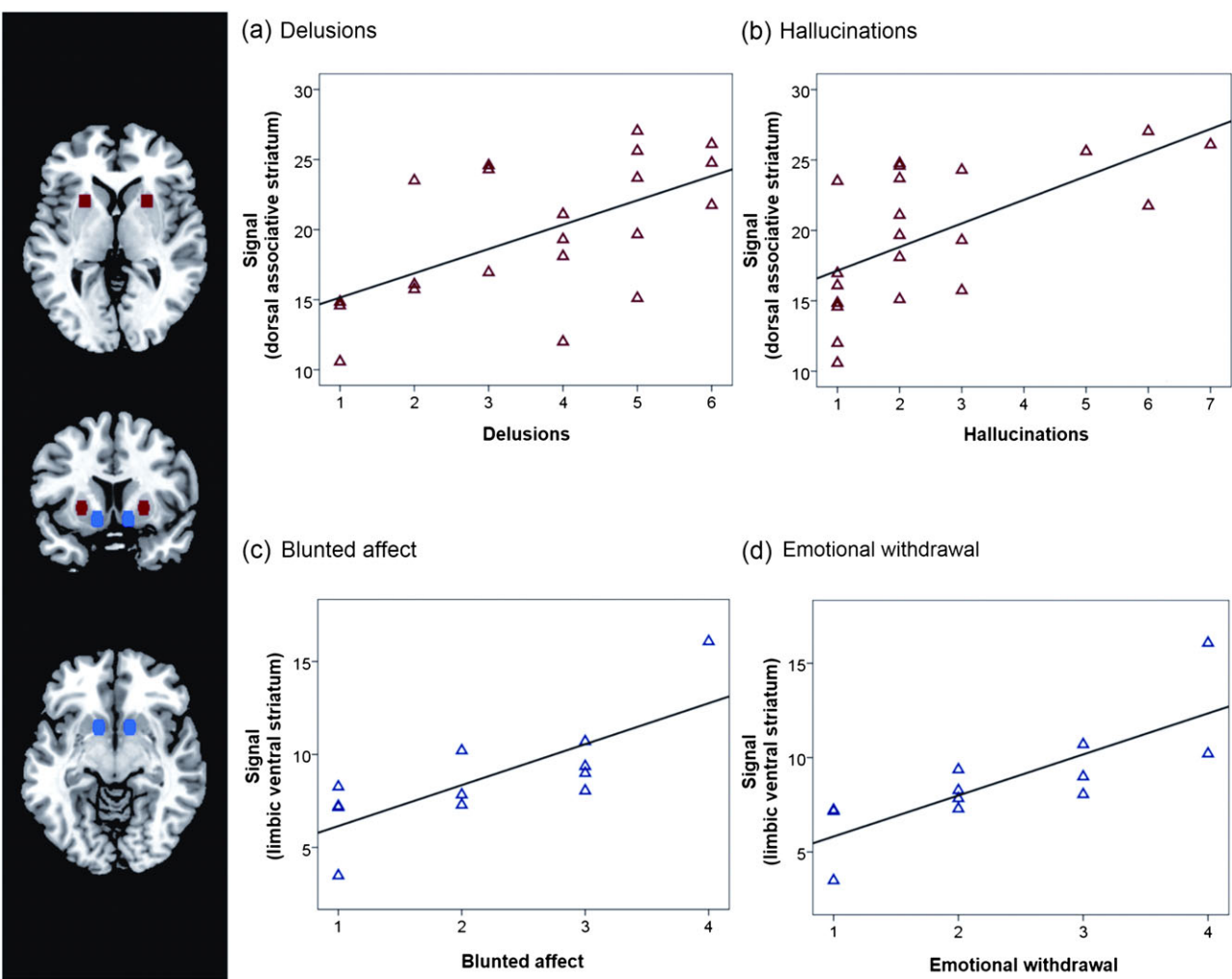


**Fig. 3.** Positive and negative symptoms of schizophrenia are related to intrinsic activity in dorsal and ventral parts of the striatum. In patients, the positive syndrome scale of positive and negative syndrome scale (PANSS) correlated with intrinsic activity in the dorsal striatum, while the negative syndrome scale was related to activity in the ventral striatum. In this figure, PANSS subscores responsible for the overall syndrome-brain relationship are plotted. From the positive syndrome scale, only (a) delusions and (b) hallucinations were significantly correlated with coherent activity in the dorsal striatum (red region of interest [ROI], Montreal Neurological Institute (MNI)-coordinates:  $\pm 24, 12, 0^{27}$ ) during psychosis ( $P < .05$ ). The negative scores (c) blunted affect and (d) emotional withdrawal were significantly correlated with activity in the ventral striatum (blue ROI, MNI:  $\pm 12, 9, -9^{27}$ ) during psychotic remission ( $P < .05$ ). ROI-signals were calculated as averaged  $z$  scores across left/right ROI from single-subject ICs of the basal ganglia network (figure 1). Partial correlations were corrected for striatal volume and antipsychotic medication (CPZ).

had significantly reduced power compared with controls ( $P = .02$ ). Patients during psychosis had a trend for reduced power compared with controls ( $P = .08$ ). Again, the other ICs with striatal involvement did not differ across groups and sessions for temporal aspects of striatal activity.

#### Intrinsic Striatal Activity Predicted Positive and Negative Symptoms

To study the relation between increased striatal activity and symptom dimensions, we correlated ROI-restricted  $z$  scores with total PANSS scores in patients. The coordinates of ROIs for functional subdivisions of the striatum (limbic/ventral and associative/dorsal) were independently derived from a previous brain imaging study.<sup>27</sup>

During psychosis, we found that synchronous activity of the dorsal striatum correlated with total positive ( $r = .53, P < .05$ ) but not with negative ( $r = .02$ ) symptoms (partial correlation, corrected for striatal volume and medication (CPZ), Bonferroni corrected for 4 tests); during psychotic remission, the correlation between activity in the ventral striatum and total negative symptoms demonstrated a trend to significance ( $r = .35, P = .09$  corrected), while there was no relation to positive symptoms ( $r = -.07$ ). Post hoc analyses of correlations with PANSS subscores revealed that the severity of delusions and hallucinations during psychosis positively correlated with activity increases within the associative striatum (figure 3, supplementary table S5,  $P < .05$ ). During psychotic remission, the severity of blunted affect and

emotional withdrawal positively correlated with activity increases within the limbic striatum (figure 3, supplementary table S5,  $P < .05$ ).

#### *Changes of Striatal Coactivity Are Not Explained by Medication or Striatal Volume Changes*

Finally, we investigated whether medication or structural changes in the striatum influence our result of coactivity changes. For each subject, we summarized his/her medication in terms of chlorpromazine equivalents (CPZ) and tested these for differences across disease states and for any correlation with striatal connectivity measures. We found no difference between psychosis and psychotic remission for the patient group (paired  $t$  test,  $P < .05$ , see table 1). Furthermore, the voxel-wise correlation analysis—restricted to the striatum—between  $z$  scores reflecting coactivity and CPZs across patients during psychosis and psychotic remission respectively revealed no significant correspondence ( $P < .05$ , FDR-corrected). Also, the analysis of volumetric data revealed no significant group differences for the striatum between healthy subjects and patients ( $P = .57$ ).

## Discussion

This study revealed changed intrinsic striatal activity in patients with schizophrenia. Changes were modulated by psychosis and related to various symptom dimensions in spatially distinct regions: Coherent intrinsic activity in the dorsal striatum was increased during psychosis and predictive for delusion and hallucination; the ventral striatum, however, showed increased activity during psychotic remission and predicted blunted affect and emotional withdrawal in the same patients. These findings extend our knowledge about striatal dysfunction in schizophrenia and suggest a link between intrinsic activity, symptom dimensions, and possibly striatal dopamine dysfunction.

#### *The Link Between Changed Intrinsic Activity in the Striatum and Symptom Dimensions in Schizophrenia*

The striatum is integrated into multiple cortico—basal ganglia—cortical loops. The ventral part projects into limbic, the associative part into associative, and the sensorimotor part into sensorimotor cortices.<sup>29,30</sup> Activity across these corticostriatal loops is coordinated particularly at the striatal level.<sup>30</sup> In order to retrieve distinct intrinsic networks with striatal contribution, we decomposed the rs-fMRI data with ICA and subsequently analyzed several components. Voxel-wise  $z$  values in a component's spatial map reflect the strength of functional connectivity to all other parts of this particular network.<sup>17,19</sup> While we found no disease-related differences of functional connectivity in the cortical networks covering parts of the basal ganglia, the BGN itself revealed strong changes of coherent intrinsic activity within the striatum.

#### *Dorsal Striatum Activity Correlates With Positive Symptoms*

We found that coherent intrinsic activity in the dorsal striatum was increased during psychosis but not during psychotic remission. Moreover, activity in the associative part correlated with positive symptoms and particularly with delusion and hallucination. With respect to regional specificity and behavioral relevance, our result is well in line with previous findings focusing on dopaminergic dysfunctions.<sup>2,3</sup> For example, Howes and colleagues<sup>2</sup> found elevated dopamine function of the associative striatum to be linked with positive signs in patients with prodromal schizophrenia. The consistency between our resting-state fMRI study and previous dopamine-related resting-state positron emission tomography studies in terms of brain-behavior relations suggest a link between intrinsic activity and dopamine dysfunction at rest.

#### *Ventral Striatum Activity Correlates With Negative Symptoms*

We found increased coherence of intrinsic activity in the ventral striatum during psychotic remission corresponding to blunted affect and emotional withdrawal in these patients. The ventral striatum is critically involved in emotion processing and reward-based learning.<sup>30</sup> In schizophrenia, task-fMRI studies on reward and emotion processing also revealed a link between activity changes in the ventral striatum and negative symptoms.<sup>31–33</sup> We interpret the increase of intrinsic connectivity in the ventral striatum with an increased frequency of negative symptom behavior. This is in accordance with rs-fMRI data of healthy subjects where repetitive sensory experiences lead to increased intrinsic connectivity in sensory systems.<sup>26</sup> Similarly, patients with major depression (MD) suffer from frequent negative feelings or repetitive behaviors such as rumination. Accordingly, studies on resting-state networks in MD reveal increased intrinsic connectivity in associated brain regions.<sup>34</sup>

#### *The Link Between Changed Spontaneous Activity in the Striatum and Dopamine Dysfunction in Schizophrenia*

We found that increased intrinsic activity in the ventral and dorsal striatum of patients differentially predicts disorder states and symptom dimensions. Our finding of locally diverging dysfunctions in the striatum correspond well with two distinct dopaminergic pathways: dopaminergic cells in the ventral tegmentum release dopamine into the ventral striatum and dopaminergic cells of the substantia nigra project to the dorsal striatum.<sup>35</sup> Although direct evidence for an interaction of intrinsic activity and dopamine signaling is still missing, there is experimental evidence for a relationship between dopamine levels and intrinsic activity in the dorsal striatum of animals and humans. In monkeys, iontophoretically applied dopamine modulates the spontaneous firing rate of neurons in the dorsal striatum,<sup>6</sup> see also Goto et al.<sup>5</sup> In patients suffering from Parkinson's disease (PD), where

dopamine levels in the dorsal striatum are reduced due to substantia nigra degeneration, resting-state fMRI data show an increase of intrinsic activity in the dorsal striatum after administration of levodopa, almost reaching levels of healthy persons.<sup>36,37</sup> In schizophrenia, psychosis is linked to elevated striatal dopamine function in the associative part,<sup>2,3</sup> which corresponds well to our data of increased intrinsic activity also in the dorsal part of the striatum. Together, these results from various domains suggest a potential link of intrinsic activity and dopamine signaling, at least in the dorsal striatum, which is particularly altered in patients with PD and schizophrenia. However, other neurotransmitter systems and structural changes might also impact on striatal dysfunction and should therefore be investigated with respect to intrinsic brain activity.

### Control Parameters and Limitations

The BGN consistently shows low-frequency BOLD signal fluctuations across both groups, a typical characteristic of functionally relevant intrinsic brain networks.<sup>19</sup> However, we also found slight differences in the low-frequency power between healthy subjects and patients (supplementary figure S2). While the meaning of alterations in the frequency range is still a matter of discussion,<sup>38</sup> a recent study reported decreased low-frequency power in a cortical IC of patients with schizophrenia.<sup>14</sup> Together, our data provide evidence for consistent changes of spatial and temporal characteristics of intrinsic striatal activity in schizophrenia.

We also aimed at controlling for several parameters related to the disease that might impact on our findings. We therefore included medication and striatal volume as confounding effects into the analyses.

**Medication.** It is important to note that the remitted subsample that we investigated approximately 9 months later only differed with respect to symptom dimensions (PANSS) but not with respect to medication and demographical aspects. Still, drug effects might confound our results from the group analysis compared with HCs. However, 2 recent studies found evidence that (1) the resting-state signal in the striatum of drug-naïve schizophrenic patients is also increased<sup>16</sup> suggesting that rs-fMRI effects are rather due to the pathology than due to drug effects. And that (2) dopaminergic substitution in PD increases resting-state connectivity in the striatum.<sup>36,37</sup> Therefore, any antidopaminergic medication in our patients should even have a contrary effect on the coherent activity in the striatum.<sup>39</sup> Finally, (3) both direction and localization of change in spontaneous activity were in accordance with the literature.<sup>3,16,36,37</sup>

**Striatal Volume.** It is also unlikely that increased striatal spontaneous activity is due to volumetric changes; again, we included striatal volume from a VBM analysis as variable of no interest into statistical analyses. Although a previous study observed volume reduction in the striatum of

schizophrenic patients depending on disorder state, medication, and duration of disorder,<sup>40</sup> we did not find any changes of striatal volume in our patient group.

A limitation of the study is the fact that we were not able to recruit all 21 patients for another reexamination and rescan during remission. Although all patients were in remission at the time of contact, 8 subjects did not agree to return to the clinic due to several reasons. Furthermore, we did not rescan HCs a second time as various test-retest studies with rs-fMRI data proved the consistency of the intrinsic functional architecture across days and months.<sup>24,25</sup> Although we cannot rule out any order effects in the patient group, we conclude that the long-term shift that exclusively occurred in the BGN and not in any other network is unlikely to be caused simply by changes over time.

### Conclusions

Overall, we found intriguing similarities between changes of intrinsic activity in the striatum, behavioral symptoms, and previous dopamine findings. Increased coherent intrinsic activity in the dorsal striatum during psychosis is predictive for delusion and hallucination; increased activity during psychotic remission in the ventral striatum is predictive for blunted affect and emotional withdrawal in the same patients. However, further studies exploring both a patient's dopamine function and intrinsic activity at the same time would be needed to reveal any direct relation between aberrant striatal dopamine function and intrinsic activity.

### Funding

This work was supported by the German Federal Ministry of Education and Research (BMBF 01EV0710 to A.M.W.), the Alzheimer Forschung Initiative (AFI 08860 to V.R.), the Kommission für Klinische Forschung of the Klinikum Rechts der Isar der Technischen Universität München (KKF 8765162 to C.S.), and through a bilatgrunn grant from the Norwegian Research Council (to T.E.).

### Supplementary Material

Supplementary material is available at <http://schizophreniabulletin.oxfordjournals.org>.

### Acknowledgments

We are grateful to the participants of the study and the staff of the Department of Psychiatry and Neuroradiology for their help in recruitment and data collection. The authors have declared that there are no conflicts of interest in relation to the subject of this study.

### References

- Howes OD, Kapur S. The dopamine hypothesis of schizophrenia: version III—the final common pathway. *Schizophr Bull*. 2009;35:549–562.

2. Howes OD, Montgomery AJ, Asselin MC, et al. Elevated striatal dopamine function linked to prodromal signs of schizophrenia. *Arch Gen Psychiatry*. 2009;66:13–20.
3. Kegeles LS, Abi-Dargham A, Frankle WG, et al. Increased synaptic dopamine function in associative regions of the striatum in schizophrenia. *Arch Gen Psychiatry*. 2010;67:231–239.
4. Agid O, Mamo D, Ginovart N, et al. Striatal vs extrastriatal dopamine D2 receptors in antipsychotic response—a double-blind PET study in schizophrenia. *Neuropsychopharmacology*. 2007;32:1209–1215.
5. Goto Y, Otani S, Grace AA. The Yin and Yang of dopamine release: a new perspective. *Neuropharmacology*. 2007;53:583–587.
6. Rolls ET, Thorpe SJ, Boytim M, Szabo I, Perrett DI. Responses of striatal neurons in the behaving monkey. 3. Effects of iontophoretically applied dopamine on normal responsiveness. *Neuroscience*. 1984;12:1201–1212.
7. Grace AA. Phasic versus tonic dopamine release and the modulation of dopamine system responsiveness: a hypothesis for the etiology of schizophrenia. *Neuroscience*. 1991;41:1–24.
8. Rolls ET, Loh M, Deco G, Winterer G. Computational models of schizophrenia and dopamine modulation in the prefrontal cortex. *Nat Rev Neurosci*. 2008;9:696–709.
9. Corlett PR, Taylor JR, Wang XJ, Fletcher PC, Krystal JH. Toward a neurobiology of delusions. *Prog Neurobiol*. 2010; 92:345–369.
10. Fletcher PC, Frith CD. Perceiving is believing: a Bayesian approach to explaining the positive symptoms of schizophrenia. *Nat Rev Neurosci*. 2009;10:48–58.
11. Kapur S. Psychosis as a state of aberrant salience: a framework linking biology, phenomenology, and pharmacology in schizophrenia. *Am J Psychiatry*. 2003;160:13–23.
12. Lynall ME, Bassett DS, Kerwin R, et al. Functional connectivity and brain networks in schizophrenia. *J Neurosci*. 2010; 30:9477–9487.
13. Bluhm RL, Miller J, Lanius RA, et al. Spontaneous low-frequency fluctuations in the BOLD signal in schizophrenic patients: anomalies in the default network. *Schizophr Bull*. 2007;33: 1004–1012.
14. Garrity AG, Pearlson GD, McKiernan K, Lloyd D, Kiehl KA, Calhoun VD. Aberrant “default mode” functional connectivity in schizophrenia. *Am J Psychiatry*. 2007;164:450–457.
15. Lui S, Li T, Deng W, et al. Short-term effects of antipsychotic treatment on cerebral function in drug-naïve first-episode schizophrenia revealed by “resting state” functional magnetic resonance imaging. *Arch Gen Psychiatry*. 2010;67:783–792.
16. Huang XQ, Lui S, Deng W, et al. Localization of cerebral functional deficits in treatment-naïve, first-episode schizophrenia using resting-state fMRI. *Neuroimage*. 2010;49: 2901–2906.
17. Calhoun VD, Adali T, Pearlson GD, Pekar JJ. A method for making group inferences from functional MRI data using independent component analysis. *Hum Brain Mapp*. 2001;14:140–151.
18. Robinson S, Basso G, Soldati N, et al. A resting state network in the motor control circuit of the basal ganglia. *BMC Neurosci*. 2009;10:137.
19. Beckmann CF, DeLuca M, Devlin JT, Smith SM. Investigations into resting-state connectivity using independent component analysis. *Philos Trans R Soc Lond B Biol Sci*. 2005;360:1001–1013.
20. American Psychiatric Association. Diagnostic and Statistical Manual of Mental Disorders—DSM IV—TR. Washington, DC: American Psychiatric Association; 2000.
21. Kay SR, Fiszbein A, Opler LA. The positive and negative syndrome scale (PANSS) for schizophrenia. *Schizophr Bull*. 1987;13:261–276.
22. Spitzer RL, Williams JB, Gibbon M, First MB. The Structured Clinical Interview for DSM-III-R (SCID). I: History, rationale, and description. *Arch Gen Psychiatry*. 1992;49:624–629.
23. Woods SW. Chlorpromazine equivalent doses for the newer atypical antipsychotics. *J Clin Psychiatry*. 2003;64:663–667.
24. Meindl T, Teipel S, Elmouden R, et al. Test-retest reproducibility of the default-mode network in healthy individuals. *Hum Brain Mapp*. 2010;31:237–246.
25. Shehzad Z, Kelly AM, Reiss PT, et al. The resting brain: unconstrained yet reliable. *Cereb Cortex*. 2009;19:2209–2229.
26. Riedl V, Valet M, Woller A, et al. Repeated pain induces adaptations of intrinsic brain activity to reflect past and predict future pain. *Neuroimage*. 2011;57:206–213.
27. Martinez D, Slifstein M, Broft A, et al. Imaging human mesolimbic dopamine transmission with positron emission tomography. Part II: amphetamine-induced dopamine release in the functional subdivisions of the striatum. *J Cereb Blood Flow Metab*. 2003;23:285–300.
28. Ashburner J, Friston KJ. Unified segmentation. *Neuroimage*. 2005;26:839–851.
29. Alexander GE, DeLong MR, Strick PL. Parallel organization of functionally segregated circuits linking basal ganglia and cortex. *Annu Rev Neurosci*. 1986;9:357–381.
30. Graybiel AM. Habits, rituals, and the evaluative brain. *Annu Rev Neurosci*. 2008;31:359–387.
31. Dowd EC, Barch DM. Anhedonia and emotional experience in schizophrenia: neural and behavioral indicators. *Biol Psychiatry*. 2010;67:902–911.
32. Goghari VM, Sponheim SR, MacDonald AW. The functional neuroanatomy of symptom dimensions in schizophrenia: a qualitative and quantitative review of a persistent question. *Neurosci Biobehav Rev*. 2010;34:468–486.
33. Jensen J, Willeit M, Zipursky RB, et al. The formation of abnormal associations in schizophrenia: neural and behavioral evidence. *Neuropsychopharmacology*. 2008;33:473–479.
34. Greicius MD, Flores BH, Menon V, et al. Resting-state functional connectivity in major depression: abnormally increased contributions from subgenual cingulate cortex and thalamus. *Biol Psychiatry*. 2007;62:429–437.
35. Moore RY, Bloom FE. Central catecholamine neuron systems: anatomy and physiology of the dopamine systems. *Annu Rev Neurosci*. 1978;1:129–169.
36. Wu T, Long X, Zang Y, et al. Regional homogeneity changes in patients with Parkinson’s disease. *Hum Brain Mapp*. 2009;30:1502–1510.
37. Wu T, Wang L, Chen Y, Zhao C, Li K, Chan P. Changes of functional connectivity of the motor network in the resting state in Parkinson’s disease. *Neurosci Lett*. 2009;460:6–10.
38. Niazy RK, Xie J, Miller K, Beckmann CF, Smith SM. Spectral characteristics of resting state networks. *Prog Brain Res*. 2011;193:259–276.
39. Kapur S, Mamo D. Half a century of antipsychotics and still a central role for dopamine D2 receptors. *Prog Neuropsychopharmacol Biol Psychiatry*. 2003;27:1081–1090.
40. Ellison-Wright I, Glahn DC, Laird AR, Thelen SM, Bullmore E. The anatomy of first-episode and chronic schizophrenia: an anatomical likelihood estimation meta-analysis. *Am J Psychiatry*. 2008;165:1015–1023.

## Supplementary Tables

**Table S1. Individual subject medication protocol and dosage**

Patient_ID	First scan during acute state of psychosis	Second scan during state of remission
1	20 mg Olanzapine	400 mg Clozapine
2	100 mg Clozapine, 80 mg Ziprasidone	<i>NO medication</i>
3	30 mg Olanzapine, 15 mg Aripiprazole	<i>no second scan</i>
4	10 mg Olanzapine, 5 mg Risperidone	2 mg Risperidone
5	30 mg Olanzapine, 5 mg Risperidone	<i>no second scan</i>
6	<i>NO medication</i>	<i>no second scan</i>
7	12,5 mg Olanzapine, 6 mg Paliperidone	<i>NO medication</i>
8	<i>NO medication</i>	6 mg Paliperidone
9	20 mg Olanzapine	12,5 Olanzapine
10	400 mg Quetiapine, 9 mg Paliperidone	<i>NO medication</i>
11	25 mg Olanzapine	<i>NO medication</i>
12	30 mg Olanzapine, 50mg Clozapine	300 mg Clozapine
13	30 mg Olanzapine, 5 mg Risperidone	600 mg Quetiapine
14	400 mg Quetiapine, 5 mg Risperidone	<i>no second scan</i>
15	25 mg Olanzapine, 50 mg Clozapine	<i>no second scan</i>
16	400 mg Amilsupride, 5mg Risperidone	600 mg Amilsupride, 400 mg Quetiapine
17	<i>NO medication</i>	600 mg Quetiapine, 5 mg Risperidone
18	200 mg Amilsupride, 15 mg Aripiprazol	<i>no second scan</i>
19	30 mg Olanzapine, 400 mg Quetiapine	<i>no second scan</i>
20	15 mg Olanzapine	<i>no second scan</i>
21	200 mg Clozapine, 12mg Paliperidone	450 mg Clozapine, 15 mg Aripiprazole

**Table S2. Striatal contributions to brain networks in healthy controls: Spatial Regression**

Network	Spatial Regression coefficient	one-sample-t-test, FDR-corrected	two-sample-t-test, SP vs. HC, FDR-corrected
Basal Ganglia Network	0.393	p<0.05 (Fig 1)	none
Artefact (White Matter)	0.006	p<0.05	-
Artefact (White Matter)	0.005	p<0.05	-
Lateral Temporal Network	0.002	p<0.05 (Fig S1)	none
Hippocampal Cingular Network	0.001	p<0.05 (Fig S1)	none
Salience Network	0.0001	p<0.05 (Fig S1)	none

A multiple spatial regression was conducted using a mask comprising the bilateral striatum (Putamen, globus pallidus, caudate nucleus) to identify independent components covering the striatum. For all networks with spatial regression coefficient >0.0001, a one-sample-t-test was performed to investigate the statistical significance of striatal contributions. For all networks with significant striatal co-activations (p<0.05, FDR-corrected), a two-sample-t-test between HC and SP was performed. The tests yielded no significant between-group differences.

**Table S3. Striatal contributions to cortical-subcortical intrinsic brain networks in healthy controls: one-sample-t-test, FDR-corrected, see Figure S1, Table S2.**

Anatomical region	L/R	cluster	Z-score	p-value (FDR-corrected)	MNI (x,y,z)
<b><i>Lateral Temporal network</i></b>					
Operculum	R	1720	7,73	<0,001	57, -15, 9
Superior temporal gyrus	R		6,95	<0,001	48, -33, 12
Operculum	L	1864	7,34	<0,001	-48, -30, 15
Precuneus	R	91	4,79	<0,001	12, -48, 69
Lingual Gyrus	L	101	4,56	<0,001	-18, -54, -3
Anterior cingulate cortex	R	170	3,96	<0,001	6, 15, 27
Middle cingulate cortex	R	170	3,96	<0,001	6, 24, 30
Cerebellum VII	L	17	3,83	<0,001	-24, -72, -45
<b>Caudate Nucleus</b>	<b>R</b>	<b>24</b>	<b>3,66</b>	<b>0,001</b>	<b>12,12, 0</b>
Postcentral Gyrus	R	8	3,64	0,001	60, -15, 48
Superior frontal gyrus	L	21	3,63	0,001	-18, 33, 39
Lingual Gyrus	R	24	3,53	0,001	15, -45, -3
Middle cingulate cortex	R	24	3,10	0,001	9, -52, 36
Middle orbital gyrus	R	19	3,47	0,001	36, 54, -3
Cerebellum Crus 2	L	10	3,45	0,001	-42, -69, -39
Cerebellum IX	L	20	3,37	0,001	-15, -54, -42
<b><i>Hippocampal-insular-cingular network</i></b>					
Insula Lobe	R	2568	7,28	<0,001	48, 9, -6
Hippocampus	L	2668	6,14	<0,001	-15, -27, -12
Hippocampus	R	2568	5,95	<0,001	18, -33, -12
Superior temporal gyrus	L	1227	7,21	<0,001	-57, 3, 0
Insula Lobe	L	1227	6,36	<0,001	-24, 3, 6
Anterior cingulate cortex	L	428	6,34	<0,001	0, 39, 12
Middle occipital gyrus	L	39	5,12	<0,001	-36, -72, 33
Thalamus	L	61	4,84	<0,001	-3, -18, 3
<b>Caudate Nucleus</b>	<b>L</b>	<b>24</b>	<b>4,59</b>	<b>&lt;0,001</b>	<b>-9, 6, 3</b>

Middle frontal gyrus	L	77	4,55	0,001	-33, 48, 12
Superior frontal gyrus	L	77	3,59	0,001	-21, 57, 18
Middle cingulate cortex	R	14	3,06	0,001	6, -36, 48
<b>Salience Network</b>					
Superior medial gyrus	R	3900	7,65	<0,001	6, 21, 42
Middle cingulate cortex	R	3900	7,61	<0,001	6, 30, 30
Middle cingulate cortex	L	3900	7,45	<0,001	-3, 24, 36
Insula Lobe	R	670	6,89	<0,001	48, 15, -3
<b>Caudate Nucleus</b>	<b>R</b>	<b>670</b>	<b>5,64</b>	<b>&lt;0,001</b>	<b>15, 12, 3</b>
Insula Lobe	L	727	6,46	<0,001	-45, 12, -6
Cerebellum Crus 1	R	181	6,21	<0,001	39, -63, -27
Cerebellum Crus 1	L	227	5,97	<0,001	-39, -60, -27
Precuneus	L	727	4,58	0,001	-9, -51, 12
Precuneus	R	113	3,62	0,001	18, -60, 42
Thalamus	L	37	3,95	<0,001	-12, -15, 15

**Table S4. Striatal subregions of changed spontaneous activity in patients with schizophrenia during psychosis and psychotic remission**

Functional subdivisions	Anatomical subdivisions (peak voxel)	L/R	p-value	MNI (x, y, z)
<b>(a) SP &gt; HC</b>				
Associative striatum	Precommissural dorsal putamen	L	0,005*	-27, 6, 6
		R	0,007*	24, 15, 3
Sensorimotor Striatum	postcommissural dorsal putamen	L	0,018*	-27, -6, 3
		R	0,002*	24, 12, -9
<b>(b) SPR &gt; HC</b>				
Limbic striatum	Precommissural ventral putamen	L	0,019*	-15, 9, -6
		R	0,038*	12, 6, -9

\*Significant for p<0.05, FDR-corrected for multiple comparisons (for comparisons SP vs HC and SPR vs HC two-sample t-test, corrected for striatal volume). Abbreviations: SP: patients with schizophrenia during psychosis; SPR: patients with schizophrenia during psychotic remission; HC: healthy controls

**Table S5. Post-hoc tests for correlations between positive/negative PANSS subscores and striatal coactivity for significant total PANSS score correlations.**

	SP	SPR
	Dorsal / Associative striatum	Ventral / Limbic striatum
<b>Positive subscores</b>		
<b>Delusions (P1)</b>	<b>0,505*</b>	
Conceptual disorganization (P2)	-0,025	
<b>Hallucinations (P3)</b>	<b>0,582*</b>	
Hyperactivity (P4)	0,521	
Grandiosity (P5)	0,033	
Suspiciousness/persecution (P6)	0,166	

Hostility (P7)	0,185	
<b>Negative subscores</b>		
<i>Blunted affect (N1)</i>		<b>0,775**</b>
<i>Emotional withdrawal (N2)</i>		<b>0,854**</b>
<i>Poor rapport (N3)</i>		0,377
<i>Passive/apathetic social withdrawal (N4)</i>		0,372
<i>Difficulty in abstract thinking (N5)</i>		-0,284
<i>Lack of spontaneity and flow of conversation (N6)</i>		-0,102
<i>Stereotyped thinking (N7)</i>		-0,332

Significant for \* $p<0.05$ , \*\* $p<0.005$  partial correlation, corrected for striatal volume and chlorpromazine equivalent dose (CPZ).

Abbreviations: SP: patients with schizophrenia during psychosis; SPR: patients with schizophrenia during psychotic remission.

## Supplementary Figures

**Figure S1. Additional intrinsic brain networks comprising parts of the striatum as revealed by the multiple spatial regression analysis (see Tables S2, S3).**

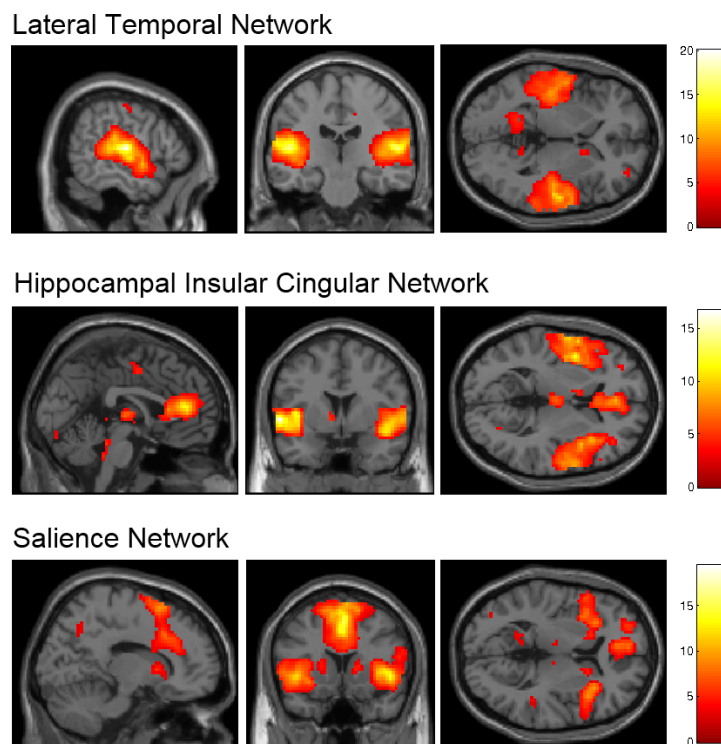
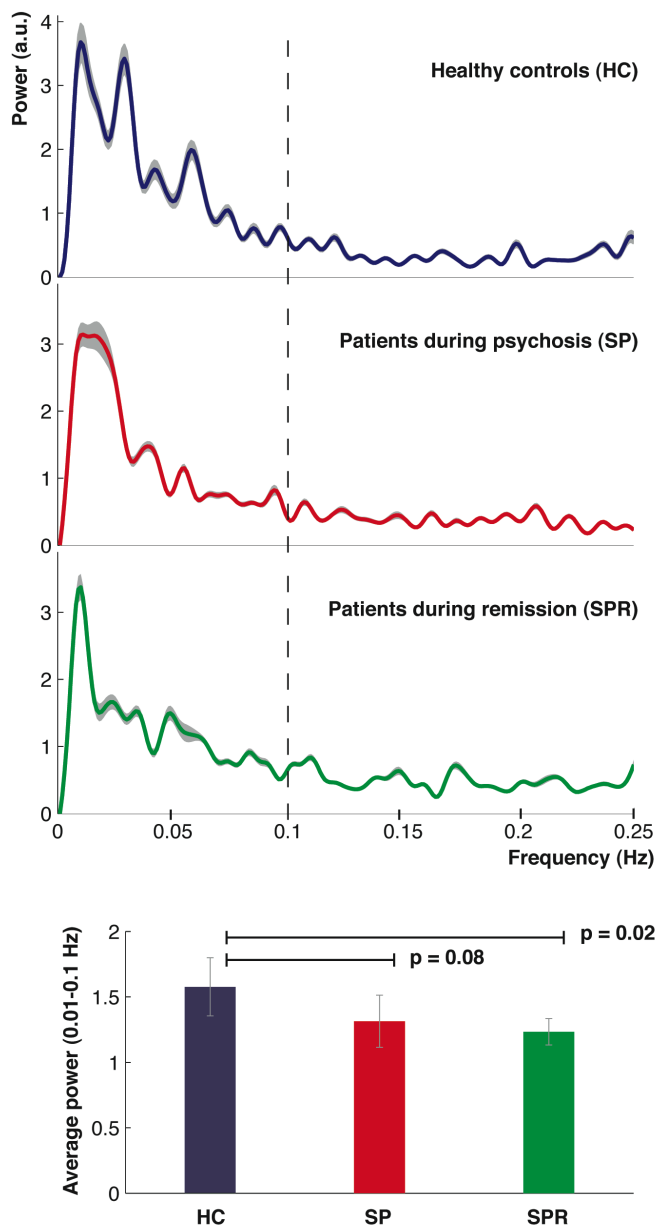


**Figure S2. Spectral power of time courses of the basal ganglia network for patients and healthy controls.**



The three frequency-power plots represent spectral power density of time courses of the basal ganglia network for healthy controls (HC), patients during psychosis (SP), and patients during psychotic remission (SPR). The bar plots (bottom) reflect average spectral power in the frequency range of 0.01 – 0.1 Hz for each group. During psychotic remission patients' spectral power is significantly reduced compared with controls ( $p=0.02$ ) and during psychosis a trend for reduced power remains ( $p=0.08$ ).

## 12 Discussion

The resting brain hosts intrinsic networks of coherent ongoing neuronal activity between distributed brain regions<sup>5,14</sup>. These ICNs persist in humans across the whole life span<sup>38-41</sup>, during waking and sleep<sup>42,43</sup>, and even in complete unconsciousness like in patients in a vegetative state<sup>65</sup>. Moreover, ICNs occur in anaesthetized rats and monkeys<sup>35,36</sup>. Therefore the intrinsic functional architecture of coherent brain activity is a fundamental organizational principle of the brain.

We participated in a multi-center study of 35 research groups that defined the intrinsic functional architecture of ongoing brain activity as an emerging tool for discovery science of the brain<sup>37</sup>. The study reported several FC methods that consistently detect ICNs of coherent low-frequency BOLD fluctuations in rs-fMRI data. This is in accordance with other studies performing test-retest analyses of data from the same subjects across days and months<sup>30,66-68</sup>. Despite this overall consistency of ICNs, our study also revealed effects of age and sex on network connectivity. While changes related to sex were subtle in our as in other studies<sup>32</sup>, age effects were more prominent. Most studies investigating the intrinsic functional architecture across the life span report overall uncoupling, or decreased FC of mainly long-range connections that might start as early as in young adulthood<sup>32,41</sup>.

### 12.1 Organized intrinsic brain activity influences behavior in healthy subjects

We then investigated the behavioral relevance of organized intrinsic brain activity. Specifically, we explored whether variations in sensory experiences relate to altered patterns of intrinsic brain activity in the resting state, beyond the immediate experience. First, we tested short-term modulation of ICN activity by exposing healthy subjects to repeated painful stimulation across 11 consecutive days<sup>59</sup>. In a different study we explored long-term differences in organized intrinsic brain activity. We tested whether aberrant visual perception of synesthetes, healthy subjects that consistently perceive unimodal stimuli (grey letters) as multimodal stimuli (grey letters as colored letters; letters associated with tones) is related to permanent changes in the intrinsic brain architecture (Dovern et al, J Neurosci, under revision).

In the study on short-term plasticity of intrinsic brain activity we exposed healthy subjects to identical painful stimuli on 11 consecutive days and explored intrinsic FC in ICNs during rest before (preREST) and after (postREST) stimulation. On a network level, we found that repeated pain selectively increased FC in the sensorimotor ICN (SMN) during postREST. We also found that the degree of increased FC during postREST correlated with the subjective experience of pain intensity the subjects had during stimulation. After 11 days, FC of the ventromedial prefrontal cortex (vmPFC) in the SMN even predicted the intensity a subject will perceive during the final, forthcoming stimulation. This study revealed experimentally induced plasticity of organized intrinsic brain activity in response to repeated pain.

These results on modulated intrinsic brain activity with repeated pain are in line with task-fMRI studies testing acute pain processing. While somatosensory cortices process sensory discriminatory information of a pain sensation, the vmPFC has been ascribed a modulatory role in pain perception<sup>69-71</sup>. Hence, our data show that repeated pain selectively alters intrinsic connectivity between brain regions initially involved in processing acute pain sensations.

“Chronic pain is a state of continuous learning”<sup>72</sup>. In our study, predictive coding in the vmPFC only evolved after subjects had repeatedly experienced, or learned, this particular situation. The anticipatory role of the vmPFC in the resting state might account for this learning effect. The literature on pain processing shows opposite directions of prefrontal activity between healthy subjects and patients suffering from chronic pain<sup>70,71,73</sup>. Healthy subjects that habituate to repeated pain show decreased activation in prefrontal cortex during pain processing<sup>71</sup>. In chronic pain patients, however, vmPFC is the only region within the pain network being more strongly involved in pain processing as compared to normal subjects<sup>70</sup>. Our data imply that a painful experience is not only coded by immediate changes of neuronal activity but also in coherent ongoing brain activity during rest. Furthermore aberrant plasticity in the intrinsic functional architecture might be related to chronic pain states.

In the following, I will relate the changes of intrinsic brain activity we found in response to pain to similar changes observed in other sensory and cognitive modalities.

Robertson et al showed that learning of a difficult spatial navigation task across several minutes changes FC in the resting state immediately after the task<sup>57</sup>. These changes selectively occurred in an ICN supposed to process attention to spatial information. In a different study, subjects had to detect a visual target on a screen and learned this task for several hours<sup>60</sup>. Again, the FC of primary visual and attention related brain regions increased from the resting state before learning the task to the resting state after successful performance of the task. Together, these and our data show that configurations of intrinsic brain activity change with the repeated experience or performance of somatosensory, visual and motor tasks. This suggests that ICNs of certain functional entities are integrated into a stable architecture of intrinsic brain activity, and are selectively modulated by recent experiences or different cognitive states. A possible interpretation of these data is that intrinsic brain activity might be involved in memory coding of past experiences and continuously adapts with learning. Two recent studies explored the FC of the hippocampus as an integrator of new memories with the cortex after learning tasks. Both studies showed that coherent brain activity between hippocampi and cortex was increased in the resting state after a memory task<sup>74</sup> and this FC correlated with later memory retrieval<sup>75</sup>.

In addition to above described short-term modulations of intrinsic brain activity, we also investigated state dependent differences in the intrinsic functional architecture. Individuals with synesthesia are healthy subjects with altered sensory experiences since birth<sup>76</sup>. They report additional color perceptions while viewing numbers or letters. These additional experiences are stable across years (e.g. an “a” always occurs in light blue) and are hypothesized to relate to hyperconnectivity between visual grapheme, color and multimodal integration sites in the cortex<sup>77,78</sup>. We therefore investigated organized intrinsic brain activity in ICNs covering primary sensory and integration sites in subjects with synesthesia and controls (Dovern et al, J Neurosci, under revision). We found both a global and a specific (visual to fronto-parietal networks) increase of FC in grapheme-color synesthesia. Moreover, this increased intrinsic network connectivity reflected the strength of synesthetic experiences. This is the first study to investigate organized intrinsic brain activity in synesthetes and also first evidence for increased functional hyperconnectivity in synesthesia.

Beyond a better understanding of the neural mechanisms of synesthesia, our results fit into recent approaches investigating influences of inherited or acquired variations of intrinsic brain circuits on human behavior like feeling, experiences, and action patterns. The question is if organized intrinsic brain activity is linked to emotional and cognitive functions. Seeley and colleagues showed that FC in a salience related ICN (SN) comprising anterior cingulate cortex and bilateral insula correlated with the level of anxiety measured in prescan resting state before the fMRI session<sup>61</sup>. In another study, Hampson et al. showed that the strength of FC in the default mode network (DMN) correlated with performance on a working memory task, during the task and also during postTASK resting state<sup>79</sup>. A very recent study also showed correlations between FC measures and personality traits<sup>80</sup>. In combination, our data suggest that differences in intrinsic network connectivity are directly related to the phenomenology of human experiences and continuously change with further experiences.

## **12.2 Intrinsic connectivity networks and neuropsychiatric diseases**

Our final two studies explored disease related changes of organized intrinsic brain activity in neuropsychiatric patients. In healthy subjects the intrinsic functional architecture of organized brain activity is rather robust with only subtle changes occurring across lifetime. Neuroimaging of brain development in preterms or during adolescence revealed that several aspects of ICNs are already present at birth<sup>81,82</sup>, while others, especially long-range connections, continuously change during adulthood and aging<sup>40,41,81,83</sup>. Furthermore, data from colleagues and our own work on network adaptations in healthy subjects suggest that the ensemble of ICNs is crucial for behavior<sup>59-61</sup>. Therefore several groups have hypothesized that the connectivity within and between ICNs might be altered in neuropsychiatric diseases such as schizophrenia, major depression, Attention Deficit Hyperactivity Disorder (ADHD) or Parkinson's Disease<sup>84,85</sup> and have tried to link changes in the intrinsic functional architecture to disease related symptoms.

We reported the first network-wide analysis of intrinsic brain activity comparing a group of neuropsychiatric patients with healthy controls. We analyzed patients with early AD, Mild Cognitive Impairment (MCI), and found prominent alterations in only 2 out of 8 ICNs in the patient group<sup>63</sup>. The MCI patients had severely impaired FC in the

DMN and an attention related ICN comprising cortical midline structures, parietal cortices and hippocampus. All other ICNs, especially primary sensory systems remained unchanged. Most importantly, cortical regions with affected FC are key regions for structural deficits in later stages of AD. As we could exclude any structural deficits in the patient group, we suggest that the subtle memory and behavioral deficits of the patients might rather be related to the functional connectivity deficits we observed in organized intrinsic brain activity.

Our study was an initial rs-fMRI approach to test the hypothesis of AD being a disconnection syndrome<sup>86</sup>. Earlier, Greicius and colleagues already revealed uncoupling of long-range FC selectively in the DMN of patients with AD<sup>87</sup> which was followed by a similar results in whole brain analyses of FC<sup>88</sup> as well as SC<sup>89</sup>. Additionally, local measures of the amplitude of LFF also revealed disease related differences in similar brain patterns<sup>90</sup>. Overall these data suggest that AD patients are associated with abnormalities in large-scale brain networks which might provide new insights into the disease mechanism<sup>91</sup>.

In addition to cortical ICNs that we investigated in MCI, we also studied intrinsic brain activity of a subcortical ICN in different stages of schizophrenia<sup>64</sup>. Striatal dysfunction is thought to be a fundamental element in schizophrenia. Striatal dopamine dysfunction impacts on reward processing and learning and is present even at rest. We acquired rs-fMRI data and psychometric assessment in schizophrenic patients during psychosis and during remission 9 months later. We found that during psychosis, coherent intrinsic activity of the striatum was increased in the dorsal part and correlated with positive symptoms such as delusion and hallucination. In psychotic remission of the same patients activity of the ventral striatum was increased and correlated with negative symptoms such as emotional withdrawal and blunted affect. Our finding of altered intrinsic activity in distinct parts of the striatum depending on predominant schizophrenic symptoms supports previous transmitter studies on schizophrenia. PET imaging revealed that elevated dopamine function of the associative, or dorsal striatum correlated with positive signs in patients with prodromal schizophrenia<sup>92</sup>. These findings extend our knowledge about striatal dysfunction in schizophrenia and suggest a link between intrinsic activity, symptom dimensions, and possibly striatal dopamine dysfunction.

Although we concentrated on subcortical ICNs in this study, colleagues also found global alterations in the intrinsic architecture of cortical networks in schizophrenia. Early work described decreased FC within the DMN of patients during rest<sup>93,94</sup>. However, further network metrics exist that reflect the global efficiency in communication between several large scale brain networks. In schizophrenia, these measures reveal less strongly integrated configuration within and between several ICNs. E.g. Lynall et al. showed globally reduced strength of FC, whereas diversity of functional connections was increased<sup>95</sup>. Topologically, functional brain networks in schizophrenia had reduced clustering and small-worldness, reduced probability of high-degree hubs, and increased robustness in the schizophrenic group<sup>95,96</sup>. These data suggest that patients with schizophrenia have a less strongly integrated and diverse profile of subcortical and cortical intrinsic brain networks already in the resting state.

### **12.3 Overall conclusion on organized intrinsic brain activity**

Subjects at rest dedicate the largest amount of energy to the brain<sup>3</sup>. This fuels ongoing neuronal activity that is not random noise but is organized into large-scale networks of coherent low-frequency signal fluctuations in fMRI<sup>14</sup>. Organized intrinsic brain activity therefore is a fundamental and ubiquitous organizational principle of the brain yet its functional meaning is still largely unknown. Early work on the intrinsic functional architecture suggested that patterns of FC simply reflect underlying anatomical connections, or SC, between brain regions<sup>36,48</sup>. This is supported by the fact that intrinsic brain activity forms patterns of ICNs robustly occurring in several species<sup>35,36</sup>, across time (test-retest reliability)<sup>66-68</sup>, and even in states of altered consciousness<sup>44</sup>. However, recent data clearly showed that only a certain amount (25%) of distinct brain regions is indeed coupled by FC when also strong SC is present<sup>49</sup>. As soon as polysynaptic connections are assumed on the structural level, no correlation exists with FC patterns. Moreover, a prominent feature of certain ICNs is strong FC between contralateral hemispheres where no direct anatomical connections exist (e.g. bilateral occipital cortices). Therefore, SC can only partly explain coherent intrinsic brain activity in ICNs.

This implies that the volatile aspects of intrinsic brain activity should be inspected in more detail. Several studies reported that the emotional or cognitive state of a subject is partly related to FC in certain ICNs. E.g. the level of anxiety or anticipated pain can already be implied from the coherence of intrinsic brain activity in certain networks<sup>59,61</sup>.

Furthermore, we have shown that consistent differences in subjective experiences of primary sensory processing can be predicted from an altered intrinsic brain architecture (Dovern et al, J Neurosci, under revision). But modulations of FC even occur on shorter time scale of days or seconds. We have shown that the repeated experience of an identical painful stimulation leads to plasticity in the intrinsic functional architecture<sup>59</sup>. Fox and colleagues even showed immediate influence of the strength of FC in the motor system on the motor force a subject applied to a lever on a trial-by-trial basis<sup>97</sup>.

We therefore suggest two layers of processing inherited in ongoing brain activity of large scale brain networks. On the one hand, intrinsic brain activity forms a robust architecture of consistent ICNs reflecting mainly anatomical connections. On the other hand, immediate changes in the coherence of spontaneous activity relate to fluctuations in cognitive functions and motor behavior. This suggests a volatile layer of intrinsic brain fluctuations influencing behavior in the range of seconds. We hypothesize that with continuous experiences, coherent intrinsic activity might stabilize networks of brain regions that are commonly activated together during sensory or cognitive processing. These organized patterns of intrinsic activity continuously adapt with ongoing experiences to reflect past and anticipate future experiences. By this, the intrinsic architecture of ongoing brain activity continuously adapts and prepares the organism for what might happen. In conclusion, the intrinsic brain state might have more impact on human behavior than does the brain's immediate response to an event.

### 13 References

1. Friston, K. J. Modalities, modes, and models in functional neuroimaging. *Science* **326**, 399–403 (2009).
2. Raichle, M. E. A brief history of human brain mapping. *Trends Neurosci* **32**, 118–126 (2009).
3. Raichle, M. E. & Mintun, M. A. Brain work and brain imaging. *Annu Rev Neurosci* **29**, 449–476 (2006).
4. Gusnard, D. A., Raichle, M. E. & Raichle, M. E. Searching for a baseline: functional imaging and the resting human brain. *Nat Rev Neurosci* **2**, 685–694 (2001).
5. Raichle, M. E. Two views of brain function. *Trends Cogn Sci (Regul Ed)* **14**, 180–190 (2010).
6. Belliveau, J. W. *et al.* Functional mapping of the human visual cortex by magnetic resonance imaging. *Science* **254**, 716–719 (1991).
7. Friston, K. J. Imaging neuroscience: principles or maps? *Proc Natl Acad Sci USA* **95**, 796–802 (1998).
8. Logothetis, N. K. What we can do and what we cannot do with fMRI. *Nature* **453**, 869–878 (2008).
9. Logothetis, N. K., Pauls, J., Augath, M., Trinath, T. & Oeltermann, A. Neurophysiological investigation of the basis of the fMRI signal. *Nature* **412**, 150–157 (2001).
10. Ogawa, S., Lee, T. M., Nayak, A. S. & Glynn, P. Oxygenation-sensitive contrast in magnetic resonance image of rodent brain at high magnetic fields. *Magn Reson Med* **14**, 68–78 (1990).
11. Bandettini, P., Wong, E. & Hinks, R. Time course EPI of human brain function during task activation. *Magnetic ...* (1992).
12. Kwong, K. & Belliveau, J. Dynamic magnetic resonance imaging of human brain activity during primary sensory stimulation. *Proceedings of the ...* (1992).
13. Ogawa, S., Tank, D. & Menon, R. Intrinsic signal changes accompanying sensory stimulation: functional brain mapping with magnetic resonance imaging. *Proceedings of the ...* (1992).
14. Fox, M. D. & Raichle, M. E. Spontaneous fluctuations in brain activity observed with functional magnetic resonance imaging. *Nat Rev Neurosci* **8**, 700–711 (2007).
15. Corbetta, M., Patel, G. & Shulman, G. L. The reorienting system of the human brain: from environment to theory of mind. *Neuron* **58**, 306–324 (2008).
16. Shulman, R. G., Rothman, D. L., Behar, K. L. & Hyder, F. Energetic basis of brain activity: implications for neuroimaging. *Trends Neurosci* **27**, 489–495 (2004).
17. Fox, P. T., Raichle, M. E., Mintun, M. A. & Dence, C. Nonoxidative glucose consumption during focal physiologic neural activity. *Science* **241**, 462–464 (1988).
18. Cole, D. M., Smith, S. M. & Beckmann, C. F. Advances and pitfalls in the analysis and interpretation of resting-state FMRI data. *Front Syst Neurosci* **4**, 8 (2010).
19. Smith, S. M. *et al.* Network modelling methods for FMRI. *NeuroImage* **54**, 875–891 (2011).
20. Friston, K. Functional and effective connectivity in neuroimaging: a synthesis. *Hum Brain Mapp* **2**, 56–78 (1994).
21. Yang, H. *et al.* Amplitude of low frequency fluctuation within visual areas revealed by resting-state functional MRI. *NeuroImage* **36**, 144–152 (2007).

22. Van Dijk, K. R. A. *et al.* Intrinsic functional connectivity as a tool for human connectomics: theory, properties, and optimization. *J Neurophysiol* **103**, 297–321 (2010).
23. Sporns, O., Tononi, G. & Kötter, R. The human connectome: A structural description of the human brain. *PLoS Comput Biol* **1**, e42 (2005).
24. Bressler, S. L. & Menon, V. Large-scale brain networks in cognition: emerging methods and principles. *Trends Cogn Sci (Regul Ed)* **14**, 277–290 (2010).
25. Biswal, B., Yetkin, F. Z., Haughton, V. M. & Hyde, J. S. Functional connectivity in the motor cortex of resting human brain using echo-planar MRI. *Magn Reson Med* **34**, 537–541 (1995).
26. Greicius, M. D., Krasnow, B., Reiss, A. L. & Menon, V. Functional connectivity in the resting brain: a network analysis of the default mode hypothesis. *Proc Natl Acad Sci USA* **100**, 253–258 (2003).
27. Fox, M. D. *et al.* The human brain is intrinsically organized into dynamic, anticorrelated functional networks. *Proc Natl Acad Sci USA* **102**, 9673–9678 (2005).
28. Beckmann, C. F., DeLuca, M., Devlin, J. T. & Smith, S. M. Investigations into resting-state connectivity using independent component analysis. *Philos Trans R Soc Lond, B, Biol Sci* **360**, 1001–1013 (2005).
29. De Luca, M., Beckmann, C. F., De Stefano, N., Matthews, P. M. & Smith, S. M. fMRI resting state networks define distinct modes of long-distance interactions in the human brain. *NeuroImage* **29**, 1359–1367 (2006).
30. Damoiseaux, J. S. *et al.* Consistent resting-state networks across healthy subjects. *Proc Natl Acad Sci USA* **103**, 13848–13853 (2006).
31. Yeo, B. T. T. *et al.* The organization of the human cerebral cortex estimated by intrinsic functional connectivity. *J Neurophysiol* **106**, 1125–1165 (2011).
32. Allen, E. A. *et al.* A baseline for the multivariate comparison of resting-state networks. *Front Syst Neurosci* **5**, 2 (2011).
33. Doucet, G. *et al.* Brain activity at rest: A multi-scale hierarchical functional organization. *J Neurophysiol* (2011). doi:10.1152/jn.00895.2010
34. Abou-Elseoud, A. *et al.* Group-ICA Model Order Highlights Patterns of Functional Brain Connectivity. *Front Syst Neurosci* **5**, 37 (2011).
35. Lu, Zuo, Gu & Waltz Synchronized delta oscillations correlate with the resting-state functional MRI signal. *Proc Natl Acad Sci USA* **104**, 18265–18269 (2007).
36. Vincent, J. L. *et al.* Intrinsic functional architecture in the anaesthetized monkey brain. *Nature* **447**, 83–86 (2007).
37. Biswal, B. B. *et al.* Toward discovery science of human brain function. *Proc Natl Acad Sci U S A* **107**, 4734–4739 (2010).
38. Kelly, A. M. C. *et al.* Development of anterior cingulate functional connectivity from late childhood to early adulthood. *Cereb Cortex* **19**, 640–657 (2009).
39. Supekar, K. *et al.* Development of functional and structural connectivity within the default mode network in young children. *NeuroImage* **52**, 290–301 (2010).
40. Fair, D. A. *et al.* Functional brain networks develop from a “local to distributed” organization. *PLoS Comput Biol* **5**, e1000381 (2009).
41. Andrews-Hanna, J. R. *et al.* Disruption of large-scale brain systems in advanced aging. *Neuron* **56**, 924–935 (2007).
42. Fukunaga, M. *et al.* Large-amplitude, spatially correlated fluctuations in BOLD fMRI signals during extended rest and early sleep stages. *Magn Reson Imaging* **24**, 979–992

- (2006).
43. Larson-Prior, L. J. *et al.* Cortical network functional connectivity in the descent to sleep. *Proc Natl Acad Sci USA* **106**, 4489–4494 (2009).
  44. Greicius, M. D. *et al.* Persistent default-mode network connectivity during light sedation. *Hum Brain Mapp* **29**, 839–847 (2008).
  45. Boveroux, P. *et al.* Breakdown of within- and between-network resting state functional magnetic resonance imaging connectivity during propofol-induced loss of consciousness. *Anesthesiology* **113**, 1038–1053 (2010).
  46. Achard, S. & Bullmore, E. Efficiency and cost of economical brain functional networks. *PLoS Comput Biol* **3**, e17 (2007).
  47. Kelly, C. *et al.* L-dopa modulates functional connectivity in striatal cognitive and motor networks: a double-blind placebo-controlled study. *J Neurosci* **29**, 7364–7378 (2009).
  48. Hagmann, P. *et al.* Mapping the structural core of human cerebral cortex. *PLoS Biol* **6**, e159 (2008).
  49. Honey, C. J. *et al.* Predicting human resting-state functional connectivity from structural connectivity. *Proc Natl Acad Sci USA* **106**, 2035–2040 (2009).
  50. Leopold, D. A. & Maier, A. Ongoing physiological processes in the cerebral cortex. *NeuroImage* (2011).doi:10.1016/j.neuroimage.2011.10.059
  51. Niazy, R. K., Xie, J., Miller, K., Beckmann, C. F. & Smith, S. M. Spectral characteristics of resting state networks. *Prog Brain Res* **193**, 259–276 (2011).
  52. Shmuel, A. & Leopold, D. Neuronal correlates of spontaneous fluctuations in fMRI signals in monkey visual cortex: Implications for functional connectivity at rest. *Hum Brain Mapp* **29**, 751–761 (2008).
  53. He, B., Snyder, A., Zempel, J., Smyth, M. & Raichle, M. Electrophysiological correlates of the brain's intrinsic large-scale functional architecture. *Proc Natl Acad Sci USA* (2008).doi:10.1073/pnas.0807010105
  54. Nir, Y. *et al.* Interhemispheric correlations of slow spontaneous neuronal fluctuations revealed in human sensory cortex. *Nat Neurosci* (2008).doi:10.1038/nn.2177
  55. Keller, C. J. *et al.* Intrinsic functional architecture predicts electrically evoked responses in the human brain. *Proc Natl Acad Sci U S A* **108**, 10308–10313 (2011).
  56. Laufs, H. *et al.* Electroencephalographic signatures of attentional and cognitive default modes in spontaneous brain activity fluctuations at rest. *Proc Natl Acad Sci USA* **100**, 11053–11058 (2003).
  57. Albert, N., Robertson, E. & Miall, R. The Resting Human Brain and Motor Learning. *Curr Biol* (2009).doi:10.1016/j.cub.2009.04.028
  58. Lee, A. K. & Wilson, M. A. Memory of sequential experience in the hippocampus during slow wave sleep. *Neuron* **36**, 1183–1194 (2002).
  59. Riedl, V. *et al.* Repeated pain induces adaptations of intrinsic brain activity to reflect past and predict future pain. *NeuroImage* **57**, 206–213 (2011).
  60. Lewis, C., Baldassarre, A., Committeri, G., Romani, G. & Corbetta, M. Learning sculpts the spontaneous activity of the resting human brain. *Proc Natl Acad Sci USA* (2009).doi:10.1073/pnas.0902455106
  61. Seeley, W. W. *et al.* Dissociable Intrinsic Connectivity Networks for Salience Processing and Executive Control. *Journal of Neuroscience* **27**, 2349–2356 (2007).
  62. Harrison, B. J. *et al.* Modulation of brain resting-state networks by sad mood induction. *PLoS ONE* **3**, e1794 (2008).

63. Sorg, C. *et al.* Selective changes of resting-state networks in individuals at risk for Alzheimer's disease. *Proc Natl Acad Sci USA* **104**, 18760–18765 (2007).
64. Sorg, C. *et al.* Increased Intrinsic Brain Activity in the Striatum Reflects Symptom Dimensions in Schizophrenia. *Schizophrenia bulletin* (2012).doi:10.1093/schbul/sbr184
65. Boly, M. *et al.* Functional connectivity in the default network during resting state is preserved in a vegetative but not in a brain dead patient. *Hum Brain Mapp* (2009).doi:10.1002/hbm.20672
66. Meindl, T. *et al.* Test-retest reproducibility of the default-mode network in healthy individuals. *Hum Brain Mapp* (2009).doi:10.1002/hbm.20860
67. Shehzad, Z. *et al.* The Resting Brain: Unconstrained yet Reliable. *Cereb Cortex* (2009).doi:10.1093/cercor/bhn256
68. Zuo, X.-N. *et al.* Reliable intrinsic connectivity networks: test-retest evaluation using ICA and dual regression approach. *NeuroImage* **49**, 2163–2177 (2010).
69. Ploghaus, A., Becerra, L., Borras, C. & Borsook, D. Neural circuitry underlying pain modulation: expectation, hypnosis, placebo. *Trends Cogn Sci (Regul Ed)* **7**, 197–200 (2003).
70. Apkarian, A. V., Bushnell, M. C., Treede, R.-D. & Zubieta, J.-K. Human brain mechanisms of pain perception and regulation in health and disease. *European journal of pain (London, England)* **9**, 463–484 (2005).
71. Bingel, U., Schoell, E., Herken, W., Büchel, C. & May, A. Habituation to painful stimulation involves the antinociceptive system. *Pain* **131**, 21–30 (2007).
72. Apkarian, A., Baliki, M. & Geha, P. Towards a theory of chronic pain. *Prog Neurobiol* **87**, 81–97 (2009).
73. Gündel, H. *et al.* Altered cerebral response to noxious heat stimulation in patients with somatoform pain disorder. *Pain* (2007).doi:10.1016/j.pain.2007.10.003
74. Tambini, A., Ketz, N. & Davachi, L. Enhanced brain correlations during rest are related to memory for recent experiences. *Neuron* **65**, 280–290 (2010).
75. van Kesteren, M. T. R., Fernández, G., Norris, D. G. & Hermans, E. J. Persistent schema-dependent hippocampal-neocortical connectivity during memory encoding and postencoding rest in humans. *Proc Natl Acad Sci USA* **107**, 7550–7555 (2010).
76. Grossenbacher, P. G. & Lovelace, C. T. Mechanisms of synesthesia: cognitive and physiological constraints. *Trends Cogn Sci (Regul Ed)* **5**, 36–41 (2001).
77. Rouw, R. & Scholte, H. S. Increased structural connectivity in grapheme-color synesthesia. *Nat Neurosci* **10**, 792–797 (2007).
78. Hänggi, J., Wotrubá, D. & Jäncke, L. Globally altered structural brain network topology in grapheme-color synesthesia. *J Neurosci* **31**, 5816–5828 (2011).
79. Hampson, M., Driesen, N. R., Skudlarski, P., Gore, J. C. & Constable, R. T. Brain connectivity related to working memory performance. *J Neurosci* **26**, 13338–13343 (2006).
80. Adelstein, J. S. *et al.* Personality is reflected in the brain's intrinsic functional architecture. *PLoS ONE* **6**, e27633 (2011).
81. Doria, V. *et al.* Emergence of resting state networks in the preterm human brain. *Proc Natl Acad Sci USA* **107**, 20015–20020 (2010).
82. Fransson, P. *et al.* Resting-state networks in the infant brain. *Proc Natl Acad Sci USA* **104**, 15531–15536 (2007).
83. Fair, D. A. *et al.* Maturing thalamocortical functional connectivity across development. *Front Syst Neurosci* **4**, 10 (2010).

84. Zhang, D. & Raichle, M. E. Disease and the brain's dark energy. *Nat Rev Neurosci* **6**, 15–28 (2010).
85. Greicius, M. Resting-state functional connectivity in neuropsychiatric disorders. *Curr Opin Neurosci* **21**, 424–430 (2008).
86. Delbeuck, X., Van der Linden, M. & Collette, F. Alzheimer's disease as a disconnection syndrome? *Neuropsychology review* **13**, 79–92 (2003).
87. Greicius, M. D., Srivastava, G., Reiss, A. L. & Menon, V. Default-mode network activity distinguishes Alzheimer's disease from healthy aging: evidence from functional MRI. *Proc Natl Acad Sci USA* **101**, 4637–4642 (2004).
88. Wang, K. *et al.* Altered functional connectivity in early Alzheimer's disease: A resting-state fMRI study. *Hum Brain Mapp* **28**, 967–978 (2007).
89. He, Y., Chen, Z. & Evans, A. Structural insights into aberrant topological patterns of large-scale cortical networks in Alzheimer's disease. *J Neurosci* **28**, 4756–4766 (2008).
90. Wang, Z. *et al.* Spatial patterns of intrinsic brain activity in mild cognitive impairment and alzheimer's disease: A resting-state functional MRI study. *Hum Brain Mapp* (2010).doi:10.1002/hbm.21140
91. He, Y., Chen, Z., Gong, G. & Evans, A. Neuronal Networks in Alzheimer's Disease. *Neuroscientist* (2009).doi:10.1177/1073858409334423
92. Kegeles, L. S. *et al.* Increased synaptic dopamine function in associative regions of the striatum in schizophrenia. *Arch Gen Psychiatry* **67**, 231–239 (2010).
93. Garrity, A. G. *et al.* Aberrant "default mode" functional connectivity in schizophrenia. *Am J Psychiatry* **164**, 450–457 (2007).
94. Bluhm, R. L. *et al.* Spontaneous low-frequency fluctuations in the BOLD signal in schizophrenic patients: anomalies in the default network. *Schizophrenia bulletin* **33**, 1004–1012 (2007).
95. Lynall, M.-E. *et al.* Functional connectivity and brain networks in schizophrenia. *J Neurosci* **30**, 9477–9487 (2010).
96. Liu, Y. *et al.* Disrupted small-world networks in schizophrenia. *Brain* (2008).doi:10.1093/brain/awn018
97. Fox, M. D., Snyder, A. Z., Vincent, J. L. & Raichle, M. E. Intrinsic fluctuations within cortical systems account for intertrial variability in human behavior. *Neuron* **56**, 171–184 (2007).

## **14 Acknowledgments**

I am deeply grateful for the love and support of Kathrin and my parents and I have been enjoying the hours of discussions and exchange on brain and other matters with Afra and Christian.

## **15 Statutory declaration and statement**

Ich versichere hiermit eidesstattlich, dass die vorgelegte Dissertation von mir selbstständig und nur unter Verwendung der angegebenen Hilfsmittel angefertigt wurde.